Cement Fatigue and HPHT Well Integrity with Application to Life of Well Prediction

by

Catalin Teodoriu, Jerome Schubert, and Ignatius Ugwu
Petroleum Engineering Department, Texas A&M University
College Station, Texas

Final Project Report
Prepared for the Minerals Management Service
Under the MMS/OTRC Cooperative Research Agreement
1435-01-04-CA-35515
Task Order M07AC12464
MMS Project Number 602

December 2008

OTRC Library Number: 12/08A195

For more information contact:

Offshore Technology Research Center
Texas A&M University
1200 Mariner Drive
College Station, Texas 77845-3400
(979) 845-6000

or

Offshore Technology Research Center
The University of Texas at Austin
1 University Station C3700
Austin, Texas 78712-0318
(512) 471-6989

A National Science Foundation Graduated Engineering Research Center

EXECUTIVE SUMMARY

Problem Statement

For an oil/gas well to maintain its integrity and be produced effectively and economically, it is pertinent that a complete zonal isolation is achieved during the life of the well. This complete zonal isolation, however, can be compromised due to factors that come into play during the operative life of the completed well. Such factors may come in the form of thermal or pressure loads generally regarded as HTHP (High Temperature-High Pressure) loads which can manifest themselves as a static/cyclic load or both depending on how they are exerted. Cement structures experiencing cyclic loading conditions can fail as a result of fatigue due to extensive degradation of the microstructure of the cement material depending on stress levels and number of cycles.

There has been a lot of research and experimental investigations on the mechanism of fatigue failure of structures like buildings, bridges etc. but the fatigue behavior of well cement is still relatively unknown to engineers. Research in the area of well cement design has led to improved cement designs and cementing practices but yet many cement integrity problems persist and this further strengthens the need to understand the mechanism of cement fatigue. Even though most structural failures are as a result of fatigue rather than static loading, insights on the role of both static and fatigue loading conditions on the failure of cement sheath would hopefully lead to improvements in well design.

Project Objective

The objective of this project is to develop a better understanding of the performance of the casing–cement bond under HPHT well conditions, leading to a model to predict well life. This would entail two major tasks:

- to identify the factors that affect the casing–cement integrity under HPHT conditions
- to understand better the fatigue of well cement.

Based on the knowledge acquired from completing these tasks, it will be possible to analyze the mechanics of casing–cement systems under HPHT conditions for the long term integrity of the system.

Approach

The first approach taken in this project was a comprehensive literature review on the fatigue of construction cement/concrete since no literature presently exists on the fatigue of well cement and understanding of the differences between both kinds of cement. The literature review was focused on:

- the state of the art in the fatigue of cement,
- casing cement interaction models currently being utilized by operators, and
- casing–cement integrity under HPHT conditions.

The findings here are discussed in chapters 1 and 2. The knowledge from the literature review was then applied in modeling and understanding the mechanism of fatigue in well cement.

Furthermore, an analytical model of wellbore stresses based on wellbore parameters was developed and used in addition to finite element analysis to conduct stress analysis on a casing–cement–formation model in order to study the integrity of the cement sheath under different HPHT loading scenarios. This is presented in chapters 3 and 4 of this report. This model can be integrated in a simple-to-use computer software package capable of recording the history of the well and predicting its fatigue life.

Finally, recommendations for future work are given in chapter 5.

NOMENCLATURE

ID	Internal diameter
HPHT	High Pressure-High Temperature
S-N Diagram	Stress-cycle diagram
LS	Low Strength
HS	High Strength
BWOC	By Weight of Cement
BVOB	By Volume of Blend
BWOW	By Weight of Water
FEA	Finite Element Analysis
SF	Safety Factor
E	Young's modulus
v	Poisson's ratio
α	Coefficient of thermal expansion
ΔT	Temperature change
p_i	Internal pressure
p_f	Formation pressure
σ_a	Stress amplitude
σ_m	Mean stress

TABLE OF CONTENTS

LIST OF FIGURES

LIST OF TABLES

1. INTRODUCTION

For a well, whether oil or gas, to maintain its integrity and produce effectively and economically, it is pertinent that a complete zonal isolation is achieved during the life of the well. This complete zonal isolation, however, can be compromised due to factors that come into play during the operative life of the completed well. Such factors may come in the form of thermal or pressure loads generally regarded as HPHT (high temperature-high pressure) loads which can manifest themselves as a static/cyclic load or both, depending on how they are exerted. Depending on the magnitude of loading (stress level), the number of cycles and even the mechanical properties of the well cement, cyclic loading could result in failure by extensive breakdown of the microstructure of the cement.

There have been a lot of experimental investigations on the mechanism of fatigue failure of structures like buildings and bridges but the fatigue behavior of well cement is still relatively unknown to engineers. Research has led to improved cement designs and cementing practices, yet many cement integrity problems persist and this further strengthens the need to understand the mechanism of cement fatigue. Even though most structural failures are a result of fatigue rather than static loading, insights on the role of both static and fatigue loading conditions on the failure of cement sheath would hopefully lead to improvements in well design.

1.1 Background

1.1.1 HPHT Well Integrity

A well can be said to have maintained its integrity if it effectively achieves zonal isolation over its life. However, maintaining integrity is not always the case in real life oilfield practice as case histories abound where the integrity of the well was compromised due to failure of the cement sheath, leading to loss of money and production.

In order to keep up with the world's energy demands, oil and gas producing companies have taken the initiative to explore offshore reserves or drill deeper into previously existing wells. The consequence of this, however, is that they have to deal with the high temperatures and pressures encountered at increasing depths. The industry acknowledges the threshold for high temperature and high pressure conditions as 300°F and 10,000 psi respectively [1]. For temperatures and pressures above these values, only a rigorous design would ensure the integrity of the well. High pressure / high temperature (HPHT) scenarios can be seen in the case of the Tuscaloosa trend in Louisiana drilled to a depth of 23,000 ft and with bottom hole temperature of 400°F and pressures between 17,000 to 20,000 psi, or even in case of the Shearwater field [2] in the East Central Graben area of the North Sea with a depth of 16,000 ft, temperature of 360°F and pressure of 15,200 psi, to mention but a few.

These actual HPHT industrial experiences highlight the inadequacy of conventional cementing procedures to provide adequate zonal isolation. High temperatures and pressures or even post-cementing stresses imposed on the cement

sheath as a result of casing pressure testing and formation integrity tests set in motion events which could compromise the long term integrity of the cement sheath due to fatigue. Knowledge of the mechanism of fatigue in cement and factors that affect it such as the magnitude of the load, strength and composition of the cement, mechanical properties of the cement and pattern of load cycles are important to achieve a realistic design of a cement system that will be subjected to fatigue loading. Such a design will go a long way to ensure the long term integrity of a well operating under HPHT conditions.

1.1.2 Fatigue in Cement/Concrete

The nature of fatigue in well cement is generally unknown and only a few studies exist on the fatigue of construction cement. The differences between oil well cement and cement used in the construction industry will be discussed in the next chapter. The fatigue strength of cement/concrete can be affected by factors such as the composition and mechanical properties of the cement, environmental and loading conditions, and water-cement ratio of concrete. A number of studies have been conducted on the fatigue of construction cement and it was found that due to the heterogeneous nature of cement, experimental results show a large scattering in the concrete behavior due to the cyclic loading and few data sets may not be sufficient to give an adequate description of cement behavior under fatigue loading.

Studies were conducted by Kim and Kim[3] on the fatigue behavior of high strength concrete using a type I Portland cement to which Elkem micro silica (powder)

was added. A constant minimum stress level of 25% of the static uniaxial compressive strength was maintained while the cyclic tests were conducted at maximum stress levels of 75, 80, 85 and 95% of the static strength. The first cycle of loading was loaded at a standard rate, and the other cycles were loaded at a frequency of 1 Hz. The test results (Fig.1.1) indicated that, under the same stress levels, fatigue life decreases as the concrete strength increases, and then the fatigue resistance of high strength concrete seems to be inferior to that of low strength concrete. Figure 1.2 shows the relationships between the number of loading cycles and the fatigue strains of low strength (LS) and high strength (HS) concrete. Although the fatigue strain of HS concrete is smaller than that of LS concrete, the slope of the strain increment curve of HS concrete is steeper than that of LS concrete, i.e., the rate of strain increment increases with the strength of concrete. Therefore high strength concrete is more brittle than low strength concrete under fatigue loading.

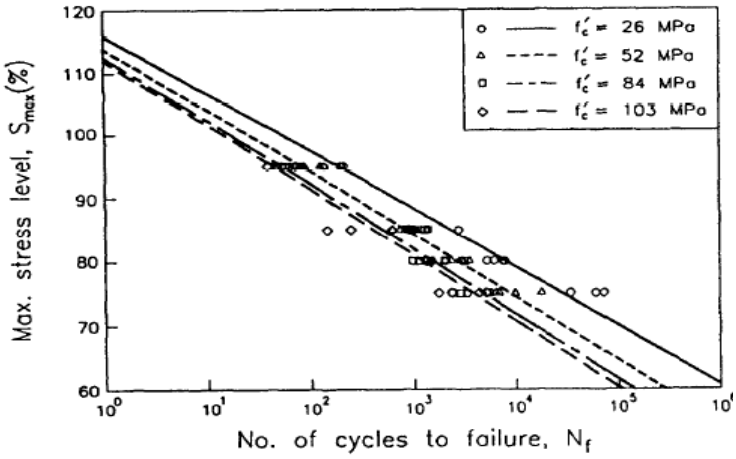

Fig 1.1: Comparison of Maximum Stress Levels to Number of Cycles for Different Cement Strengths [3]

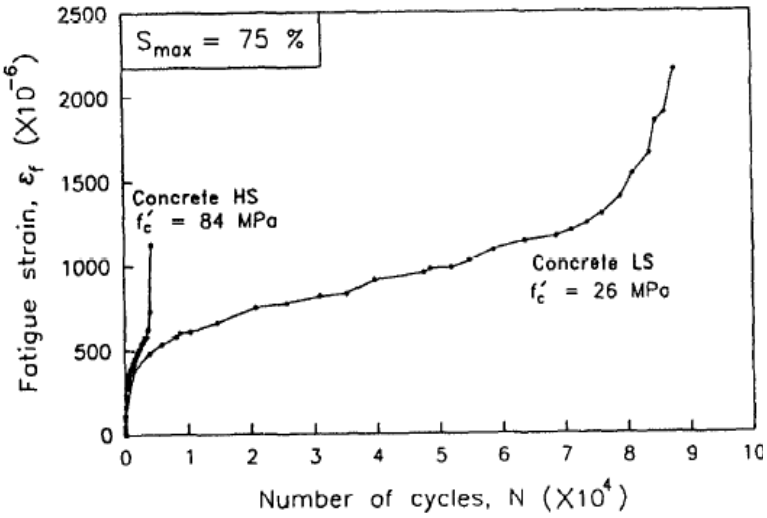

Fig 1.2: Comparison of Fatigue Strain for High and Low Strength Cements [3]

Antrim[4] conducted fatigue studies on hardened ordinary Portland (type I) cement paste using 2 specimens; one with a high water-cement ratio of 0.7 and another with a low water-cement ratio of 0.45. A high stress level of 80% (percentage of the ultimate static compressive strength of the cement) was used in conducting this investigation. It was observed that the degree to which shrinkage stresses were present in the specimens was proportional to the water content. This lead to the 0.7 mixture undergoing more shrinkage due to a more extensive capillary pore system. It was also observed that at equivalent percentages of the compressive strength, the 0.7 water-cement mixture was capable of withstanding more cycles to failure than the 0.4 water-cement mixture. From these results, the author suggested that shrinkage stresses play a greater role in fatigue strength because they serve to restrain crack propagation[4]. Crack propagation was slower in the open capillary structure cement (0.7 mixture) than in the dense structure cement

(0.4 mixture) because the high water-cement ratio paste is less brittle and can re-adjust its structure, thus delaying the build up of stress concentrations.

Breitenbucher et al. [5] noticed in their investigations that cyclic loading could lead to the reduction of stiffness of concrete and that fatigue strain plays a role in the degradation of the mechanical properties of concrete. The level of damage due to fatigue loading can be ascertained from the degradation of stiffness at a certain number of cycles. It was also observed that as the longitudinal strain increases at 60% stress level, the concrete properties (Young's modulus, fracture energy) decrease faster up to the first 2.0 millions of cycles thereafter, whereas the compressive strength almost remained constant. There was no observed failure due to fatigue for at least 25.5 million cycles. Similar observations were made at 70% and 75% stress levels. This shows that the effect of the number of load cycles appears to be negligible and therefore the damage is governed only by the evolution of fatigue strain. These results were also corroborated by the findings of Breitenbucher and Ibuk [6], who in addition noticed that small differences in the upper load can largely affect the formation of micro-cracks.

Hayeb et al.[7] obtained results similar to those of Breitenbucher et al.[5] The inclusion of steel fibers in ordinary cement paste helped to improve its damage resistance. From Fig. 1.3, it is observed that at stress levels of 80%, failure occurred at 2.7×10^4 cycles and at a reduced stress level of 72%, the specimens did not fail even after 2×10^6 cycles. A sharp decline in Young's modulus during the first 10^4 cycles was observed with no appreciable decay in the composite strength. These were also in line with the findings of Breitenbucher and Ibuk[6].

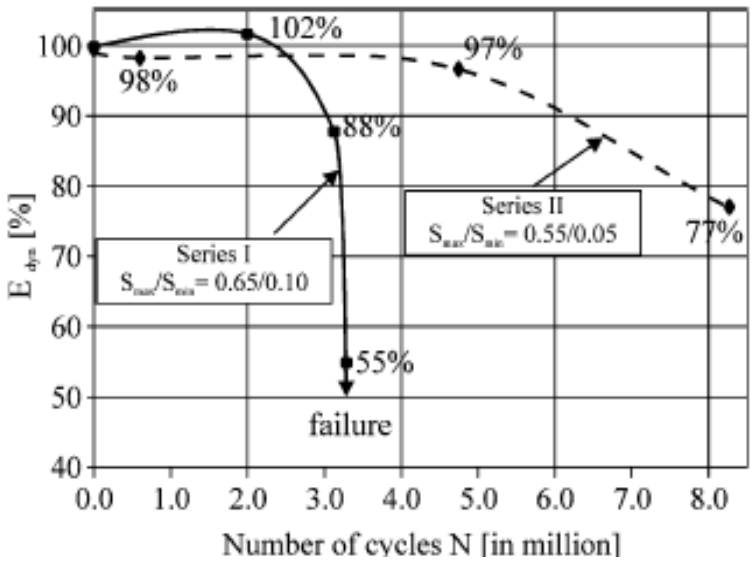

Fig 1.3: Damage Development Depending on Different Cyclic Load Levels [6]

From the existing literatures reviewed, it can be observed that the fatigue of cement can be affected by the following:

- compressive strength of cement [3]
- water-cement ratio of cement mixture [4]
- stress levels at which cyclic loading occurs [5,6]
- elasticity of the cement [6]
- use of solid particles, which may increase the fatigue resistance [6,7].

It should be noted that these studies were conducted using construction cement/concrete but they should be indicative of the fatigue of well cement as both contain the same base material.

2. OILFIELD CEMENTING

2.1 Well Cement

Well cements are specially formulated for the exploratory drilling of oil and gas wells. Well cementing serves various purposes [8], which includes:

- providing support and protection to the casing, and
- enabling zonal isolation by preventing the movement of fluids through the annular space outside the casing, stopping the movement of fluids into fractured formation or simply by plugging off an abandoned portion of the well. This is the primary goal of well cementing.

The choice of a particular cement for zonal isolation centers largely on downhole and formation conditions. But in general, oil well cements should have some features [9] which are necessary for a successful completion job and which would qualify them to be used for well cementing purposes. Such features include the following:

- the cement should be able to maintain its integrity in terms of durability and being free from strength retrogression during the operational life of the well at the prevailing downhole conditions;
- there should be an optimal setting time for the cement; too reactive a slurry will result in a short setting time and an insufficiently reactive slurry may take too long to set;
- the cement slurry should have low viscosity to make it pump-able;
- the cement should be high sulphate resistant;

- the cement should have a low permeability.

Well cement and construction cement have one thing in common - they are both Portland cements. Their difference lies in the fact that well cement, in addition to its Portland cement base, is mixed with additives in order to tailor it to a particular application and is also manufactured to a higher level of consistency. Portland cement is manufactured as a result of a chemical reaction between limestone and clay at temperatures of about 2,600°F to 3,000°F. There are four principal compounds in Portland cement, which are

- tricalcium silicate, C_3S,
- dicalcium silicate, C_2S,
- tricalcium aluminate, C_3A, and
- tetracalcium aluminoferrite, C_4AF.

Portland cement, when set, develops compressive strength due to hydration as a result of reaction between water and these constituting components of the cement. The rate of hydration depends on temperature, size of cement particle and the percentage of each component present, with C_3A hydrating most rapidly followed by C_3S, then by C_4AF and finally by C_2S. This hydration reaction results in reduction of volume which makes Portland cement shrink when set. Expansive cement, which is a modified Portland cement, is used to compensate for volume decrease due to shrinkage and to induce a tensile stress in the reinforcement.

Pure Portland cement looses its compressive strength and increases its permeability at temperatures above 230°F as a result of strength retrogression arising

from the breakdown of its crystalline structure at such temperatures. This would render the Portland cement unusable for high temperature applications. The strength retrogression could be explained as follows [10].

When Portland cement is mixed with water, tricalcium silicate (C_3S) and dicalcium silicate (C_2S) hydrate to form calcium silicate hydrate (C-S-H) gel and hydrated lime $(Ca(OH)_2)_2$. At temperatures higher than 230°F, C-S-H gel converts to α-dicalcium silicate hydrate (α-C_2SH). Conversion to the α-C_2SH phase results in the loss of compressive strength and an increase in permeability. Conversion of C-S-H gel to α-C_2SH at 230°F and higher can be prevented by adding crystalline silica.

The American Society for Testing and Materials (ASTM) Specification C-150 classifies eight types of Portland cement, with type I cement being the normal, general-purpose cement used for construction purposes [11]. More than 92% of Portland cement produced in the United States is type I and II (or Type I/II). Type III accounts for about 3.5% of cement production. Type IV cement is only available on special request, and type V may also be difficult to obtain (less than 0.5% of production).

The American Petroleum Institute on the other hand, has defined Specifications for materials and testing for well cements (API Specification 10A) , which includes requirements for eight classes of oil well cements (classes A through H) and three grades (Grades O - ordinary, MSR - moderate sulphate resistant, and HSR - high sulphate resistant). Each class is applicable for use at a certain range of well depths, temperatures, pressures, and sulphate environments. Cement classes A, B, C, G, and H are primarily used in the United States for well cementing. The petroleum industry also uses

conventional types of Portland cement with suitable cement-modifiers. Tables 2.1 and 2.2 show the ASTM and API cement classifications and their uses.

Table 2.1: ASTM Cement Classifications [11]

ASTM Cement Class	Use
I	General purpose cement, when there are no extenuating conditions. Similar to API class A.
II	Aids in providing moderate resistance to sulfate attack. Similar to API class B.
III	When a high early strength is required. Similar to API class C.
IV	When a low heat of hydration is desired (in massive structures).
V	When high sulfate resistance is required.
IA[4]	A type I cement containing an integral air-entraining agent
IIA[4]	A type II cement containing an integral air-entraining agent
IIIA[4]	A type III cement containing an integral air-entraining agent

Table 2.2: API Cement Classifications [9]

API class	Operating Temperatures (°F)	Suitability
A	80 - 170	Good for 0 - 6,000 ft depth. Used when special properties are not required.
B	80 - 170	Good for 0 - 6,000 ft depth. Used for moderate to high sulphate resistance.
C	80 - 170	Good for 0 - 6,000 ft depth. Used for moderate to high sulphate resistance and when high early strength is required.
D	170 - 230	Good for 6,000 - 10,000 ft depth. Used for moderate to high sulphate resistance and moderately high temperatures and pressures.
E	170 - 290	Good for 10,000 - 14,000 ft depth. Used for moderate to high sulphate resistance and high temperatures and pressures.
F	230 - 320	Good for 10,000 - 16,000 ft depth. Used for moderate to high sulphate resistance and extremely high temperatures and pressures.
G	80 - 200	Good for 0 - 8,000 ft depth. Used for moderate to high sulphate resistance. Has improved slurry acceleration and retardation.
H	80 - 200	Same as class G.

2.1.1 New Cements vs. Conventional Well Cements

Special situations call for innovative actions; the need to drill deeper and produce oil and gas under HPHT environments has motivated drilling engineers to come up with what is regarded as “designer” or “supercement” systems which are actually conventional

cements that are modified so as to improve long term sealing integrity in HPHT wells. In some cases, these designer cements are non-Portland based. The non-Portland based cements may include Pozzolanic cements, Epoxy Resin[12], geo-polymers, graphite and fibers (glass, steel) which polymerize at suitable temperatures and/or time to produce a flexible and mechanically improved cement system. Pozzolanic cements are not actually cements but react at ordinary temperature with calcium hydroxide in the presence of moisture to form compounds with cementitious properties.

The modified conventional cement systems include:

- expansive cements (e.g. super cement bond log),
- non-shrinking cement systems,
- foamed cement,
- thixotropic cement, and
- POZMIX cement (Pozzolan and Portland cement mix).

Each of these "designer" cements is chosen based on the prevailing well conditions as the cement for the design of one well may not be appropriate for the design of another. Investigations[12] have been conducted on the effectiveness of these new cement systems in securing long term integrity for HPHT wells. These have been conducted using new cement systems which include a Portland based expansive cement system and a non-Portland based (Epoxy Resin) cement system. According to experimental results, the expansive cement exhibited good qualities, which makes it a good candidate for a HPHT scenario. When set, it generates an internal compressive strength which enables it to counter tensile stresses as opposed to conventional cement

systems. The tensile stress generated by the pressure within the wellbore annulus serves first to reduce the compressive pre-stress present in the cement before the material realizes a net tensile stress. As a result, the effective compressive strength of the cement is increased by the compressive preload applied. This is illustrated in Fig. 2.1:

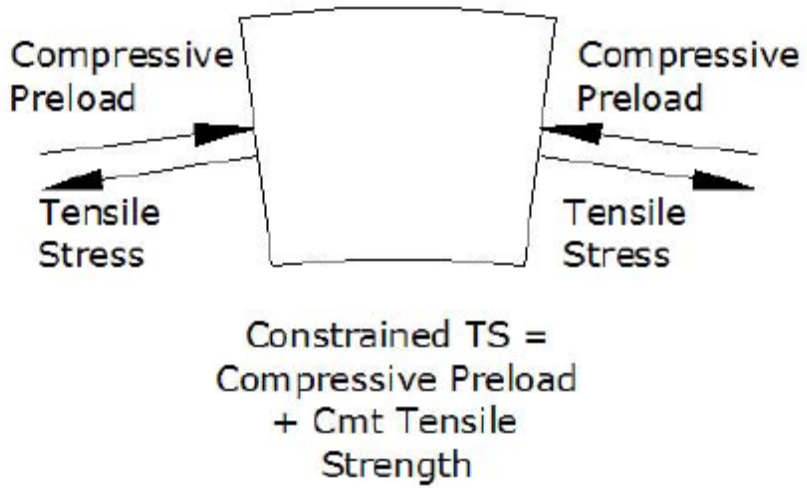

Fig 2.1: Stresses That Act on a Pre-Stressed Cement System [12]

Some of the positive results with this kind of cement include;

- *Improved Annular Seal under HPHT Conditions*

  Test results, when compared to a conventional Portland cement system (Portland cement, retarded, with 35% silica), showed the expansive cement system providing a very good seal in a hard formation. Based on the number of cycles applied at each pressure level (up to 10,000 psi with increments of 1,000 psi and temperature of

200°F), the expansive cement absorbed 5 times more energy before failure than the conventional cement system.

- *Improved Mechanical Shear Bonding*

From the mechanical shear bond testing, the conventional cement had about 140 psi bond strength as opposed to 1,840 psi for the expansive cement, an increase of approximately 13 times.

- *Improved Hydraulic Bonding*

The resistance of various materials to allowing water to flow through or past a plug was measured at ambient temperatures. The conventional system had a hydraulic bond of 3,800 psi as opposed to 6,000 psi for the expansive cement system.

It should, however, be noted that expansive cement functions by expanding against confinement and the higher the level of confinement, the better its performance since expansive cements are generally strong in compression and weak in tension. As a consequence, it would not be so good an idea to use expansive cement in soft/weak formations as it tends to de-bond from the casing–cement interface.

The same investigators also conducted investigations on non-Portland based epoxy resin cement systems but with more inconclusive than positive results as compared to the expansive cement system. They observed that for epoxy resin the pumping time is relatively insensitive to pressure and weighting materials, which makes its design simpler than conventional cement systems. Different hardeners and diluents can be added to push the temperature higher. The HPHT annular seal testing failed

laboratory investigations but was successful in field trials, and this led the investigators to conclude that more tests and observation are necessary to understand the mechanism of sealing using epoxy resin. The mechanical shear bond, however, was both high and constant, and seems to be due to the material folding up and mechanically resisting the imposed motion of the tubulars.

Foamed cement has also been employed to solve difficult HPHT well integrity problems. This can be seen in the case of Shearwater field 1 [13, 2]. The presence of higher than anticipated B annulus pressures in wells drilled at the Shearwater field in the East Central Graben area of the North Sea resulted in serious concerns about the long term integrity of the wells. The field is regarded as a HPHT well with initial reservoir temperature and pressure of 360°F and 15,200 psi, respectively at 17,900 MD. The unusually high B annulus pressures were more likely a result of:

- the formation of micro annuli between the cement /formation interface, and
- contamination of the cement by flowing hydrocarbons from tight crystalline limestone within the surrounding formation.

The Shearwater field team proposed the use of a foamed cement system citing the following advantages:

- *Improved Mud Displacement, Expansive Properties and Fluid Loss*

  Compared to conventional cement systems, foamed cement possesses superior mud removal properties, has less overall fluid loss and compensates for shrinkage common with conventional cement systems.

- *Improved Ductility*

Compared to conventional systems, foamed cements are more flexible and possess the ability to withstand both high temperature and high pressure cycling-induced stresses.

- *High Tensile Strength*

The high tensile strength of foamed cement would make it more resistant to tensile cracking.

- *Economy and Safety*

Under a HPHT scenario, foamed cement provides a cost effective life cycle design even though the initial cost may be higher than that of conventional cement, and it also reduces health safety and environmental risks.

The use of a foamed cement system proved very effective in dealing with the Shearwater field problems. However, it was pointed out that a comprehensive analysis is required to assess the risk of damage to the cement sheath due to downhole well events. It was also suggested that cement systems should be pre-tested in a laboratory to ensure that they meet the requirements determined by the analysis.

2.2 Cement Additives

Depending on downhole conditions, certain qualities may be required of the cement used in completing the well. Additives when added to the Portland cement base could be used to achieve the desired qualities. They could also be used to extend the properties of the

base cement. For instance, with additives, Portland cement may be modified to sustain very high temperatures up to 700°F and large pressures up to 30,000 psi.

Some of the most commonly used additives in oil field cementing include:

- *Accelerators*

These are cement additives that generally tend to reduce the thickening time of cement slurry and increase the rate of development of compressive strength. Since the hydration process, which results in the setting of cement, occurs at a faster rate at higher temperatures, the setting of cement might be a problem while cementing wells drilled in areas of low temperatures and also result in long waiting times. To counter such, accelerators like $CaCl_2$, NaCl, sodium silicate, sea water, etc are used to speed up the thickening time.

- *Retarders*

Retarders are the opposite of accelerators as the name suggests. They act to increase the thickening time of cement slurry. They are mostly lignosulfonates, which are polymers derived from wood pulp. Examples include calcium, sodium and chemically modified lignosulfonates.

- *Weighting Agents*

These are added to cement to increase the density of the final cement mix. They are very important when designing wells with high temperature and high pressure conditions in order to give the base cement more strength to sustain high pressures

and also to prevent strength retrogression at high temperatures. Examples include ilmenite ($FeTiO_3$), hematite (Fe_2O_3) and barite ($BaSO_4$).

- *Fluid Loss Control Agents*

This set of additives prevents phase separation under downhole temperature and pressure conditions. Such a separation would result in fluid being lost to the formation. They are usually synthetic polymers.

- *Extenders*

This set of additives helps to lower the density of the cement mix. Examples include bentonite, pozzolans, microspheres, sodium silicates, etc.

Other additives include dispersants and lost circulation control agents.

2.3 Well Cementing Design Process

The drilling and completion of a well is a capital project that runs into millions of dollars. Hence it is necessary to have a comprehensive design of the cement used for completion of a particular well and also to avoid remedial cement work which would add extra cost to the project. Cement design is usually streamlined to a particular well according to prevailing downhole conditions, which is ensured by testing in the lab to determine if the design would be satisfactory.

Ravi and Xenakis [14] discussed a three-step approach to cement design. Step one involves a detailed engineering analysis. It requires identifying the nature of the formation - is it a hard or a loose formation? It requires identifying all forces that would come into play as the well is being produced - are there high temperatures, high

pressures or both? Is it normally or abnormally pressured? Step one also includes static and fatigue loading analysis to determine if the cement sheath would sustain the series of cyclic loads it would encounter during its lifetime. The answers to step one questions lead to step two. which involves designing the cement slurry based on factors identified in step one. Here properties of the cement like tensile strength, Young's modulus, Poisson's ratio, plasticity parameters, shrinkage/expansion during hydration, and post-cement slurry hydration are chosen so as to effectively match the effects of downhole conditions. Thereafter, laboratory investigations are conducted on the designed slurry.

The data from the laboratory tests and the analysis of step one are then analyzed together to evaluate performance. Step three involves adhering to best drilling and cementing practices, such as centering the casing and effectively cleaning out the hole of all mud so as not to undermine the performance of the designed slurry. It also involves monitoring during the life of the well. Fig.2.2 below summarizes the design process.

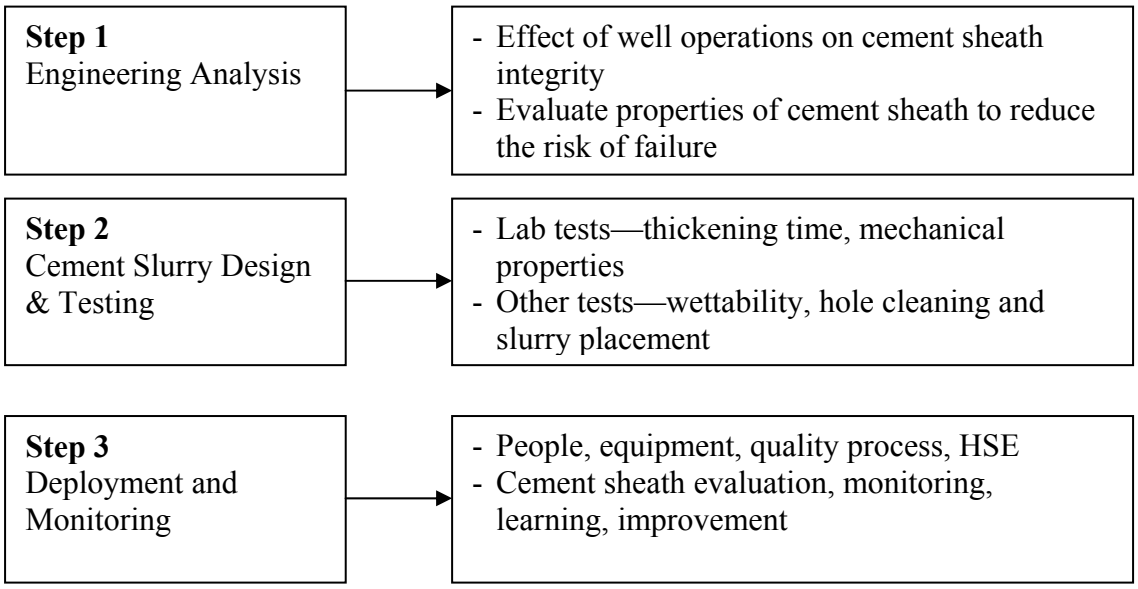

Fig 2.2: Three-step Process for Cement Design [14]

2.4 Cement Integrity Issues Due to Temperature and Pressure

Knowledge of the stress and deformation fields in the vicinity of a HPHT well is very critical in evaluating its structural capability. A combination of large temperature ranges and high pressure variations exerts excessive load between the protection casing strings and ultimately on the cement sheath. Studies have been conducted on the effects of high temperature or high pressure or both on well integrity. Some studies describing such efforts are presented below.

2.4.1 Effect of High Temperature

- ***Case Study 1***

Very high temperatures change the crystalline structure of cement. Stiles [15] conducted studies to investigate the effect of ultra-high temperatures on the mechanical properties of cement. Five different cement formulations were exposed to a high temperature of 645°F and the variations of the Young's modulus, tensile strength and Poisson's ratio of these cement systems at this temperature (and pressure of 2,133 psi) were observed over a 2-year period. The cement systems used are described below:

System 1 – Conventional (Class G) cement system with 40% BWOC silica flour, 4.3% BWOC gypsum, fluid loss control additive and $CaCl_2$ accelerator. It was mixed at 15.4 lb/gal.

System 2 – A low density thixotropic cement system with 92% Class A cement with 40% BWOC silica flour, 8% gypsum, fluid loss control additive and $CaCl_2$ accelerator and mixed at 14.5 lb/gal.

System 3 – A foamed cement system of density 11.65 lb/gal with Class G cement (with 40% BWOC silica flour) as base slurry, a surfactant additive with 26% gas production by volume. It was mixed at 15.8 lb/gal.

System 4 – High strength low density cement of density 11.65 lb/gal, containing hollow ceramic microspheres designed with maximized solid volume fraction technique with silica content in excess of 40% BWOC and with added fluid loss control additive and $CaCl_2$ accelerator.

System 5 – A flexible and expanding low density cement system of density 12.5 lb/gal containing flexible solid particles and an MgO base expanding agent designed with maximized solid volume fraction technique similar to system 4. The flexible particles were added at 50% BVOB.

From the analysis of the experimental data, it was observed that the conventional and foamed cement systems exhibited brittleness after curing at 645°F while other systems possessed mechanical parameters (low Young's modulus and high tensile strength) that are as good as or better than the flexible blends. From this study it can also be deduced that the ratio of tensile strength to Young's modulus gives an indication of resistance to failure under tension. The thixotropic cement and the flexible cement had the highest tensile strength to Young's modulus ratio.

2.4.2 Combined Effect of Temperature and Pressure

The combined presence of high temperatures downhole with high pressure loads leads to excessive pressure loading in annuli of the casing strings. The pressure load may be a result of an increase in pressure around the wellbore region due to pressure integrity tests, increase of mud weight, casing perforation, stimulation, gas production, etc and these effects can result in considerable damage to the mechanical properties of the cement sheath. Godwin and Crook[16] observed that failure in the cement sheath due to excessive pressure would normally occur in the bottom one-half to three-quarters of the casing string, while failure due to excessive temperature would normally occur in the upper one-fourth to two-thirds of the casing string.

- ***Case Study 2***

Godwin and Crook[16] investigated the effects of high temperatures and excessive annulus pressure using laboratory experiments and field trials. They circulated hot oil at a temperature of 350°F through the annulus of the test specimen while gradually increasing the pressure up to 10,000 psi with 2,000 psi increments using the following cement systems:

System 1 – Cement/siliceous material mixture system with 30% BWOW latex, 1.25% fluid loss control additive and 0.5% gelling agent. It was mixed at 12.1 lbm/gal with 10.81 gal mix water/sack. The yield was 2.49 ft^3/sack. Compressive strength, Young's modulus and Poisson's ratio was 1,000 psi, 0.69 x 10^6 psi and 0.42, respectively.

System 2 – Cement/Pozzolan mixture system with 30% BWOW latex, 2 gal/sack fluid loss control additive, 10 lbm silica additive and 0.25% gelling agent. It was mixed at 13.1 lbm/gal with 6.48 gal mix water/sack. The yield was 1.76 ft^3/sack. Compressive strength, Young's modulus and Poisson's ratio was 2,500 psi, 0.8 x 10^6 psi and 0.32, respectively.

System 3 – is the same as system 2 but without the latex and it was mixed at 13.1 lbm/gal. Compressive strength, Young's modulus and Poisson's ratio was 2,000 psi, 0.9 x 10^6 psi and 0.3, respectively.

System 4 – Class H cement system with 35% BWOC silica flour mixed at 18 lbm/gal. Compressive strength, Young's modulus and Poisson's ratio was 9,600 psi, 2.4 x 10^6 psi and 0.11, respectively.

The results indicated a collapse in the crystalline structure of system 1 at pressures of 8,000 psi and no appreciable change in the permeability of systems 2 through 4 with increasing casing pressures. All the cement systems withstood pressures of 2,000 psi and fractures were observed at pressures of 4,000 psi with catastrophic effects after 6,000 psi stress cycles. A microanulus occurred in cement 2 with internal pressures up to 6,000 psi. System 1 exhibited elastic properties and provided full casing support until its failure at 6,000 psi. Field trials were also conducted with systems 2, 3 and 4. After being subjected to a 12,150 psi internal casing pressure (casing pressure plus casing fluid hydrostatic pressure), system 4 failed while system 3 remained intact. No evaluation logs were run for system 2.

2.4.3 Casing–Cement–Formation Interactions

As the awareness of the need to analyze the structural behavior of the cement is currently increasing, so does the need for guidelines and quantitative results. This has led to the use of simple models or the more complex finite element models to analyze the casing–cement–formation system and the selection of the cement based on the results of this analysis. Fleckenstein et al.[17] propose finite element analysis as the best way to analyze the casing–cement–formation properties during the design phase. This proposal has been corroborated by others [18, 19, 20, 21].

Finite element methods offer a means of effectively modeling pressure and temperature effects. Utilizing computer programs, analysis of the stress situation downhole can be achieved in multiple dimensions by partially discretizing the system and solving the problem using FEA. With FEA, stress variations at different points along the cement sheath radius can be effectively modeled. Several studies [18, 19, 20, 21] show how finite element analysis was effectively used to model HPHT wells in order to understand and overcome cement sheath failure problems. Ravi et al [22] caution that cement which may be suitable under one set of conditions may not be suitable under a different set of conditions. Thus, a rigorous design procedure using finite element analysis should be used to select the cement system that will satisfy each specification.

- ***Case Study 3 - Casing–Cement Interactions***

Fleckenstein et al.[17] used finite element analysis to investigate the role that mechanical properties of the cement plays in withstanding the internal casing pressure. They modeled a cemented wellbore with two cement systems - a soft and hard cement. The soft (ductile) cement had a high Poisson's ratio and low modulus of elasticity and the hard (brittle) cement had a low Poisson's ratio and relatively high modulus of elasticity.

The hard cement was Class H cement mixed with 35% silica flour at 18 ppg, with the following mechanical properties: 9,500 psi compressive strength, 2,400,000 psi Young's modulus and 0.11 Poisson's Ratio. The soft cement system was a cement/siliceous material mixed with 30% latex at 12.1 ppg with 1,000 psi compressive strength, 690,000 psi Young's modulus and 0.42 Poisson's Ratio. These cement systems

were also studied by Godwin and Crook[16]. The results indicated that there is little difference in the constraining effect of the different cement slurries. However, a confining stress outside the cement sheath would increase the burst resistance of the casing.

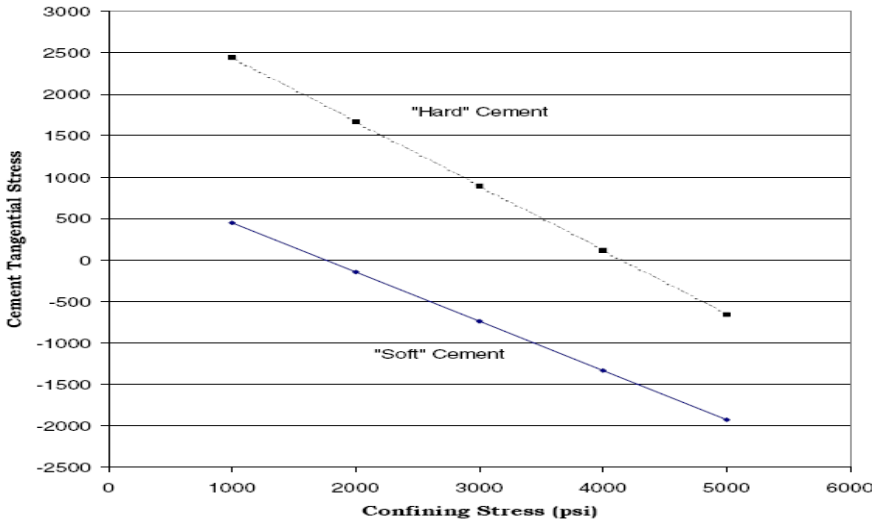

Fig 2.3: Tangential Stress for Hard and Soft Cement Systems [17]

- ***Case Study 4 - Casing–Cement–Formation Interactions***

The confining stress on the cement sheath may come from the formation and its effect on the cement sheath was also modeled. It was run with a 10,000 psi internal burst pressure acting upon the inner surface of the 5-½" casing and a 3,000 psi confining stress from the formation.

The results show reductions in von Mises stress from 6,099 psi to 4,292 psi and in tangential stress from 894 psi (tension) at the casing outer diameter to -283 psi

(compression) at the borehole wall. The investigators noticed a difference in the von Mises stress that is generated by the hard and soft cement systems. At 1,000 psi, hard cement generate twice the von Mises stress when compared with the soft cement but this reduces as the confining stress increases with a reduction of less than 20% at 5,000 psi confining stress.

From these investigations the authors deduced that radial cracking is less likely to occur with soft cement systems because hard cement systems are likely to generate significant tangential stresses (Fig. 2.3), which increases the likelihood of forming radial cracks in the presence of high internal burst pressures.

It should also be noted [23] that with the use of flexible and expanding cement systems the stiffness of the formation plays an important role. If the stiffness of the formation is low (low Young's modulus) compared to the cement system, de-bonding and formation of microannulus at the cement casing interface may occur.

3. CEMENT FAILURE DUE TO STATIC LOADING

3.1 Analytical Model of Wellbore Stresses

3.1.1 Background

As a result of production operations, a cemented casing is usually subjected to a variety of stresses in the form of cyclic pressure and temperature variations. Figure 3.1 shows the nature and profile of tangential and radial stresses under different loading conditions. Considering an infinitesimal element within the cement sheath, these stresses act in a three-dimensional fashion and the cement sheath can therefore be regarded as being under a triaxial stress state, as shown in Figure 3.2. The third component (not shown in the diagram) is the axial stress component which is perpendicular to the two stresses shown in Figure 3.2. The radial stress is always compressive in nature while the tangential stress could be tensile or compressive depending on the loading conditions.

The casing–cement–formation set up can be analyzed as a pressurized composite cylinder with three concentric cylinders. Perfect bonding is assumed to exist between the cement and casing and between the cement and formation. The pressure and/or temperature changes induce stress concentrations near the casing–cement and the cement–formation boundaries.

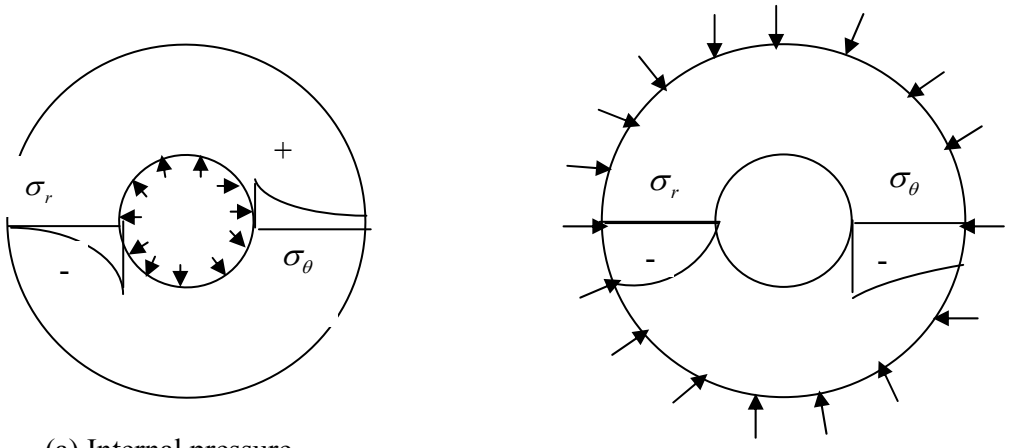

(a) Internal pressure

(b) External pressure

Fig 3.1: Radial and Hoop Stress Profile Due to Loading Conditions [26]

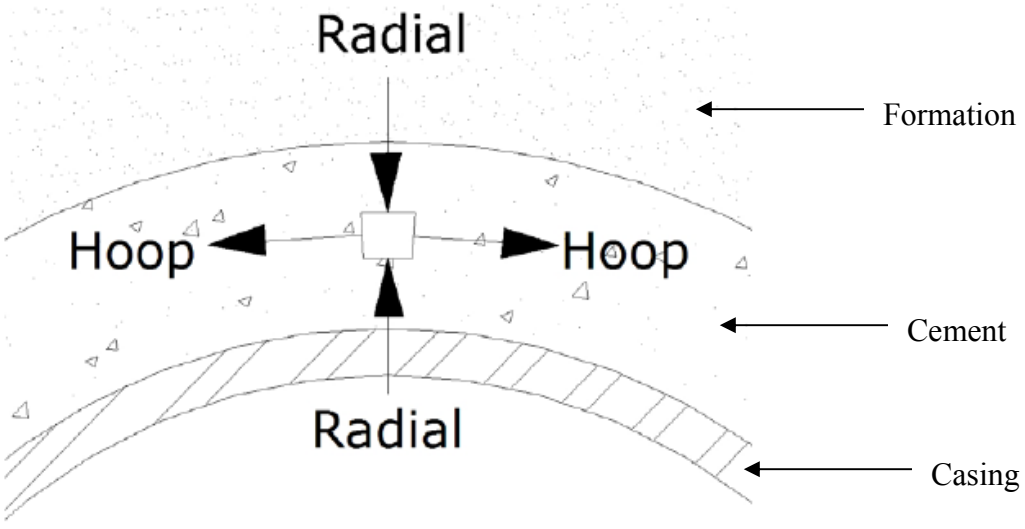

Fig 3.2: Stresses Acting on a Cement Sheath [12]

3.1.2 Assumptions

The following assumptions were made to facilitate the analytical modeling of the wellbore:

- Axisymmetric deformations exist for the composite cylinder.
- The composite cylinder undergoes plane strain deformation. This implies that the composite cylinder is under a triaxial stress state.
- Casing–cement and cement–formation interfaces are perfectly bonded with no discontinuities. This implies that the radial displacements and radial stresses are continuous across the boundary.
- No initial stress exists in the cement.
- The casing is regarded as a thin-walled pressure vessel.
- The cement sheath and formation is treated as a thick-walled pressure vessel.

3.1.3 Failure Criteria

The failure criteria employed in predicting the failure of cement sheath in this model includes

- maximum normal stress criterion,
- Mohr-Coulomb's criterion, and
- experimental investigation.

The maximum normal stress criterion predicts that an isotropic material will fail when the largest principal stress reaches a limiting value. This implies that failure would occur when

$$\frac{\sigma_1}{\sigma_f} \geq 1 \tag{3.1}$$

where σ_1 is the maximum principal stress and σ_f is the limiting stress. If σ_1 is tensile, then σ_f is the limiting tensile stress and the other two smaller principal stresses σ_2 and σ_3 play no role (with $\sigma_1 > \sigma_2 > \sigma_3$). If applied to a compressive stress state, this criterion becomes

$$\frac{|\sigma_3|}{\sigma_f} \geq 1 \tag{3.2}$$

where $|\sigma_3|$ is the magnitude of the minimum principal stress. It is should be noted that this criterion would be inaccurate if all three principal stresses are compressive.

With Mohr-Coulomb's criterion, σ_2 does not play any role and failure is predicted to occur when

$$\frac{\sigma_1}{\sigma_{tensile}} - \frac{\sigma_3}{\sigma_{compressive}} \geq 1 \tag{3.3}$$

where $\sigma_{tensile}$ and $\sigma_{compressive}$ are the tensile and compressive strengths, respectively.

The classical theories of failure discussed above become insufficient even as an approximation when the tangential, radial and axial stresses are all compressive. In such cases, different failure theories based on experiments would be required to determine the onset of failure. Avram et al.[24] discussed concrete fracture under triaxial stresses and

proposed a new failure criterion given by Eq. (3.4) below which complies with Mohr-Coulomb's criterion.

$$\frac{\sigma_1}{f_c} = 1 + 3.7\left(\frac{\sigma_3}{f_c}\right)^{0.86} \tag{3.4}$$

where f_c is the compressive strength of the cement, σ_1 is the major principal compressive stress at failure and σ_3 is the minor principal compressive stress with $|\sigma_1| > |\sigma_2| > |\sigma_3|$. Fig 3.3 and Fig 3.4 show the experimental results and failure envelope, respectively, for concrete under a triaxial compressive state.

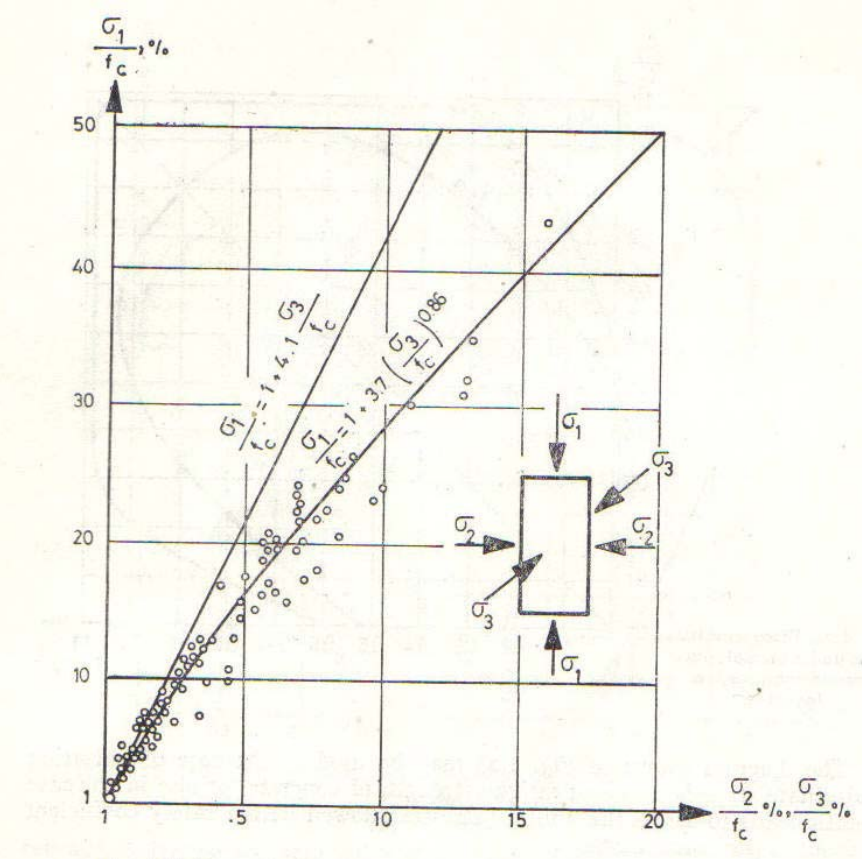

Fig 3.3: Concrete Failure Criterion under Triaxial Compressive Stresses [24]

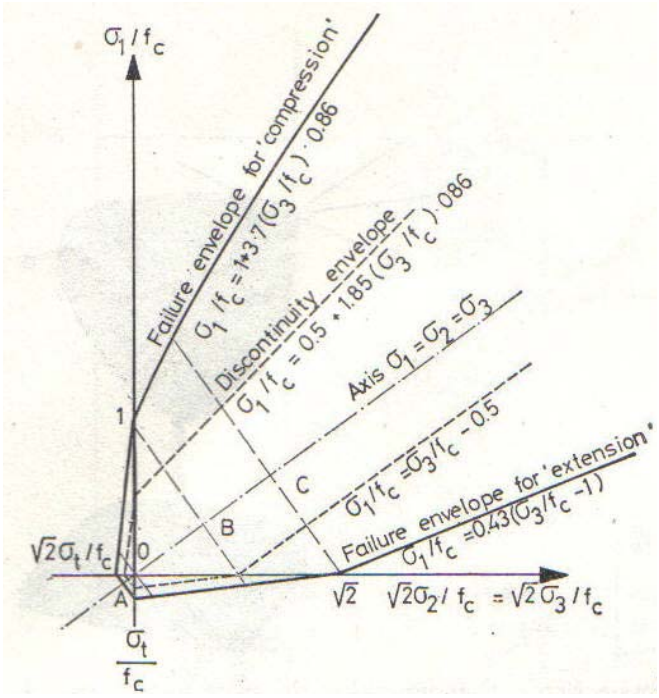

Fig 3.4: Failure Envelope for Triaxial Compression and Tensile Stress State [24]

It should be noted that this experimental failure criterion was proposed for plain concrete and may only give an approximation of failure for well cement.

3.1.4 Analytical Model

In the composite cylinder model under consideration, the internal pressure p_i acting on the inner surface of the casing in conjunction with temperature increase will expand the casing radially, while the cement sheath will resist the expansion. As a result, a contact pressure (p_{c1}) will develop at the interface between the casing and the cement.

Considering the casing–cement interface as shown in Fig. 3.5, p_{c1} is the contact pressure formed at the cement–casing interface and p_i is the internal pressure.

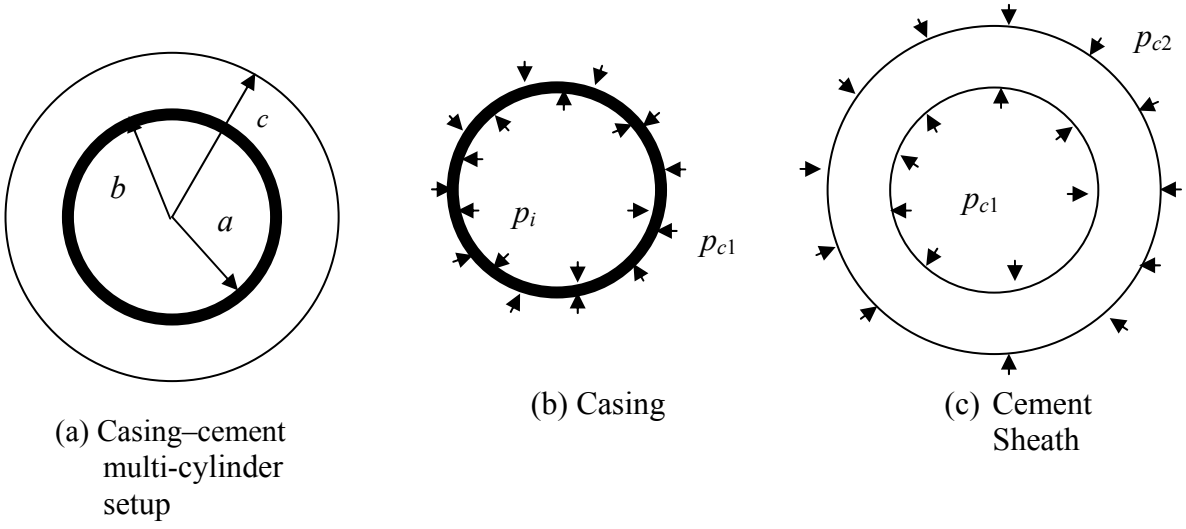

(a) Casing–cement multi-cylinder setup

(b) Casing

(c) Cement Sheath

Fig 3.5: Contact Pressure on Casing–Cement Interface

The hoop strain is given by

$$\varepsilon_\theta = \frac{1}{E}\left[\sigma_\theta - \nu\left(\sigma_z + \sigma_r\right)\right] + \alpha\,\Delta T \tag{3.5}$$

where α is the coefficient of thermal expansion and ΔT is the temperature change. The axial strain is

$$\varepsilon_z = \frac{1}{E}\left[\sigma_z - \nu\left(\sigma_\theta + \sigma_r\right)\right] + \alpha\,\Delta T \tag{3.6}$$

Since the axial strain is negligible considering the large depth, then $\varepsilon_z \approx 0$ (i.e. plane strain assumption). It follows from Eq. (3.6) that

$$\sigma_z = \nu\left[\sigma_r + \sigma_\theta\right] - \alpha\,E\,\Delta T \tag{3.7}$$

Substituting Eq. (3.7) into Eq. (3.5) yields

$$\varepsilon_\theta = \frac{1}{E}\left[\sigma_\theta\left(1-\nu^2\right) - \left(\nu+\nu^2\right)\sigma_r + \left(1+\nu\right)\alpha\,E\,\Delta T\right] \tag{3.8}$$

The radial expansion is thus obtained as

$$\delta_r = \frac{r}{E}\left[\sigma_\theta\left(1-\nu^2\right) - \left(\nu+\nu^2\right)\sigma_r + \left(1+\nu\right)\alpha E \Delta T\right] \tag{3.9}$$

Let the radii *a*, *b* and *c* in Fig 3.5(a) be represented by r_a, r_b and r_c, respectively. Considering the casing as a thin-walled vessel we have at $r = b$

$$\sigma_r = -p \quad \text{and} \quad \sigma_\theta = \frac{p\, r_m}{t_s} \tag{3.10}$$

where $p = p_i - p_{c1}$, r_m is the mean radius of the casing and t_s is the thickness of the casing. Substituting Eq. (3.10) into Eq. (3.9) leads to

$$\delta_{r\text{-casing}} = \left\{ \frac{a\left(p_i - p_{c1}\right)}{E_s}\left[\frac{r_m}{t_s}\left(1-\nu_s^2\right) + \left(\nu_s + \nu_s^2\right)\right]\right\} + \left[\left(1+\nu_s\right) a\, \alpha_s\, \Delta T\right] \tag{3.11}$$

Considering the cement sheath as a thick-walled cylinder and assuming $\partial\left(\Delta T\right)/\partial r = 0$, the tangential and radial stress are given by

$$\sigma_r = \frac{p_{c1} b^2}{c^2 - b^2}\left(1 - \frac{c^2}{r^2}\right) - \frac{p_{c2} c^2}{c^2 - b^2}\left(1 - \frac{b^2}{r^2}\right) \tag{3.12}$$

$$\sigma_\theta = \frac{p_{c1} b^2}{c^2 - b^2}\left(1 + \frac{c^2}{r^2}\right) - \frac{p_{c2} c^2}{c^2 - b^2}\left(1 + \frac{b^2}{r^2}\right) \tag{3.13}$$

At $r = b$, Eq. (3.12) and Eq. (3.13) reduce to

$$\sigma_r = -p_{c1} \tag{3.14}$$

$$\sigma_\theta = p_{c1}\left(\frac{c^2 + b^2}{c^2 - b^2}\right) - p_{c2}\left(\frac{2c^2}{c^2 - b^2}\right) \tag{3.15}$$

When Eq. (3.14) and Eq. (3.15) are substituted into Eq. (3.9), this gives the radial expansion in the cement sheath at $r = b$ as

$$\delta_{r-cement} = \frac{b}{E_c}\left\{\left(1-\nu_c{}^2\right)\left[p_{c1}\left(\frac{b^2+c^2}{c^2-b^2}\right) - p_{c2}\left(\frac{2c^2}{c^2-b^2}\right)\right] + p_{c1}\left(\nu_c + \nu_c^2\right)\right\} + \left[\left(1+\nu_c\right) b\,\alpha_c\,\Delta T\right] \tag{3.16}$$

Since both radial expansions are equal, it follows from Eq. (3.11) & Eq. (3.16) that

$$p_{c1}\left\{\frac{b}{E_c}\left[\left(1-\nu_c^2\right)\left(\frac{b^2+c^2}{c^2-b^2}\right)+\left(\nu_c+\nu_c^2\right)\right] + \frac{a}{E_s}\left[\frac{r_m}{t_s}\left(1-\nu_s^2\right)+\left(\nu_s+\nu_s^2\right)\right]\right\}$$

$$- p_{c2}\left[\frac{b}{E_c}\left(\frac{2c^2}{c^2-b^2}\right)\left(1-\nu_c^2\right)\right] = \frac{a\,p_i}{E_s}\left[\frac{r_m}{t_s}\left(1-\nu_s^2\right)+\left(\nu_s+\nu_s^2\right)\right] + \left[\left(1+\nu_s\right) a\,\alpha_s\,\Delta T\right] - \left[\left(1+\nu_c\right) b\,\alpha_c\,\Delta T\right] \tag{3.17}$$

Eq. (3.17) can be put in the form

$$A\,p_{c1} + B\,p_{c2} = C \tag{3.18}$$

where

$$A = \left\{\frac{b}{E_c}\left[\left(1-\nu_c^2\right)\left[\frac{b^2+c^2}{c^2-b^2}\right]+\left(\nu_c+\nu_c^2\right)\right] + \frac{a}{E_s}\left[\frac{r_m}{t_s}\left(1-\nu_s^2\right)+\left(\nu_s+\nu_s^2\right)\right]\right\} \tag{3.19}$$

$$B = -\left[\frac{b}{E_c}\left(\frac{2c^2}{c^2-b^2}\right)\left(1-\nu_c^2\right)\right] \tag{3.20}$$

$$C = \frac{p_i\,a}{E_s}\left[\frac{r_m}{t_s}\left(1-\nu_s^2\right)+\left(\nu_s+\nu_s^2\right)\right] + \left[\left(1+\nu_s\right) a\,\alpha_s\,\Delta T\right] - \left[\left(1+\nu_c\right) b\,\alpha_c\,\Delta T\right] \tag{3.21}$$

Similarly, considering the cement–formation interface as shown in Fig.3.6, p_{c2} is the contact pressure formed at the cement–formation boundary as a result of the confining pressure from the formation pressure, p_f.

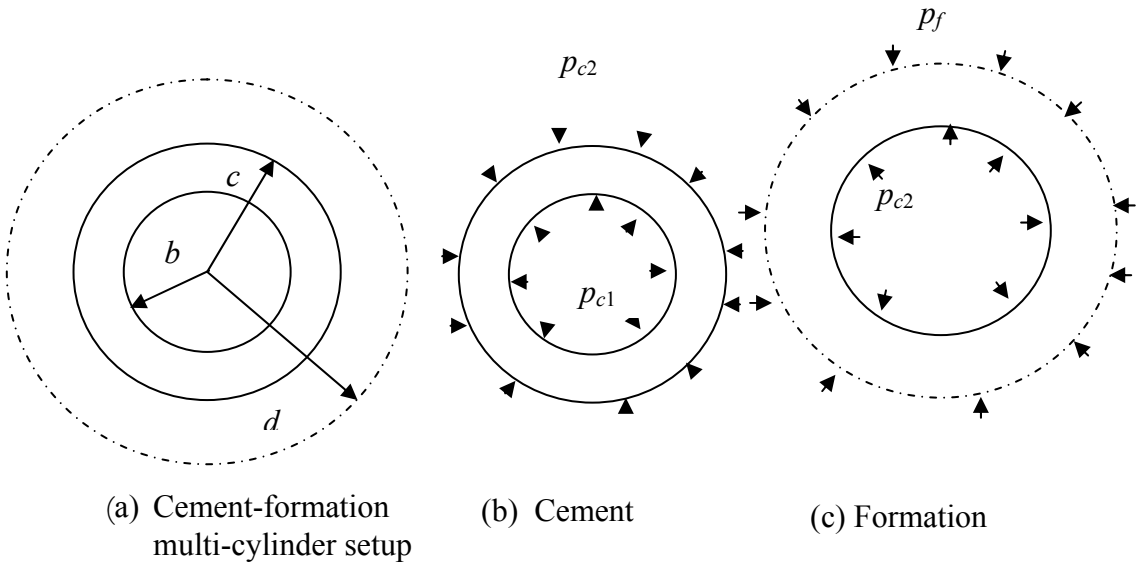

Fig 3.6: Operative Stresses on Cement–Formation Interface

Considering the cement sheath and assuming $\partial(\Delta T)/\partial r = 0$, at $r = c$,

$$\sigma_r = -p_{c2} \tag{3.22}$$

$$\sigma_\theta = p_{c1}\left(\frac{2b^2}{c^2 - b^2}\right) - p_{c2}\left(\frac{c^2 + b^2}{c^2 - b^2}\right) \tag{3.23}$$

This gives the radial expansion in the cement sheath at $r = c$ when Eq. (3.22) and Eq. (3.23) are substituted into Eq. (3.9) as

$$\delta_{r-cement} = \frac{c}{E_c}\left\{\left(1-\nu_c^2\right)\left[p_{c1}\left(\frac{2b^2}{c^2-b^2}\right)-p_{c2}\left(\frac{c^2+b^2}{c^2-b^2}\right)\right]+p_{c2}\left(\nu_c+\nu_c^2\right)\right\} + \left[\left(1+\nu_c\right)c\,\alpha_c\,\Delta T\right] \tag{3.24}$$

Considering the formation as a thick-walled pressure vessel with a finite radius *d* into the formation and also assuming $\partial(\Delta T)/\partial r = 0$, at $r = c$

$$\sigma_r = -p_{c2} \tag{3.25}$$

$$\sigma_\theta = p_{c2}\left(\frac{c^2+d^2}{d^2-c^2}\right) - p_f\left(\frac{2d^2}{d^2-c^2}\right) \tag{3.26}$$

when Eq. (3.24) and Eq. (3.25) are substituted into Eq. (3.9) , it follows that

$$\delta_{r-formation} = \frac{c}{E_f}\left\{\left(1-\nu_f^2\right)\left[p_{c2}\left(\frac{c^2+d^2}{d^2-c^2}\right)-p_f\left(\frac{2d^2}{d^2-c^2}\right)\right]+p_{c2}\left(\nu_f+\nu_f^2\right)\right\} + \left[\left(1+\nu_f\right)c\,\alpha_f\,\Delta T\right] \tag{3.27}$$

Since both radial expansions are equal, it follows from Eq. (3.24) and Eq. (3.27) that

$$p_{c2}\left\{\frac{c}{E_f}\left[\left(1-\nu_f^2\right)\left(\frac{d^2+c^2}{d^2-c^2}\right)+\left(\nu_f+\nu_f^2\right)\right]+\frac{c}{E_c}\left(1-\nu_c^2\right)\left(\frac{b^2+c^2}{c^2-b^2}\right)-\left(\nu_c+\nu_c^2\right)\right\}$$
$$-p_{c1}\left[\frac{c}{E_c}\left(\frac{2b^2}{c^2-b^2}\right)\left(1-\nu_c^{\,2}\right)\right] = p_f\left[\frac{c}{E_f}\left(\frac{2d^2}{d^2-c^2}\right)\left(1-\nu_f^2\right)\right]$$
$$-\left[\left(1+\nu_f\right)c\,\alpha_f\,\Delta T\right]+\left[\left(1+\nu_c\right)c\,\alpha_c\,\Delta T\right] \tag{3.28}$$

Eq. (3.28) can be put in the form

$$D\,p_{c1} + K\,p_{c2} = F \tag{3.29}$$

where

$$D = -\left[\frac{c}{E_c}\left(\frac{2b^2}{c^2 - b^2}\right)\left(1 - v_c^2\right)\right] \tag{3.30}$$

$$K = \left\{\frac{c}{E_f}\left\{\left(1 - v_f^2\right)\left[\frac{d^2 + c^2}{d^2 - c^2}\right] + \left(v_f + v_f^2\right)\right\} + \frac{c}{E_c}\left[1 - v_c^2\right]\left(\frac{b^2 + c^2}{c^2 - b^2}\right) - \left(v_c + v_c^2\right)\right\} \tag{3.31}$$

$$F = \left[\frac{p_f\, c}{E_f}\left(\frac{2d^2}{d^2 - c^2}\right)\left(1 - v_f^2\right)\right] - \left[\left(1 + \nu_f\right) c\, \alpha_f\, \Delta T\right] + \left[\left(1 + \nu_c\right) c\, \alpha_c\, \Delta T\right] \tag{3.32}$$

From a simultaneous solution of Eq.(3.18) and Eq. (3.29), the contact pressures p_{c1} and p_{c2} are given as

$$p_{c1} = \frac{FB - KC}{DB - AK} \tag{3.33}$$

$$p_{c2} = \frac{C - \left[\frac{FB - KC}{DB - AK}\right] A}{B} \tag{3.34}$$

From the analysis presented above, the circumferential, radial and axial stresses present in the cement sheath as shown in Fig. 3.7 can then be determined.

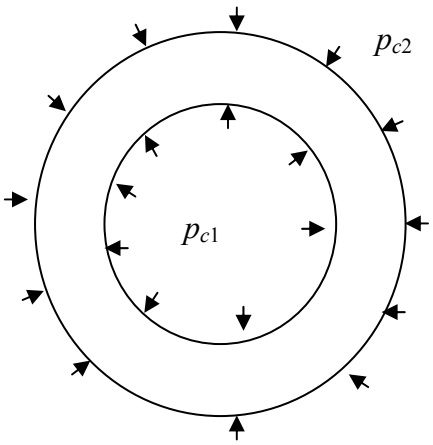

Fig 3.7: Contact Stresses on Cement Sheath

The radial, tangential and axial stresses in the cement sheath are then calculated using the following formulas

$$\sigma_{r-cement} = p_{c1}\frac{b^2}{c^2 - b^2}\left[1 - \frac{c^2}{r^2}\right] - p_{c2}\frac{c^2}{c^2 - b^2}\left[1 - \frac{b^2}{r^2}\right] \tag{3.35}$$

$$\sigma_{\theta-cement} = p_{c1}\frac{b^2}{c^2 - b^2}\left[1 + \frac{c^2}{r^2}\right] - p_{c2}\frac{c^2}{c^2 - b^2}\left[1 + \frac{b^2}{r^2}\right] \tag{3.36}$$

$$\sigma_{z-cement} = \nu_c\left[\sigma_r + \sigma_\theta\right] - \alpha E \Delta T \tag{3.37}$$

The maximum shear stress, $\tau_{\max}$, is given by the expression

$$\tau_{\max} = \frac{\left(p_{c1} - p_{c2}\right)b^2 c^2}{\left(c^2 - b^2\right)r^2} \tag{3.38}$$

At $r = b$

$$\tau_{\max} = \frac{\left(p_{c1} - p_{c2}\right)c^2}{\left(c^2 - b^2\right)} \tag{3.39}$$

At $r = c$

$$\tau_{\max} = \frac{\left(p_{c1} - p_{c2}\right)b^2}{\left(c^2 - b^2\right)} \tag{3.40}$$

The effective stress σ_e in the cement sheath is given by

$$\sigma_e = \sqrt{\frac{1}{2}\left[\left(\sigma_z - \sigma_\theta\right)^2 + \left(\sigma_r - \sigma_z\right)^2 + \left(\sigma_\theta - \sigma_r\right)^2\right]} \tag{3.41}$$

3.2 Analytical and Finite Element Studies

The analytical model developed above, which gives an insight into the magnitude of the stress imposed on the cement sheath, is a very powerful and flexible tool which can enable cement designers to optimize their design and also be able to design effectively for HTHP conditions. This is possible because it puts into consideration all the parameters that come into play downhole as the well is produced. A Microsoft Excel spreadsheet was created using the developed equations above and it was further used in the analytical and finite element studies presented in below.

The contact pressure at the cement–casing interface p_{c1} and the contact pressure at the cement–formation interface p_{c2} were calculated from equations (3.33) and (3.34) and equations (3.35) to (3.37) gave the radial, tangential and axial stresses in the cement, respectively.

The model was also extended to calculate the radial, tangential and axial stresses in the casing and formation with the following equations:

$$\sigma_{r\text{-}casing} = p_i \frac{a^2}{b^2 - a^2}\left[1 - \frac{b^2}{r^2}\right] - p_{c1} \frac{b^2}{b^2 - a^2}\left[1 - \frac{a^2}{r^2}\right] \tag{3.42}$$

$$\sigma_{\theta\text{-}casing} = p_i \frac{a^2}{b^2 - a^2}\left[1 + \frac{b^2}{r^2}\right] - p_{c1} \frac{b^2}{b^2 - a^2}\left[1 + \frac{a^2}{r^2}\right] \tag{3.43}$$

$$\sigma_{z\text{-}casing} = \nu_s\left[\sigma_r + \sigma_\theta\right] - \alpha E \Delta T \tag{3.44}$$

And for the formation we have

$$\sigma_{r-formation} = p_{c2} \frac{c^2}{d^2 - c^2}\left[1 - \frac{d^2}{r^2}\right] - p_f \frac{d^2}{d^2 - c^2}\left[1 - \frac{c^2}{r^2}\right] \tag{3.45}$$

$$\sigma_{\theta-formation} = p_{c2}\frac{c^2}{d^2-c^2}\left[1+\frac{d^2}{r^2}\right] - p_f\frac{d^2}{d^2-c^2}\left[1+\frac{c^2}{r^2}\right] \quad (3.46)$$

$$\sigma_{z\text{-}formation} = \nu_f\left[\sigma_r + \sigma_\theta\right] - \alpha E \Delta T \quad (3.47)$$

Using this model, the response of the cement sheath to different static and fatigue loading conditions was studied for three cement systems:

Cement System 1 – Ductile cement system with compressive strength of 3,000 psi, tensile strength of 1,000 psi, a Young's modulus of 0.69 x 10^6 psi and a Poisson's ratio of 0.4;

Cement System 2 – Brittle cement system with compressive strength of 9,500 psi, tensile strength of 3,000 psi, a Young's modulus of 2.4 x 10^6 psi and a Poisson's ratio of 0.1;

Cement System 3 – A low Young's modulus and a low Poisson's ratio cement system with compressive strength of 2,500 psi, tensile strength of 1,000 psi, a Young's modulus of 1 x 10^6 psi and a Poisson's ratio of 0.25.

These cement systems will be studied for the following cases:

Scenario 1 – well pressure: 15,000 psi, formation pressure: 1,000 psi;

Scenario 2 – well pressure: 15,000 psi, formation pressure: 0 psi;

Scenario 3 – well pressure: 4,000 psi, formation pressure: 10,000 psi.

Other parameters used as inputs to the model include:

Temperature change, ΔT: 150°F

Casing Young's modulus, E_s, and Poisson's ratio, v_s : 2.9 x 10^7 psi and 0.3

Shear bond strength of cement: 1,000 psi

Casing outer diameter, b: 9.625 in

Casing wall thickness, t_s: 0.545 in

Casing inner diameter, a: 8.535 in

Cement wall thickness: 2.125 in

Formation outer diameter, d: 20 in

Formation Young's modulus, E_f, and Poisson ratio, v_f: 3 x 10^6 psi and 0.42

Density of cement mix: 14 lb/gal

Cement expansion coefficient, α_c: 0.000006 in/ °F

The finite element analysis was done with ANSYS workbench 11.0 and since the casing–cement–formation is axisymetric a single quadrant was used for the 2D modeling.

To validate the analytical model, the analytical results and finite element simulations were compared. For the finite element analysis, an internal pressure of 15,000 psi was applied inside the casing with no formation pressure. The meshing was done with 6,648 elements and 20,607 node density. Plane strain state was assumed. The boundary conditions applied include

- displacement U = 0, $\tau_{xy} = 0$ on X = 0;
- displacement V = 0, $\tau_{yx} = 0$ on Y= 0 ;
- $\sigma_r = p_i$ on $r = a$;
- $\sigma_r = p_f$ on $r = d$.

The casing–cement–formation model was also assumed fully bonded with no separation at the boundaries.

Figure 3.8 shows the distribution of equivalent von Mises stress under the loading condition described above and Figure 3.9 below compares the analytical values for von Mises equivalent stress with those from the finite element analysis. The analytical and finite element values were close with an error of about 1%.

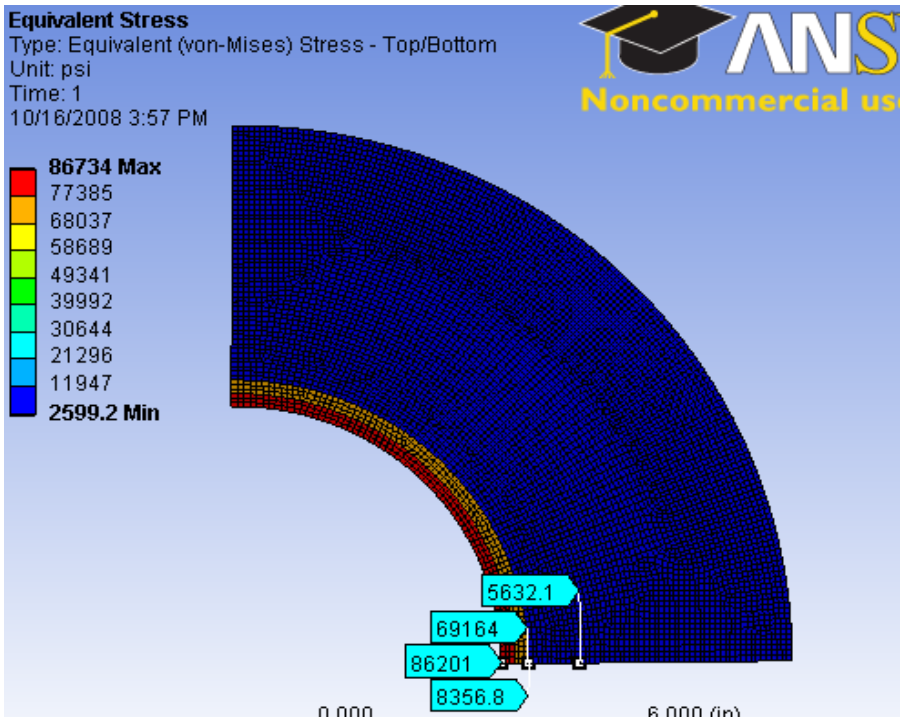

Fig 3.8: Equivalent Stress for Casing–Cement–Formation Model with Meshing

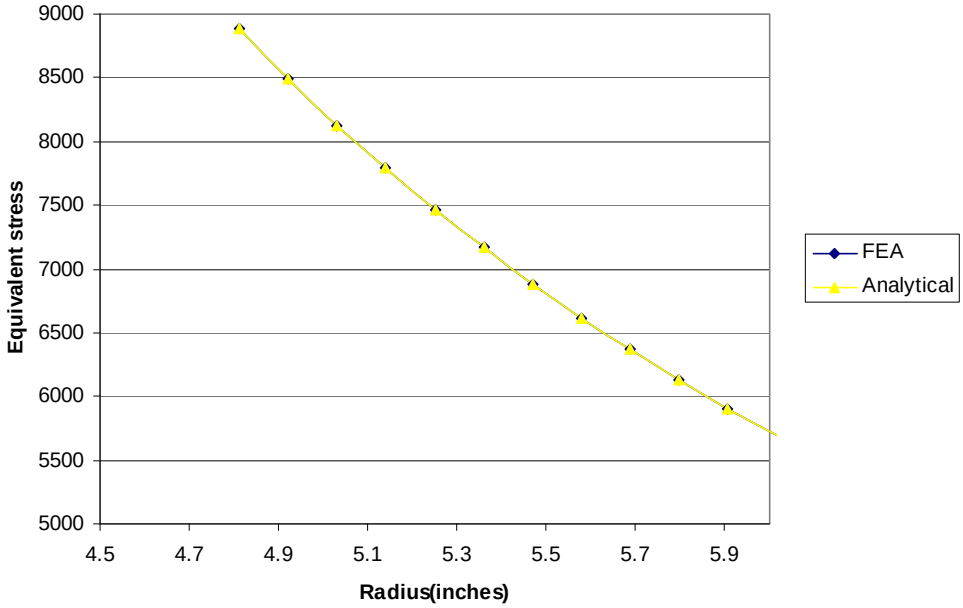

Fig 3.9: Equivalent Stress Comparison For Analytical and FEA Models

3.3 Fatigue Studies

To study the fatigue of the cement sheath, finite element analysis was utilized. The fatigue properties of concrete were used for this analysis. Such properties include S-N curves, strain-life curves and stress-strain curve. Tables 3.1 and 3.2 give the fatigue material data used in the finite element modeling for cement systems 1 and 2 based on data extracted from Fig.1.3. The fatigue life for the cement systems will be predicted from these curves using ANSYS. The S-N curve is shown in Fig.3.10.

Table 3.1: Stress-Life Data for Cement System 1 (Strength: 26 MPa/ 3,771 psi)

No of Cycles	Stress (psi)
0.99692	4332.322
4.65426	4031.543
57.8064	3590.166
683.674	3203.529
8084.64	2852.871
100398	2535.519
1.00E+06	2276.105

Table 3.2: Stress-Life Data for Cement System 2 (Strength: 84 MPa /12,183 psi)

No of Cycles	Stress (psi)
1.01527	13376.842
1.87358	13009.757
19.6824	11594.051
165.699	10353.456
1740.34	9208.586
16164.6	8206.784
1.46E+05	7314.037

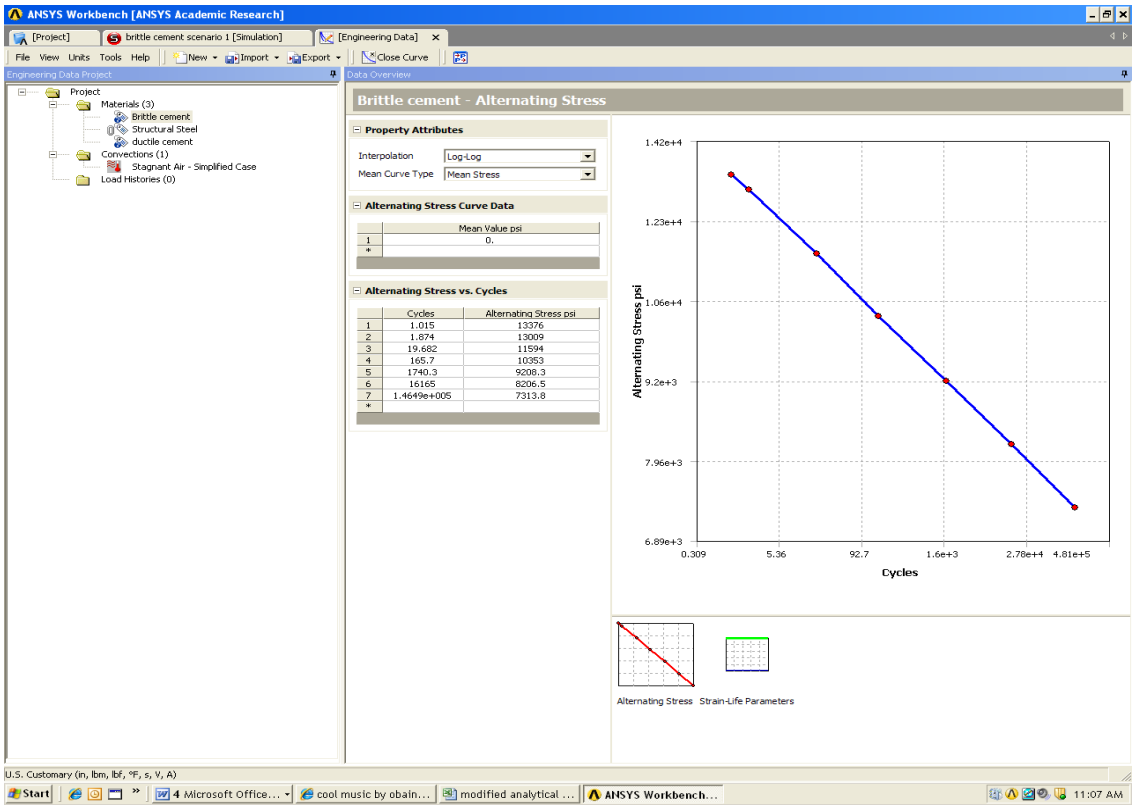

Fig 3.10: S-N Curve for Fatigue Analysis in ANSYS

Newman and Choo [25] gave a relationship between the number of cycles to failure and the load ratio derived through experimental studies for concrete with densities greater than 12.5 lb/gal as

$$\frac{f_{c.\max}}{f_c} = 1 - 0.0685(1 - R)\log_{10} N \qquad (3.48)$$

where $f_{c.\max}$ is the maximum compressive stress of the cyclic loading,

f_c is the compressive strength of the concrete,

R is the stress ratio $f_{c.\max}/f_{c.\min}$, and

N is the number of cycles to failure.

The fatigue properties of the cement sheath were also studied under two loading conditions:

- cyclic loading at the casing coupling, and
- cyclic loading within the casing annulus.

These loading conditions, shown in Fig. 3.11 below, represent a cyclic loading condition due to shear at the coupling and that due to the internal and formation pressure on areas where there are no couplings.

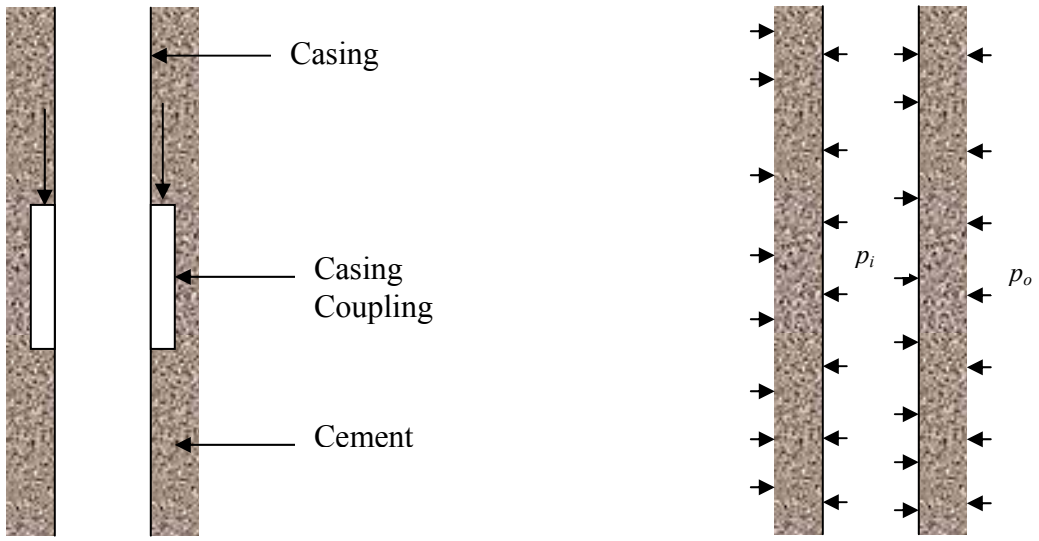

a) Cement sheath under shear at coupling

b) Cement sheath under p_i and p_o

Fig 3.11: Cyclic Loading Conditions for the Cement Sheath

For both cases a constant amplitude loading condition is assumed. A fully reversed loading is also assumed while modeling the fatigue behavior of the cement under shear cyclic loading while a zero based (compression) loading is assumed for the internal and external pressures. The Goodman diagram for fatigue analysis was chosen as it gives a good description of the fatigue behavior of brittle materials. Figure 3.12 shows the Goodman diagram. Figures 3.13 and 3.14 present the different loading conditions and options available with ANSYS.

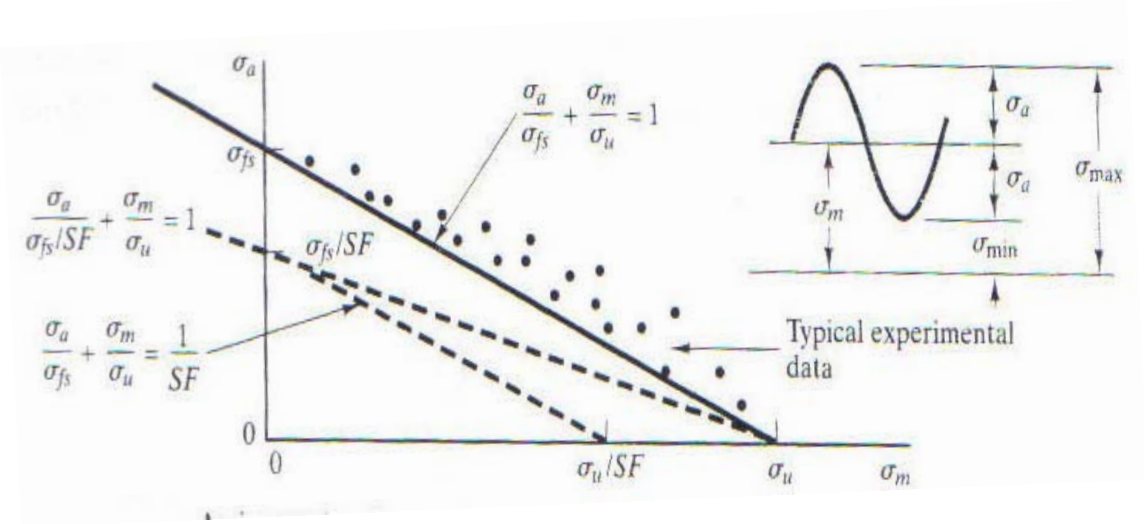

Fig 3.12: Goodman Diagram for Brittle and Ductile Materials [26]

According to the Goodman diagram, for brittle materials;

$$\frac{\sigma_a}{\sigma_{fs}} + \frac{\sigma_m}{\sigma_u} = \frac{1}{SF} \tag{3.49}$$

where *SF* is the safety factor and

$$\sigma_m = \frac{(\sigma_{\max} + \sigma_{\min})}{2} \tag{3.50}$$

$$\sigma_a = \frac{(\sigma_{\max} - \sigma_{\min})}{2} \tag{3.51}$$

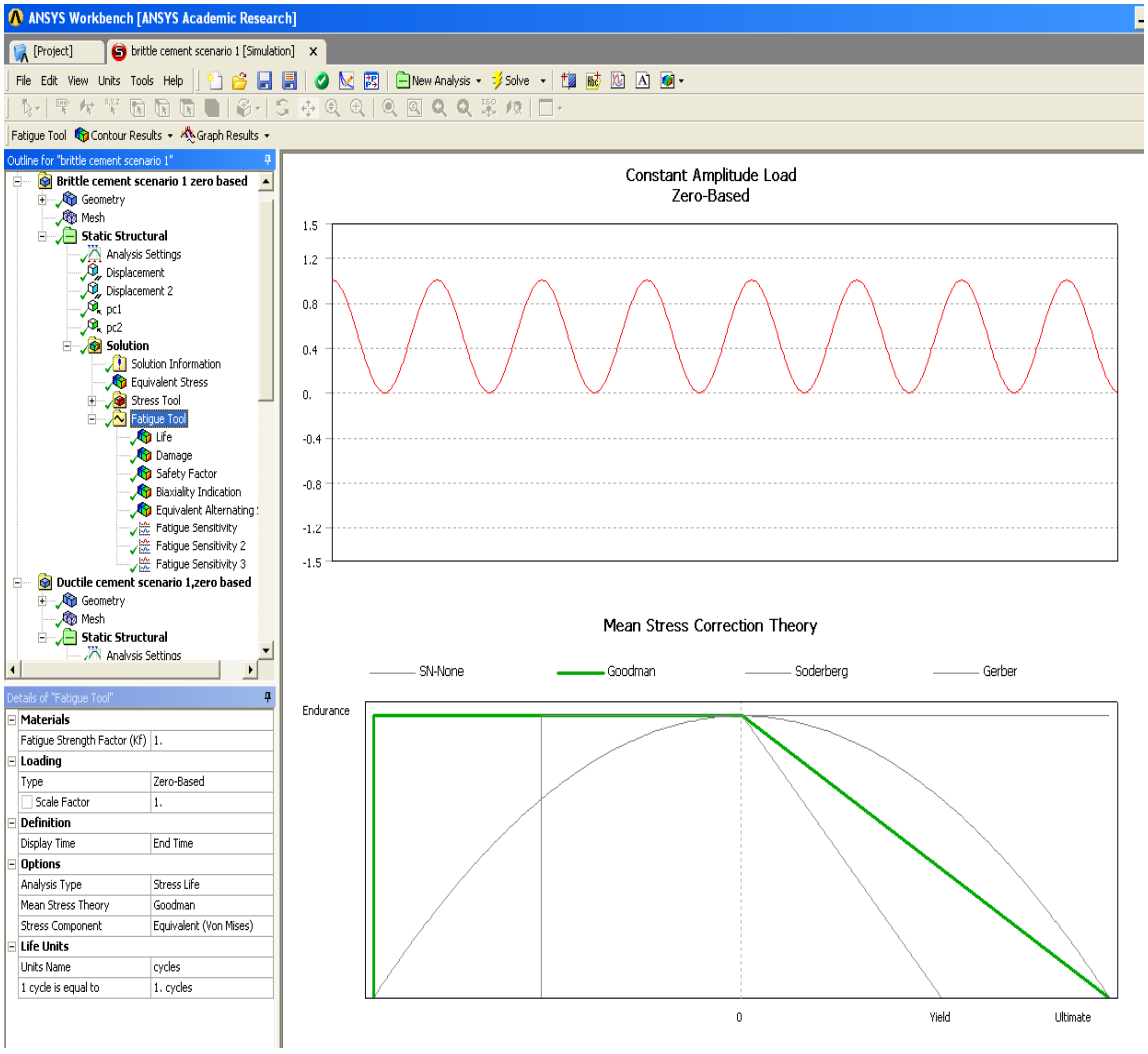

Fig 3.13: Zero Based Loading, Goodman's Diagram and Fatigue Options

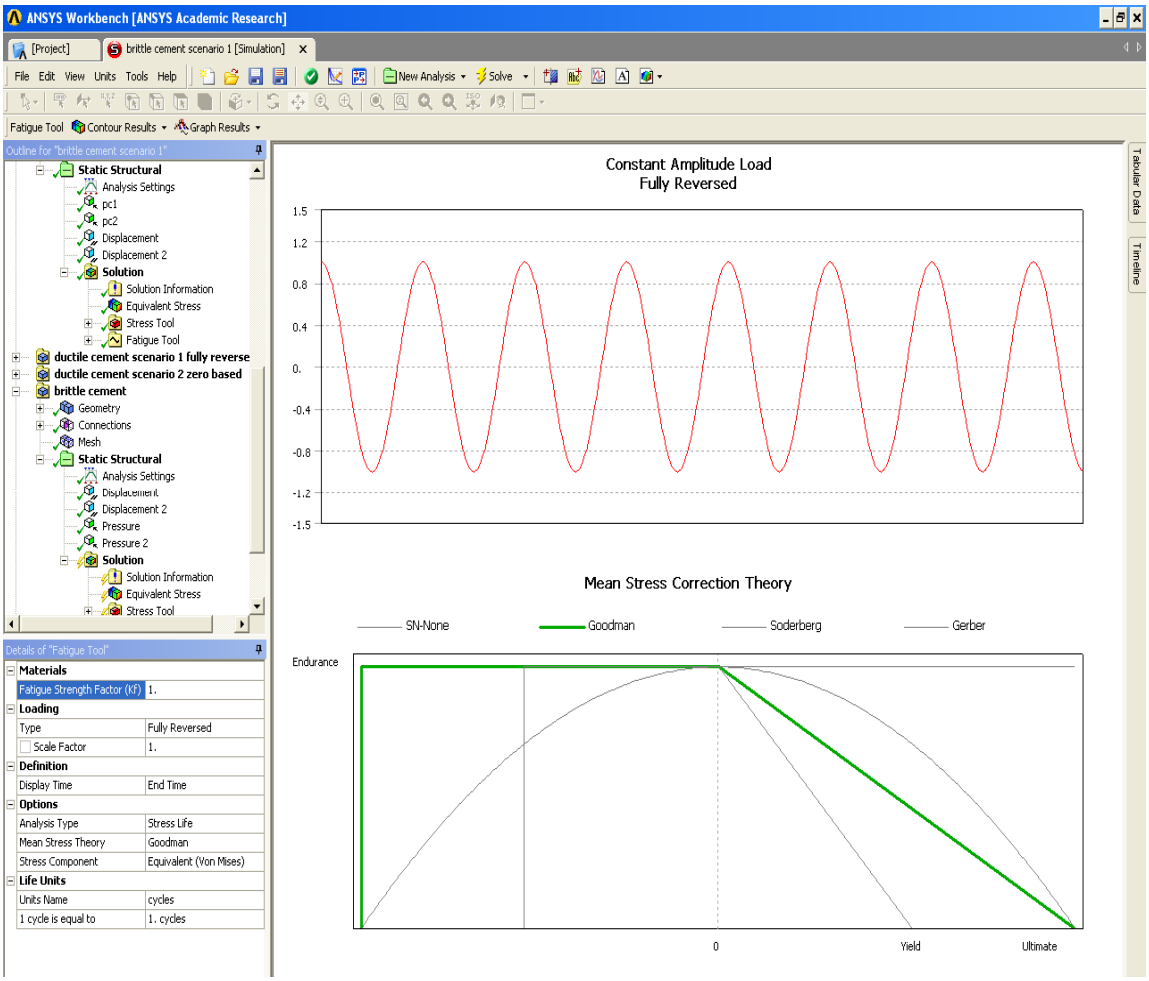

Fig 3.14: Fully Reversed Loading, Goodman's Diagram and Fatigue Options

Some of the result outputs for fatigue evaluation include:

- *Fatigue life* - The fatigue life plot gives an indication of number of cycles to failure *N* of a particular material;
- *Damage* - The fatigue damage plot gives the fatigue damage at a given design life;

- *Factor of safety* – This gives the factor of safety *SF* with respect to fatigue failure at a given design life;
- *Fatigue sensitivity* – This plot gives an indication of how loading conditions affect the fatigue performance of the material.

The Excel spreadsheet shows how fatigue equations can be linked to the analytical model to predict the fatigue life of the cement sheath under cyclic loading. Equations (3.41) to (3.44) were linked to the results from the analytical model but the idea was abandoned when the values from the proposed fatigue model did not match the finite element results. It should be noted that equations (3.48) to (3.51) were developed for structural concrete (from literature reviewed) which necessitates such equations to be developed for well cement.

4. RESULTS AND DISCUSSION

4.1 Static Studies

- *Case Scenarios without the Effect of Temperature Change*

To understand the effect of static loading on the integrity of cement sheath, the analytical model and finite element analysis were used to examine the responses of different cement systems subjected to different magnitudes of internal pressure and formation pressure as described in the previous chapter. The temperature change was neglected and the analytical model was used to show the trends in the von Mises equivalent, tangential and axial stresses in the cement sheath for the three cement systems.

1. High Inner Pressure and Low Formation Pressure

With an inner pressure of 15,000 psi and a formation pressure of 1,000 psi, the finite element model gives us an idea of the amount of stress generated within the steel casing and the actual amount transferred to the cement sheath through the casing–cement interface. The same can also be said of the transfer of stresses from the formation to the cement sheath through the cement–formation interface. Figures 4.1 and 4.2 show the trend for von Mises stress using cement system 2, for separate cases that have the same mechanical properties for the steel casing but different formation properties. From the diagrams, it is evident the amount of support the steel casing provides the cement sheath. In Fig. 4.1, the equivalent stress within the casing decreases non-linearly from 84,178 psi to 66,784 psi. At the casing–cement interface, there is a large decrease from 66,784 to

8,384 psi. Due to the fact that the properties of the cement (E_s = 2.4 x 10^6 psi, v_s = 0.4) and the formation (E_f = 3 x 10^6 psi, v_f = 0.42) are similar, there is a little change in the von Mises equivalent stress across the cement–formation interface (5,806 to 5736 psi). Fig. 4.2 shows a somewhat similar trend but with higher stresses imposed on the steel casing (93,575 to 74,325 psi) and a lower stress on the cement sheath (8,160 to 5,560 psi). As opposed to Fig. 4.1, there is a significant difference in the equivalent stress at the cement–formation interface (5,560 to 2,776 psi).

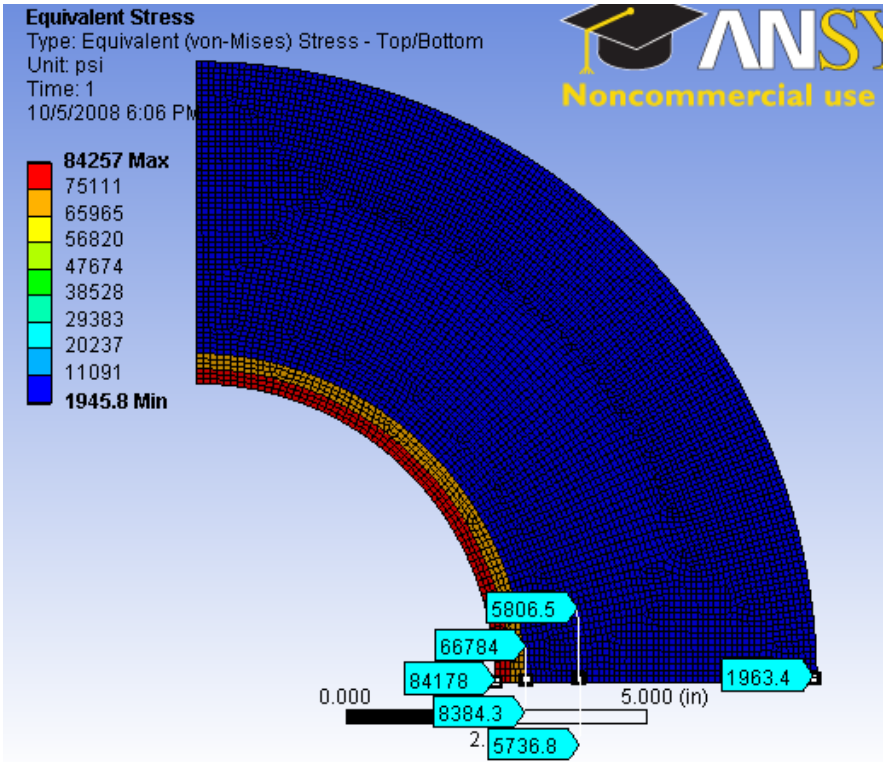

Fig 4.1: Equivalent Stress with Formation E_f = 3 x 10^6 psi and v_f = 0.42 for Scenario 1

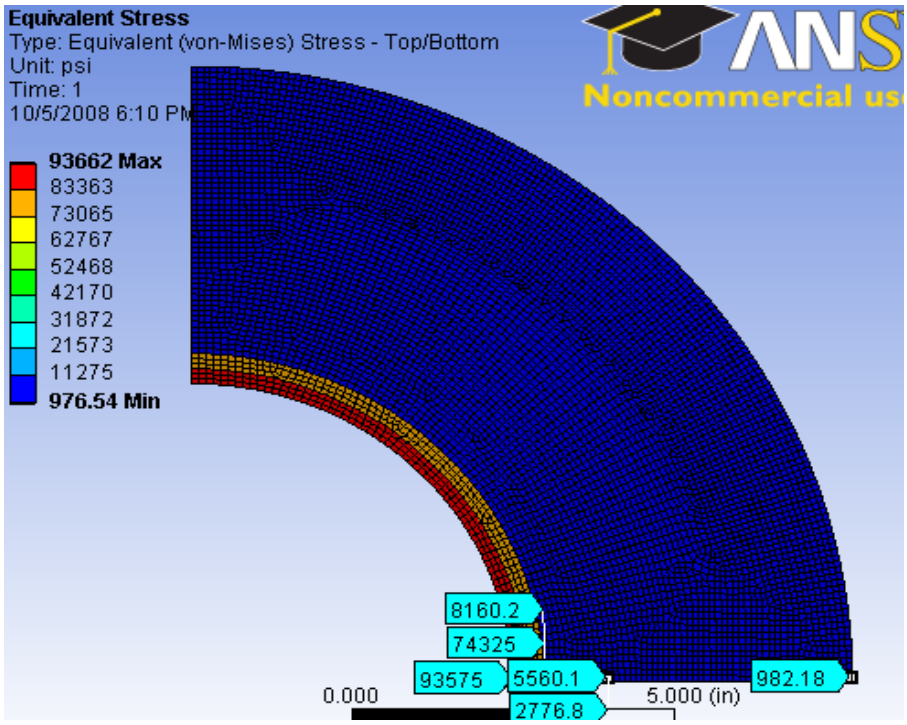

Fig 4.2: Equivalent Stress with Formation E_f = 1 x 10^6 psi and v_f = 0.3 for Scenario 1

Keeping the formation and casing properties unchanged, the analytical model was used to study the response to a high internal pressure and low formation pressures on the casing–cement–formation system as shown in Figs. 4.3 to 4.5. The results show that cement system 1 generates compressive (negative) radial and tangential stresses. The tangential stress fluctuates between a maximum value of -1,161 psi to a minimum of -590 psi. In contrast, cement systems 2 and 3 generate tensile tangential stresses. Cement system 3 possesses more of a ductile quality and generates less von Mises stress than system 2 but a little more than system 1.

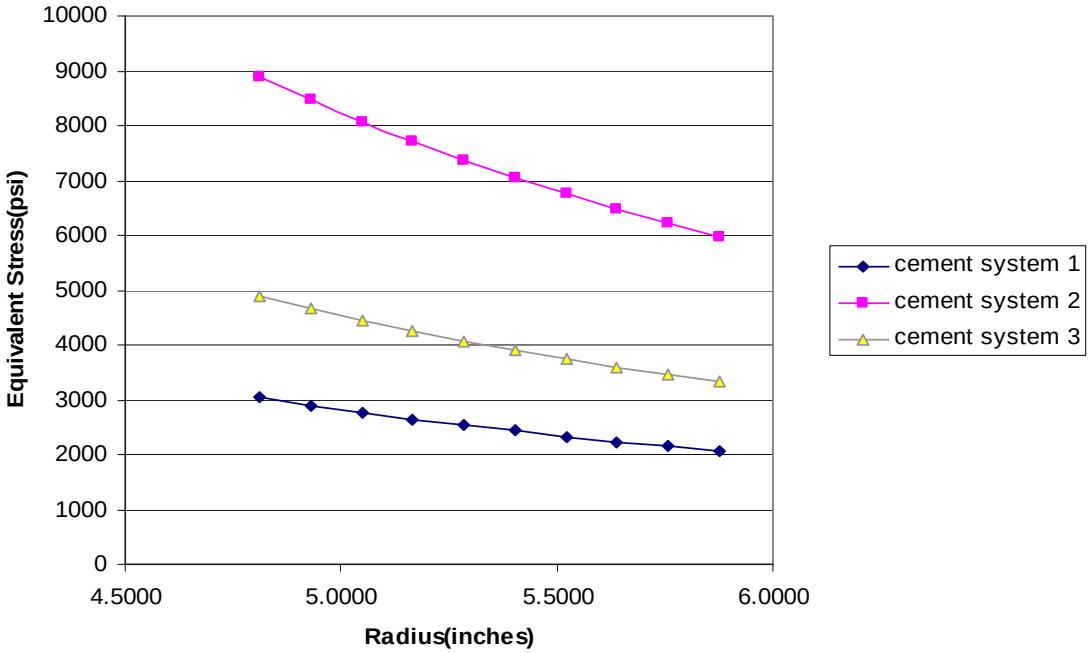

Fig 4.3: Equivalent Stress in Three Cement Systems with p_i = 15,000 psi and p_f = 1,000 psi

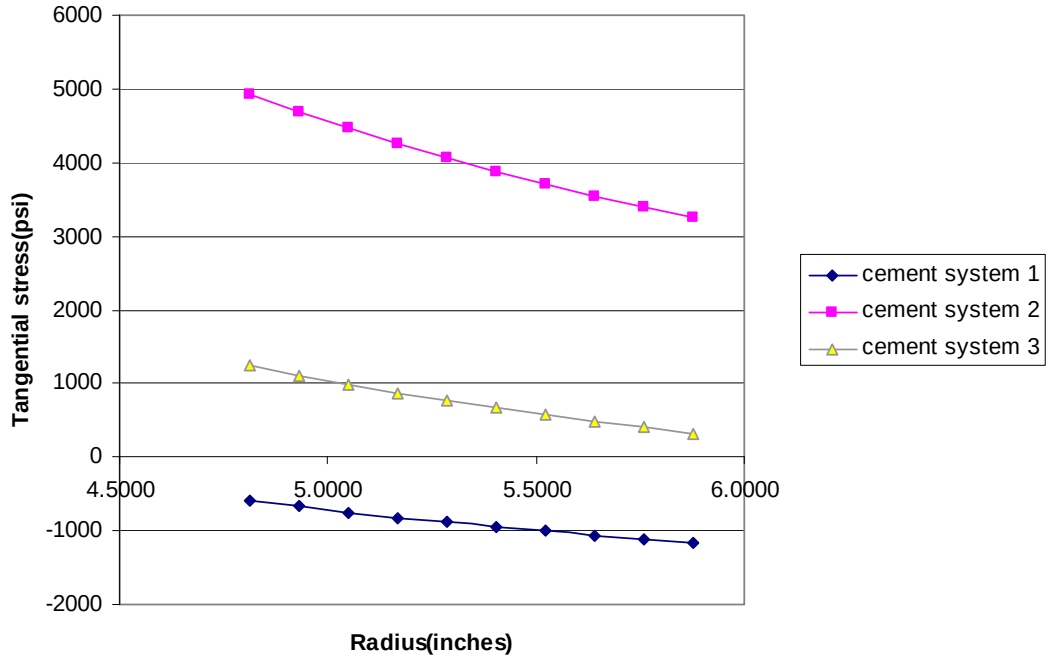

Fig 4.4: Tangential Stress in Three Cement Systems with p_i = 15,000 psi and p_f = 1,000 psi

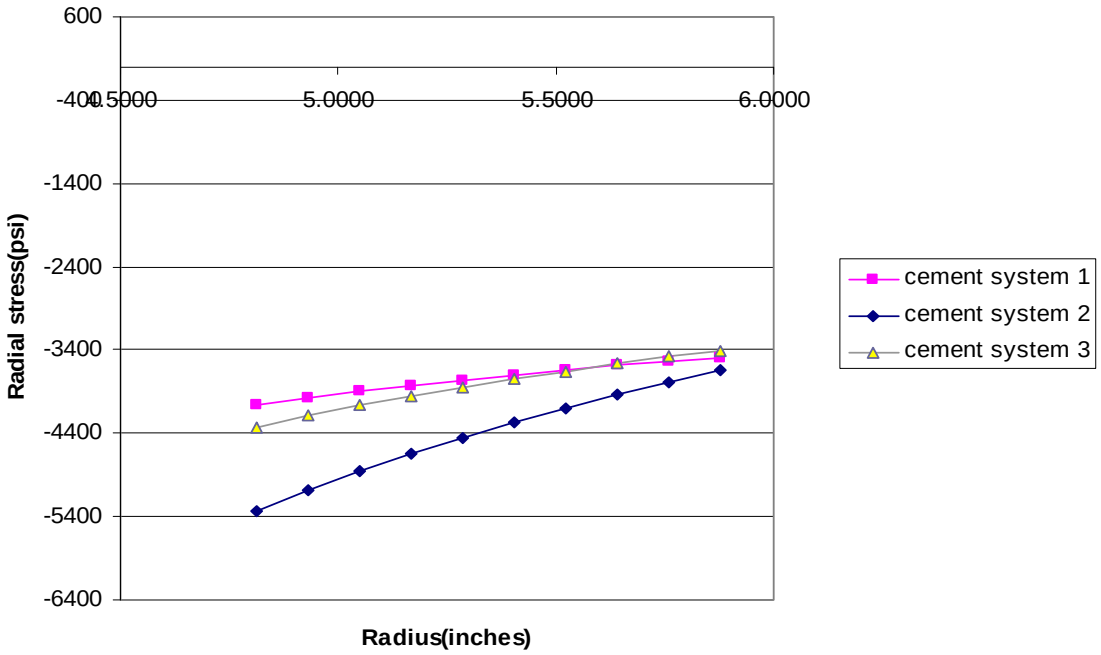

Fig 4.5: Radial Stress in Three Cement Systems with p_i = 15,000 psi and p_f = 1,000 psi

2. High Inner Pressure and Zero Formation Pressure

The trend in the radial and tangential stresses in the three cement systems subjected to a high inner pressure of 15,000 psi and a zero formation pressure is strikingly similar to the trend in scenario 1, with values for radial and tangential stresses being a little higher as shown in Figs. 4.7 to 4.9. The maximum equivalent stress in this case is 8,692 psi for cement system 2 as opposed to 9,000 psi for the same cement system under scenario 1. The same can be said about the values for the radial and tangential stresses for these two loading cases.

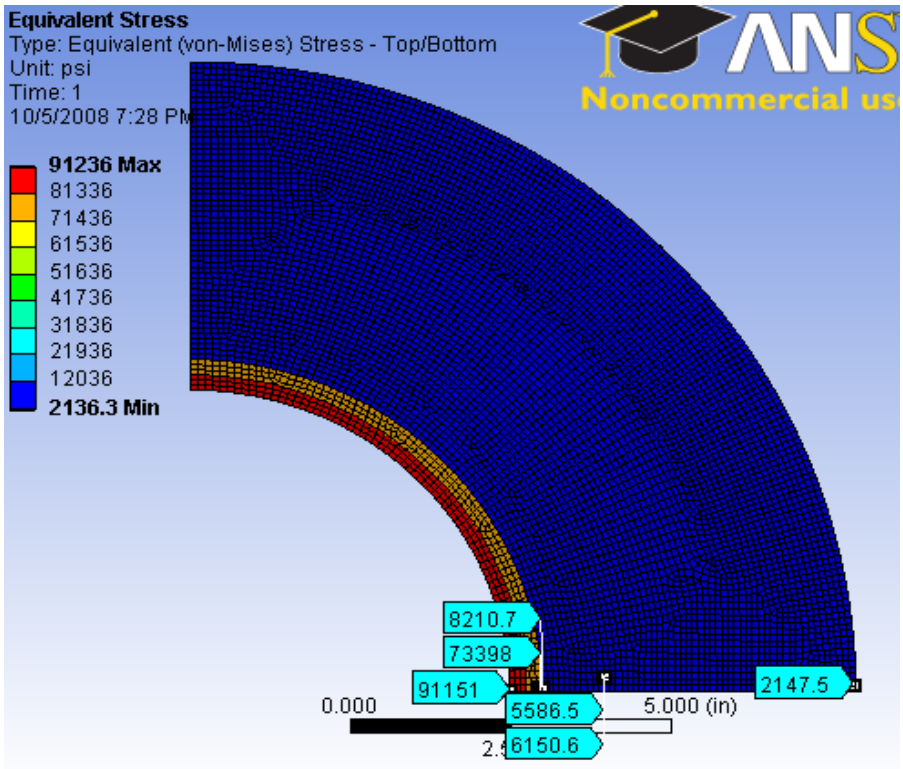

Fig 4.6: Von Mises Stress with Formation E_f = 1 x 10^6 psi and ν_f = 0.3 for Scenario 2

The finite element modeling of scenario 2 with cement system 2 (Fig. 4.6) shows a higher amount of equivalent stress on the casing (91,151 to 73,398 psi) in comparison with scenario 1 with the same formation properties (84,178 to 66,784 psi). The transitions at the boundary show a different trend from that of scenario 1. At the casing–cement interface, the pressure reduces from 73,398 psi in the casing to 8,210 psi in the cement. The trend is the opposite at the cement–formation boundary with 5,586 psi at the cement side of the boundary and 6,150 psi on the formation side.

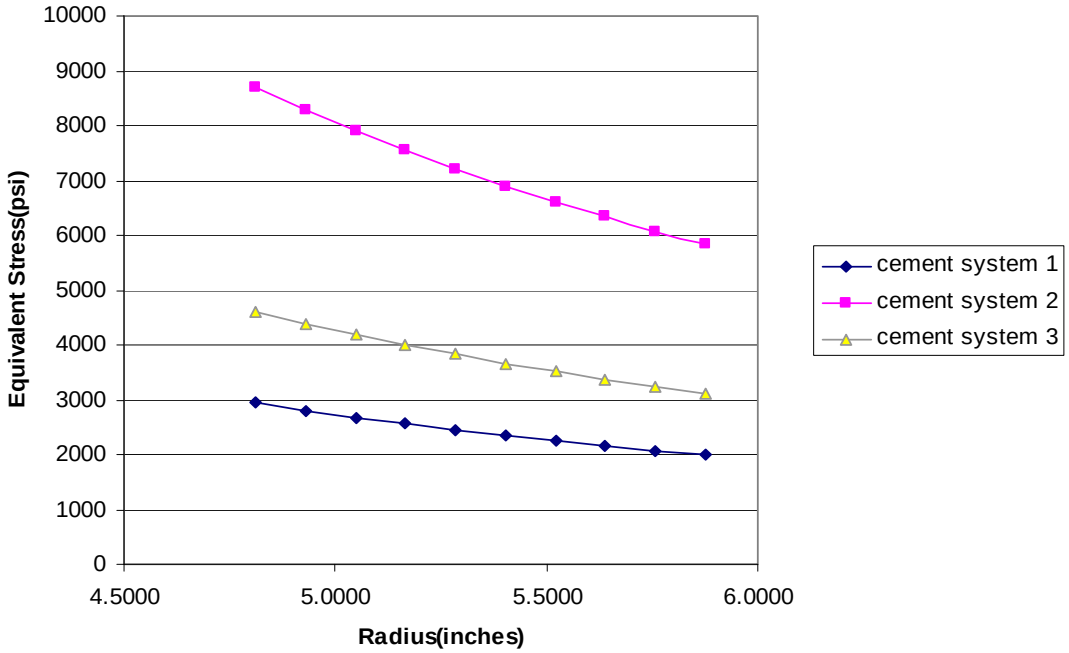

Fig 4.7: Equivalent Stress in Three Cement Systems with p_i = 15,000 psi and p_f = 0 psi

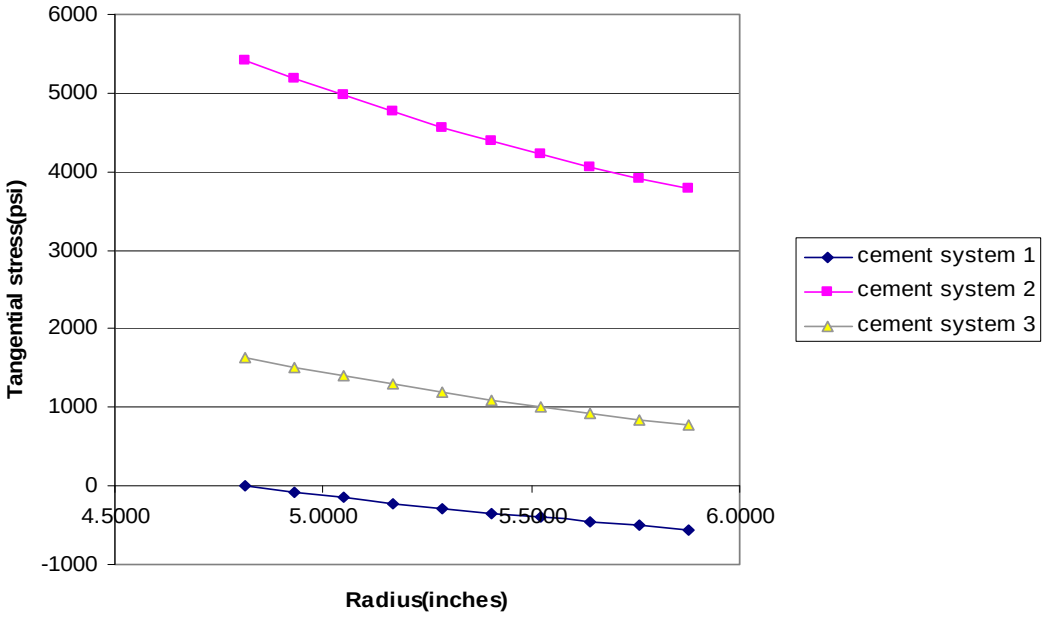

Fig 4.8: Tangential Stress in Three Cement Systems with p_i = 15,000 psi and p_f = 0 psi

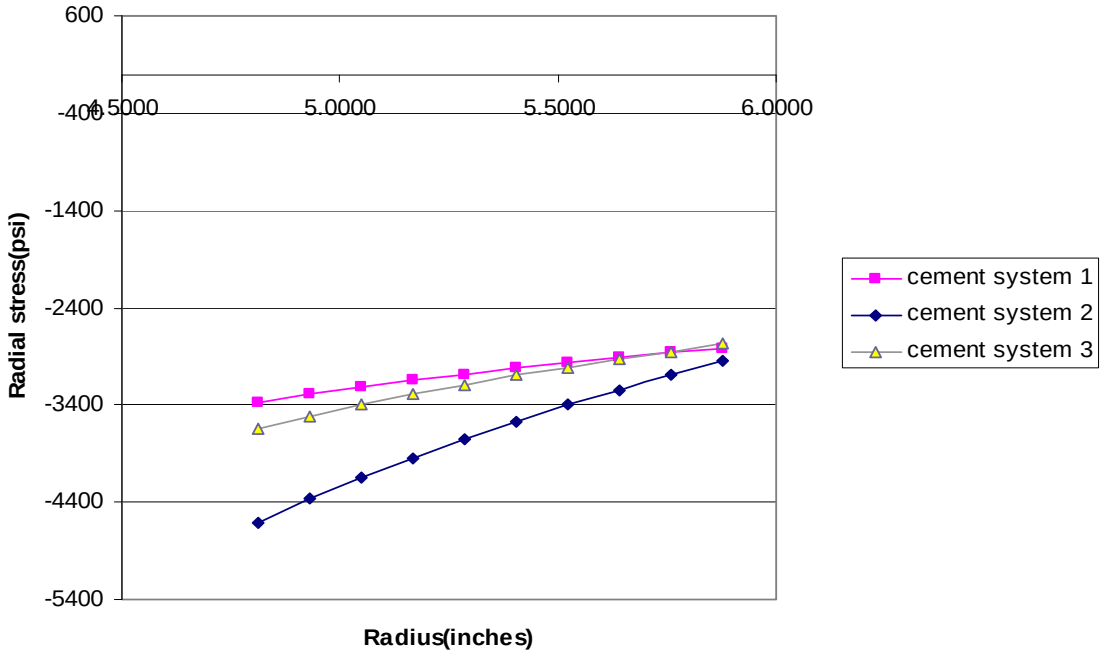

Fig 4.9: Radial Stress in Three Cement Systems with p_i = 15,000 psi and p_f = 0 psi

3. Low Inner Pressure and High Formation Pressure

Figures 4.10 to 4.12 present the case when a casing pressure of 4,000 psi and a high formation pressure of 10,000 psi are applied to the casing–cement–formation model. The trend here is significantly different from that seen in the first two scenarios. Here, both the tangential and radial stresses are compressive in nature. Cement systems 2 and 3 generate almost equal amounts of tangential stresses that are much lower than those of cement system 1. However, cement system 1 has the lowest value of radial stress (-5297 psi) of the three cement systems.

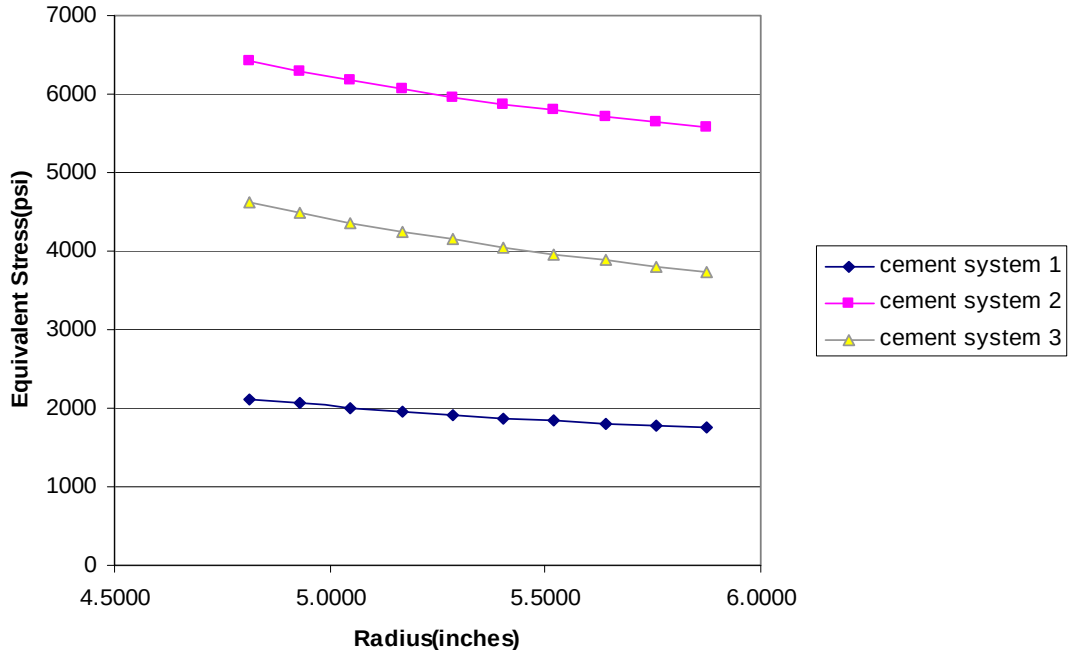

Fig 4.10: Equivalent Stress in Three Cement Systems with p_i = 4,000 psi and p_f = 10,000 psi

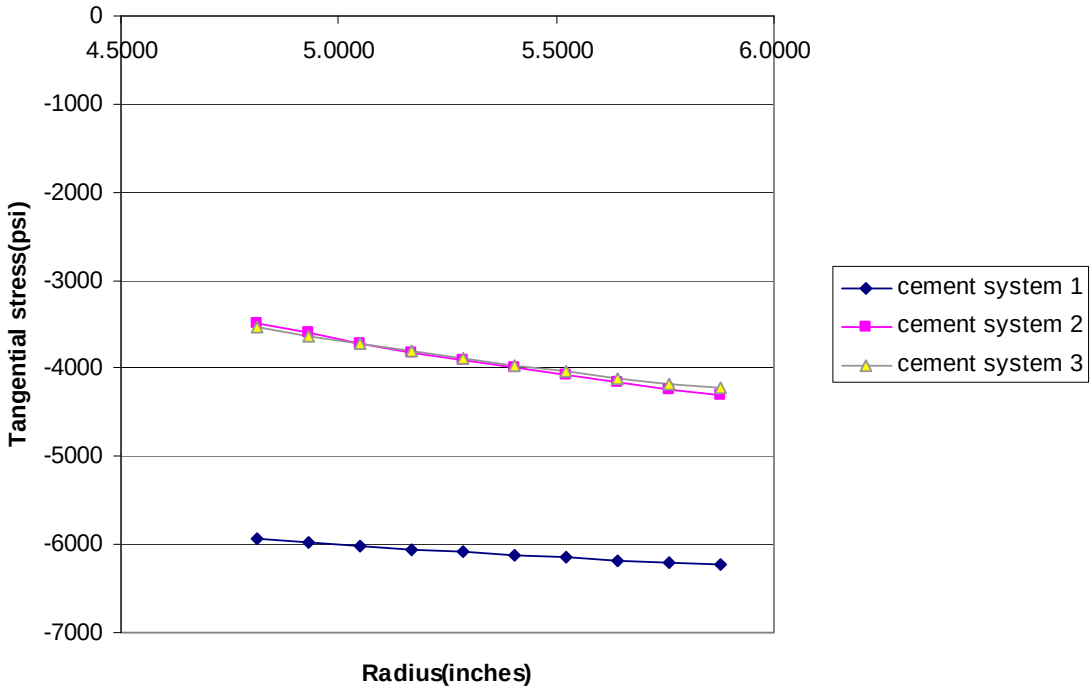

Fig 4.11: Tangential Stress in Three Cement Systems with p_i = 4,000 psi and p_f = 10,000 psi

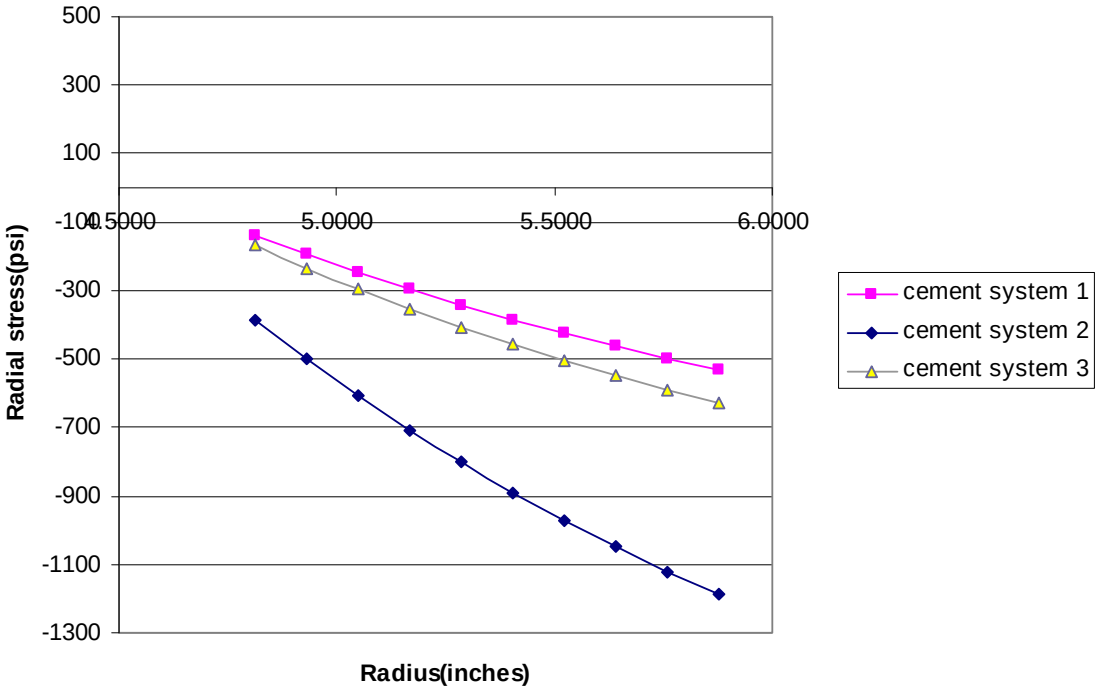

Fig 4.12: Radial Stress in Three Cement Systems with p_i = 4,000 psi and p_f = 10,000 psi

- *Case Scenarios Considering the Effect of Temperature Change*

1. High Inner Pressure, Low Formation Pressure with Temperature Change

There is no doubt that temperature change plays an important role in adding to the stresses that would ultimately lead to the failure of the cement sheath. As expected, the combined effect of temperature and pressure shows a trend that is a bit different, in terms of the magnitude of the stress, from that when the effects of pressure are considered alone. Figures 4.13 to 4.15 give us a view of that trend when an inner pressure of 15,000 psi, formation pressure of 1,000 psi and temperature change (ΔT) of 150°F are applied to the casing–cement–formation model.

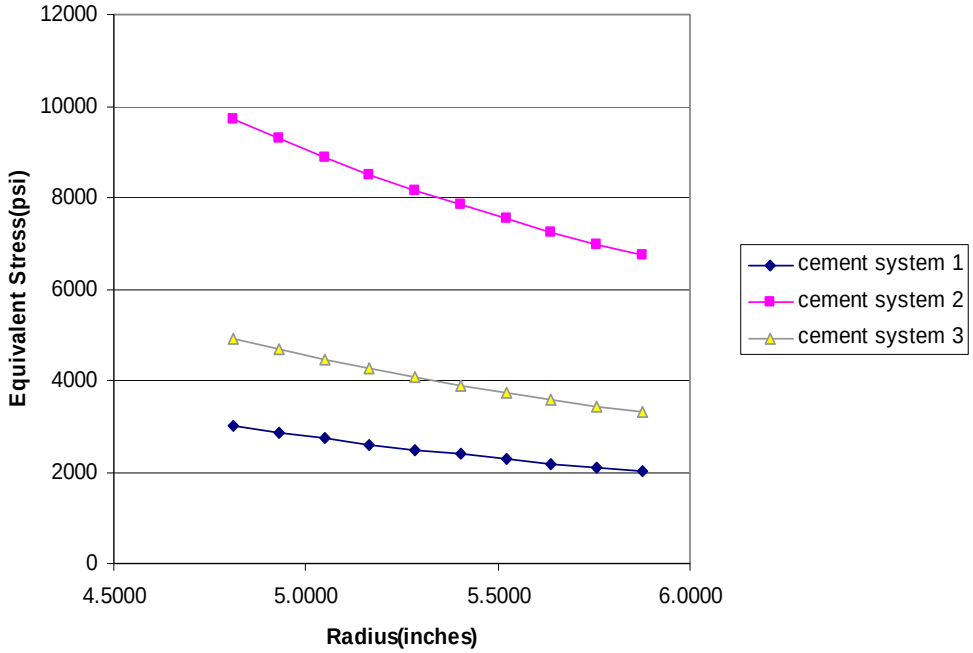

Fig 4.13: Equivalent Stress with p_i = 15,000 psi, p_f = 1,000 psi and ΔT = 150°F

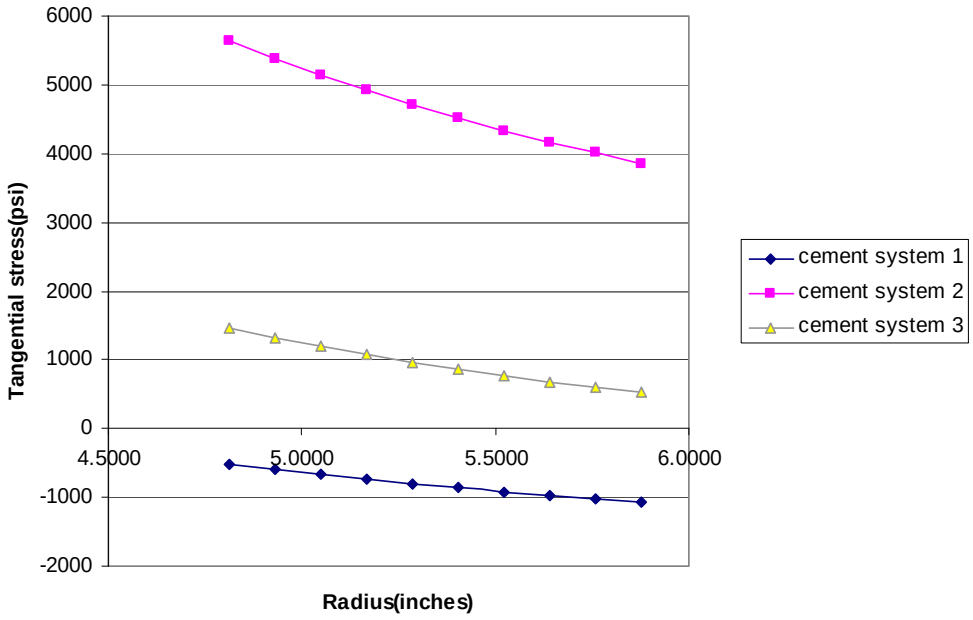

Fig 4.14: Tangential Stress with p_i = 15,000 psi, p_f = 1,000 psi and ΔT = 150°F

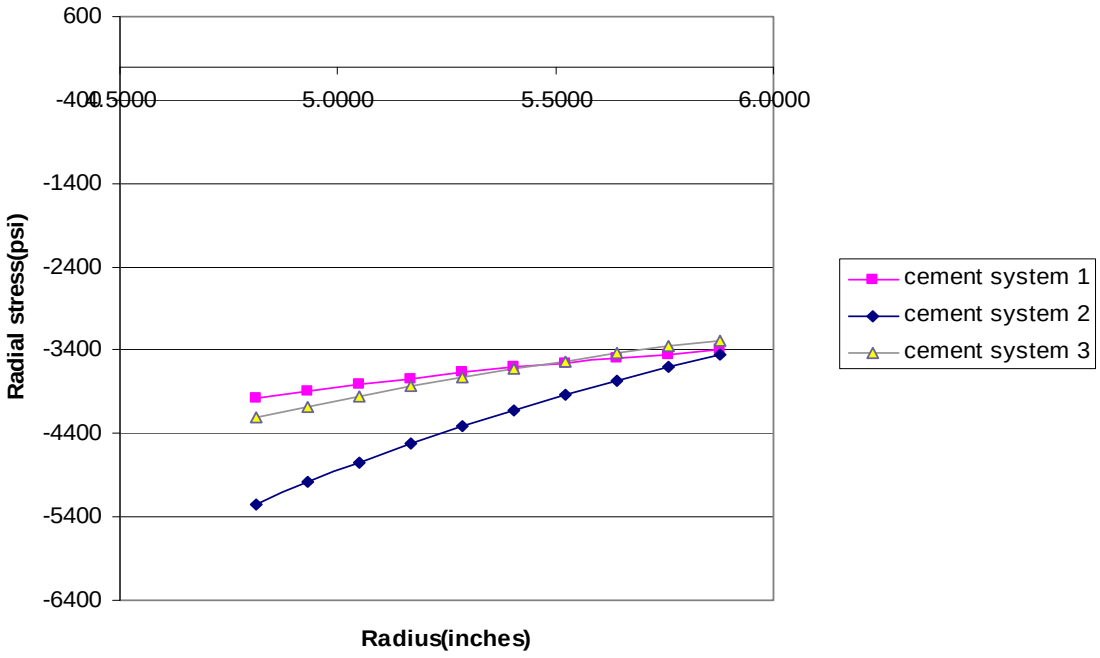

Fig 4.15: Radial Stress with p_i = 15,000 psi, p_f = 1,000 psi and ΔT = 150°F

With the effect of temperature change, the trend in the tangential stress distribution across the cement sheath remains pretty much the same although the stress value is higher. The highest von Mises stress with ΔT = 0 is about 9,000 psi (cement system 2) compared with 10,000 psi with the same cement system with ΔT = 150°F. The tangential stress distribution, however, differs as it fluctuates between a negative (compressive) value for cement system 2 to a positive (tensile) value for cement systems 1 and 3.

2. High Inner Pressure, Zero Formation Pressure with Temperature Change

In this case, the radial stress distribution profile is similar to that of Fig. 4.9 with almost the same magnitude of stress but the tangential stress profile is different. While the tangential stress profile in Fig. 4.8 was all negative (compressive) stress for cement system 1, it fluctuates from 85 psi (tensile) to -468 psi (compressive) when the effect of temperature change is considered. The equivalent stresses decreases non-linearly from the inner surface of the cement (2,928 psi for cement 1, 9,652 psi for cement 2 and 4,687 psi for cement 3) to 1,977 psi for cement 1, 6,802 psi for cement 2 and 3,164 psi for cement 3 at the outer surface. These results are shown by figures 4.16 to 4.18 below.

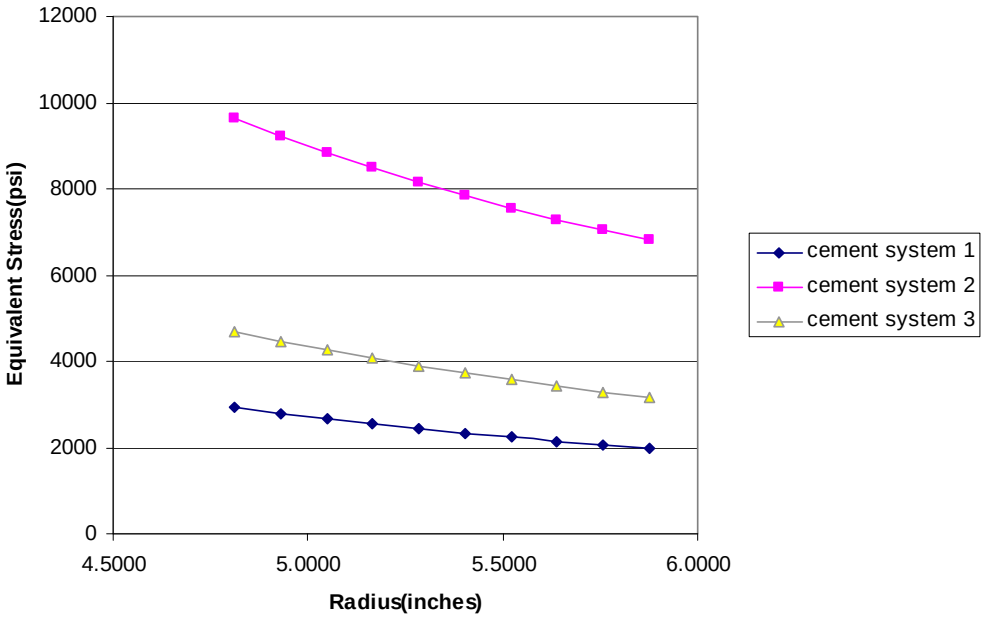

Fig 4.16: Equivalent Stress with p_i = 15,000 psi, p_f = 0 psi and ΔT = 150°F

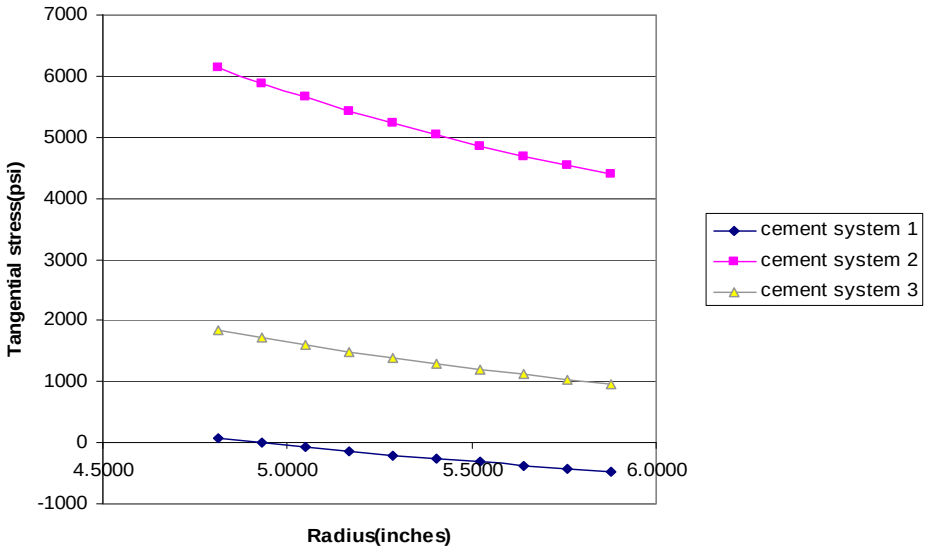

Fig 4.17: Tangential Stress with p_i = 15,000 psi, p_f = 0 psi and ΔT = 150°F

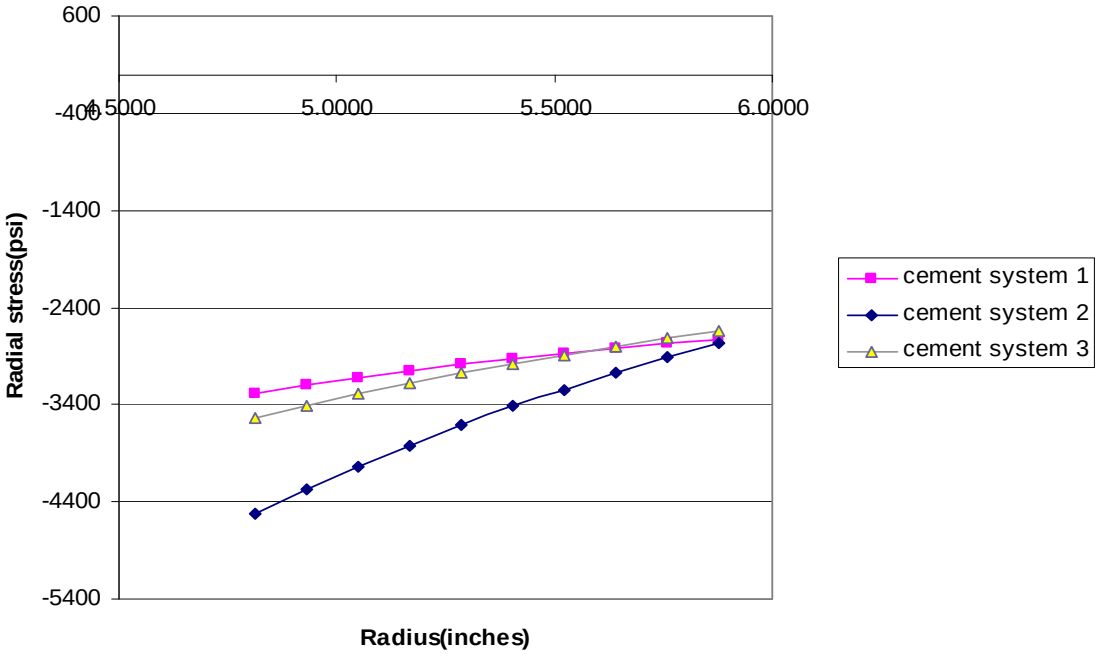

Fig 4.18: Radial Stress with p_i = 15,000 psi, p_f = 0 psi and ΔT = 150°F

3. Low Inner Pressure, High Formation Pressure with Temperature Change

This case generates higher values for tangential and radial stresses in the three cement systems as compared to the case without temperature change. The radial stress in the three cement systems also increases non-linearly from the inner surface of the cement to the outer surface where the opposite is the case without temperature change. The results are as shown in Figs. 4.19 to 4.21.

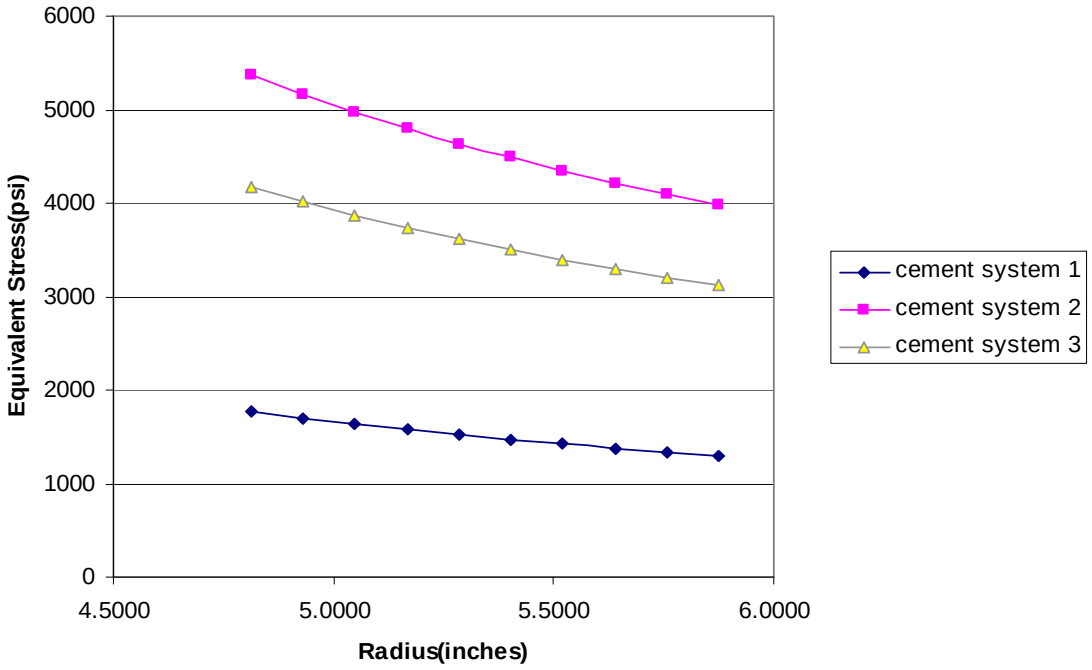

Fig 4.19: Equivalent Stress with p_i = 4,000 psi, p_f = 10,000 psi and ΔT = 150°F

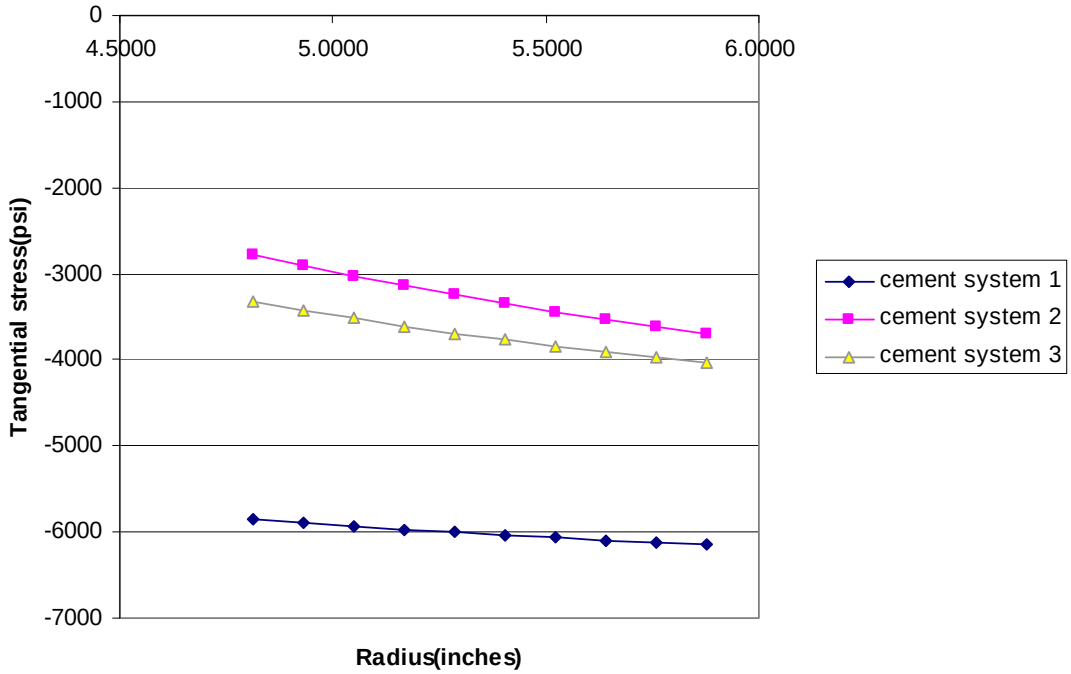

Fig 4.20: Tangential Stress with p_i = 4,000 psi, p_f = 10,000 psi and ΔT = 150°F

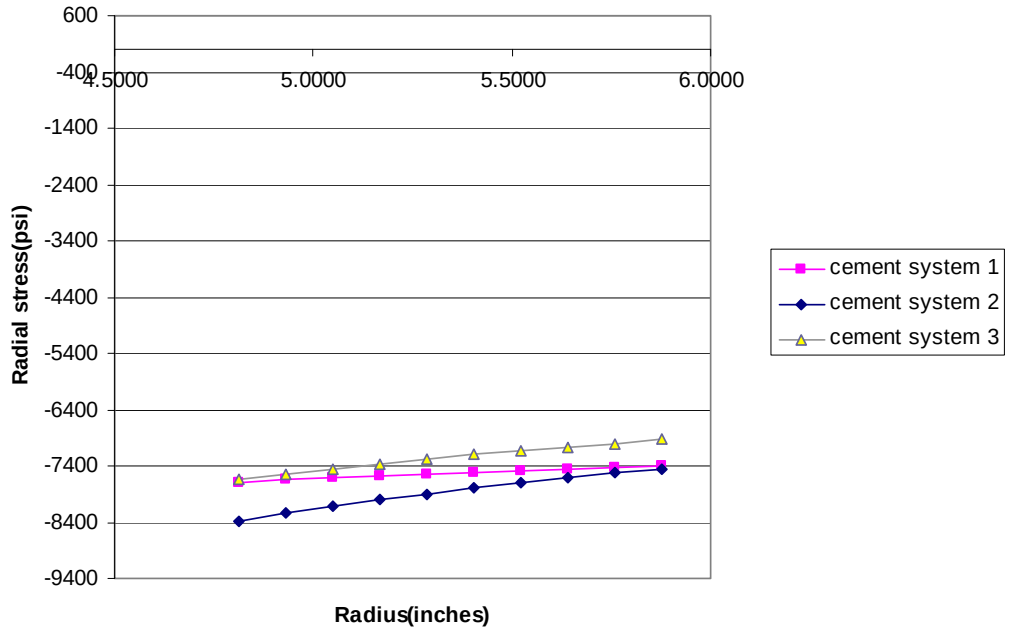

Fig 4.21: Radial Stress with p_i = 4,000 psi, p_f = 10,000 psi and ΔT = 150°F

4.2 Fatigue Loading

The aim of the fatigue study was to determine if a cement system capable of sustaining a static load would be able to sustain a similar load under cyclic loading conditions. A fatigue analysis together with a related static analysis was done with ANSYS on a casing–cement–formation setup using cement system 2 with an inner pressure of 7,000 psi and formation pressure of 2,000 psi. As was done in the static study, the properties of the casing remained the same while the fatigue behavior of cement was studied with two different formation properties; $E_f = 3 \times 10^6$ psi, $\nu_f = 0.42$ and $E_f = 1 \times 10^6$ psi, $\nu_f = 0.3$. Fully reversed and zero based loading conditions were used in the fatigue analysis.

With 7,000 psi internal pressure and 2,000 psi formation pressure, the finite element model in Fig. 4.22 gives an indication that cement system 2 would withstand such pressure loads under static loading conditions. The effective von Mises stress changes from 22,760 psi at the cement–casing boundary on the casing side to 4,330 psi on the cement sheath side and from 2,994 psi on the cement side of cement–formation boundary to 1,842 psi on the formation side of the same boundary. The equivalent alternating stresses for a zero based cyclic loading condition with the formation properties $E_f = 1 \times 10^6$ psi, $\nu_f = 0.42$, however, is a bit different as shown in Fig. 4.23.

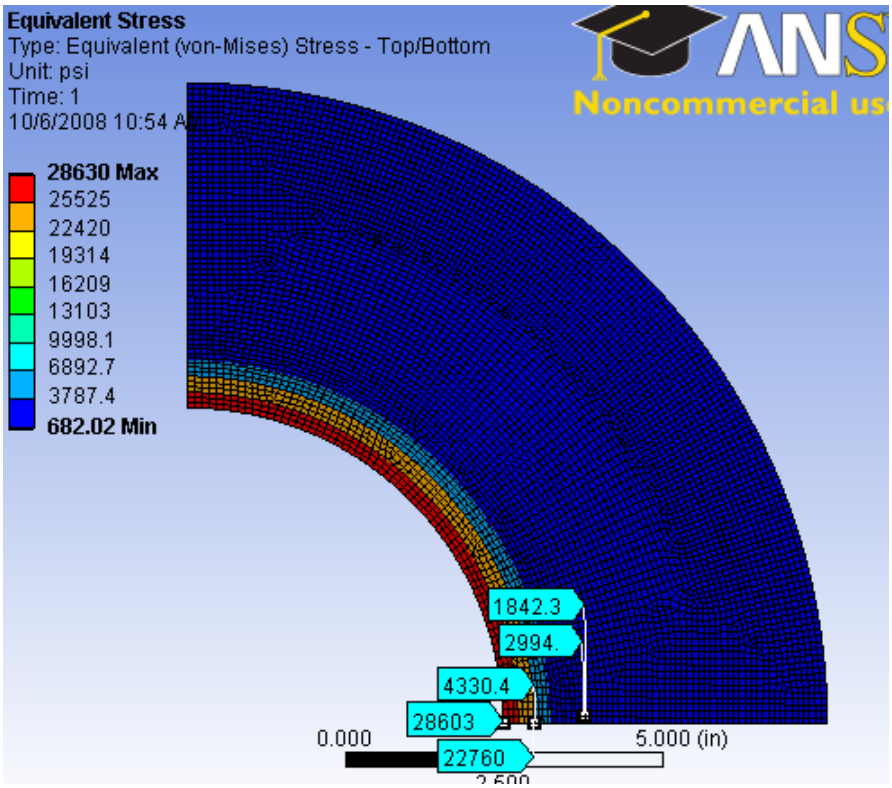

Fig 4.22: Equivalent Stress for Static Loading with Formation $E_f = 1 \times 10^6$ psi and $\nu_f = 0.42$

The zero based fatigue loading results in a lower equivalent alternating stress in the casing but higher values in the cement and the formation, as shown in Fig. 4.23. The equivalent alternating stress decreases non-linearly from 18,199 psi to 13,719 psi at the casing–cement boundary with a fatigue life of 5.86×10^5 cycles (Fig. 4.24). The cement part of the casing–cement boundary has a fatigue life of 5.6×10^4 cycles (Fig. 4.24) and an alternating stress of 7,783 psi (Fig. 4.23) psi as opposed to 4,330 psi (Fig. 4.22) under static loading conditions. The progression from the cement to the formation at the cement–formation boundary however sees a large increase in the equivalent alternating stress from 2,992 psi to 1×10^{32} psi.

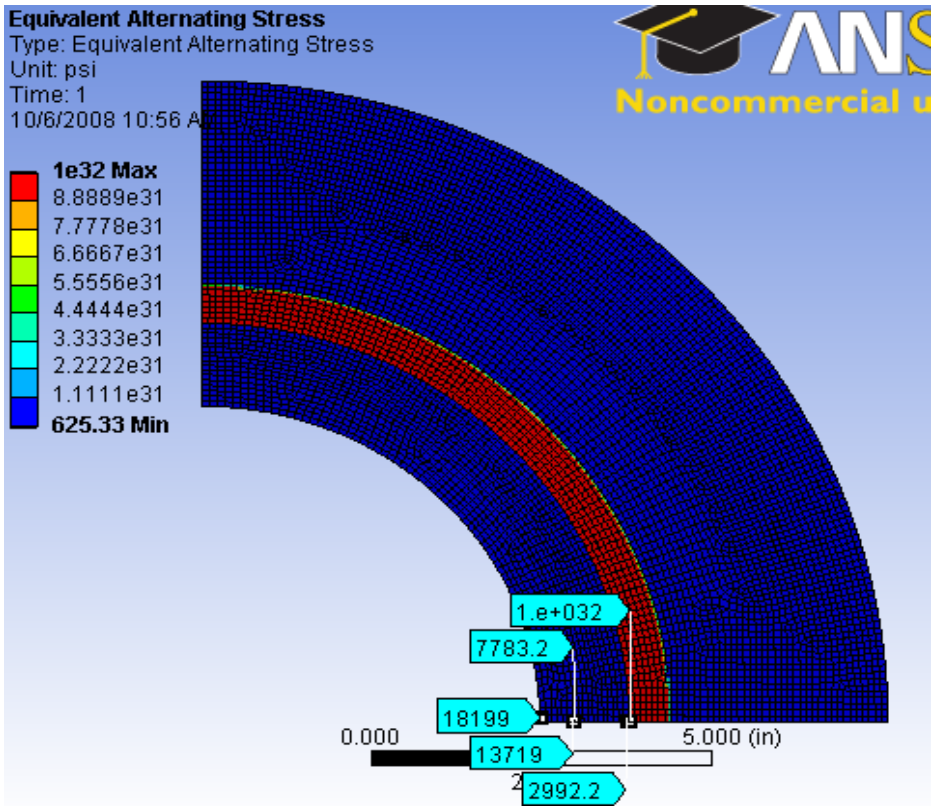

Fig 4.23: Equivalent Alternating Stress for Zero Based Loading

Figures 4.25 to 4.27 show the fatigue sensitivity plot for life, damage and safety factor but do not explicitly show the fatigue performance of the different regions of the casing–cement–formation model.

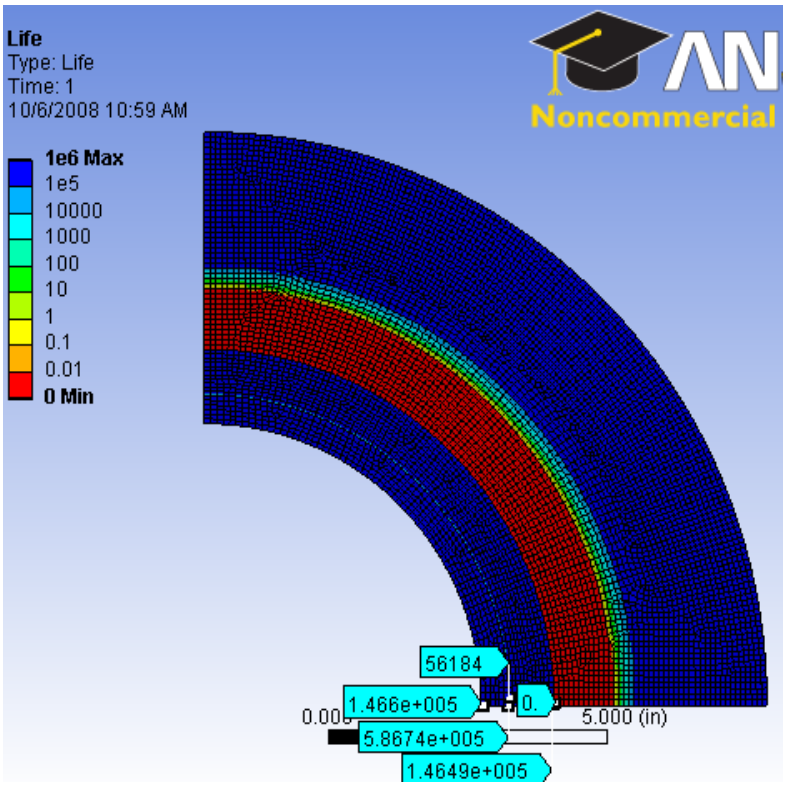

Fig 4.24: Life Cycle for Zero Based Loading

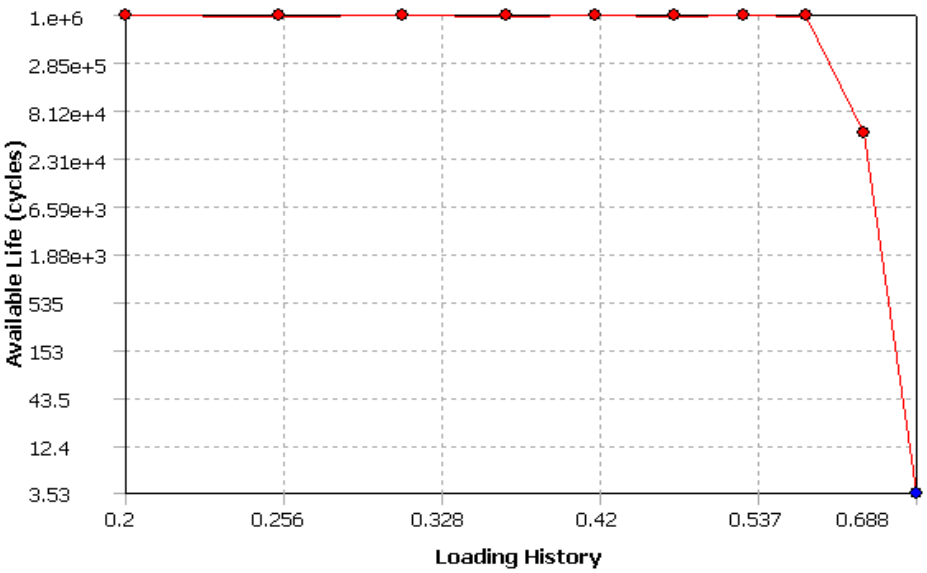

Fig 4.25: Fatigue Sensitivity to Life Plot for Zero Based Loading

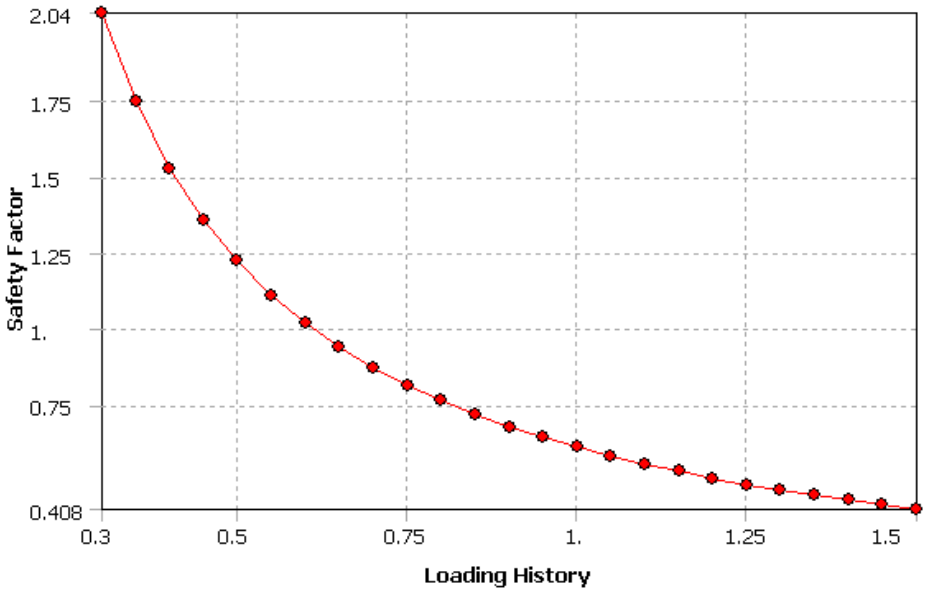

Fig 4.26: Fatigue Sensitivity to Safety Factor Plot for Zero Based Loading

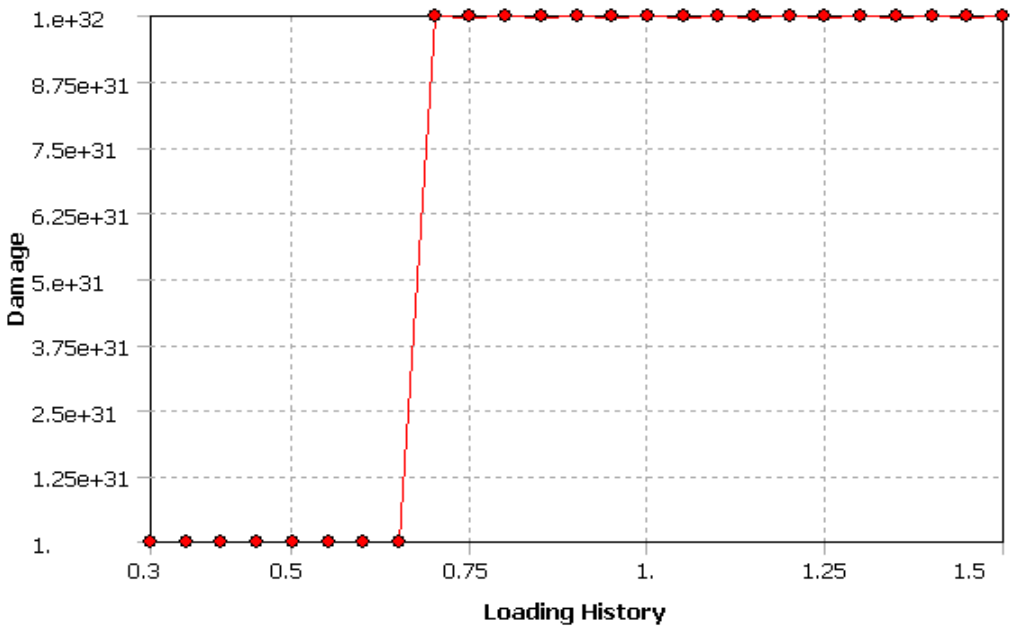

Fig 4.27: Fatigue Sensitivity to Damage Plot for Zero Based Loading

With the formation properties changed to $E_f = 1 \times 10^6$ psi and $\nu_f = 0.3$, while the casing and cement properties remain the same, an insight is gained on how mechanical properties like Young's modulus and Poisson's ratio affect the stress distribution and the ability to withstand fatigue loading. Figure 4.27 shows the response to fatigue with zero based load and formation properties $E_f = 1 \times 10^6$ psi and $\nu_f = 0.3$. Under the different formation properties, both cases show similar trends in the static equivalent stresses and alternating stresses but, as shown in Figs. 4.28 and 4.29, the formation with more ductile properties ($E_f = 1 \times 10^6$ psi and $\nu_f = 0.3$) has slightly higher stress values for the static equivalent stresses and almost the same value of alternating stress.

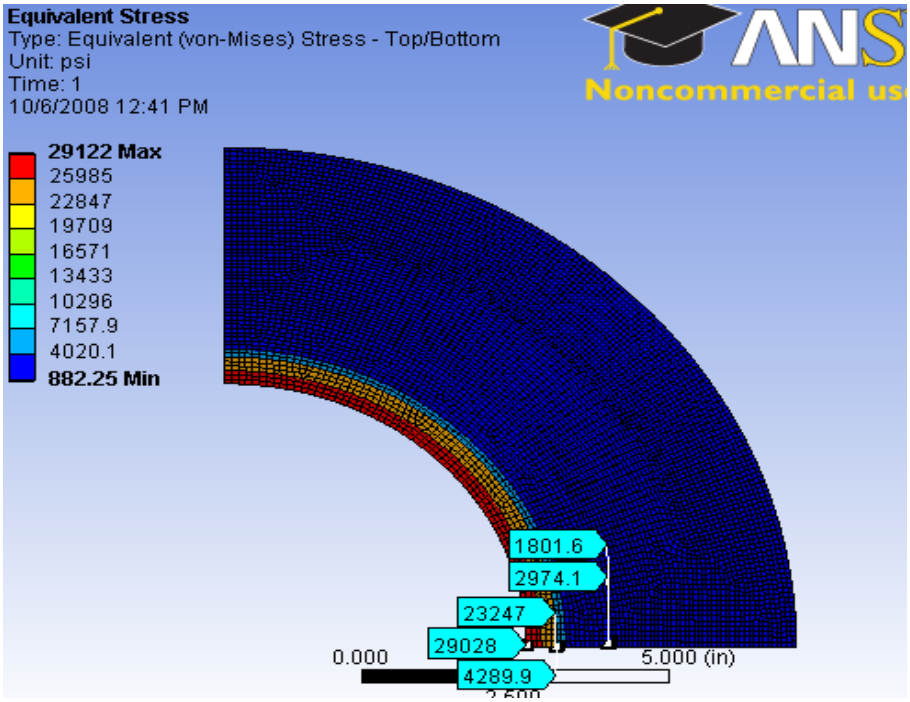

Fig 4.28: Equivalent Stress for Static Loading with Formation Property: $E_f = 1 \times 10^6$ psi, $\nu_f = 0.3$

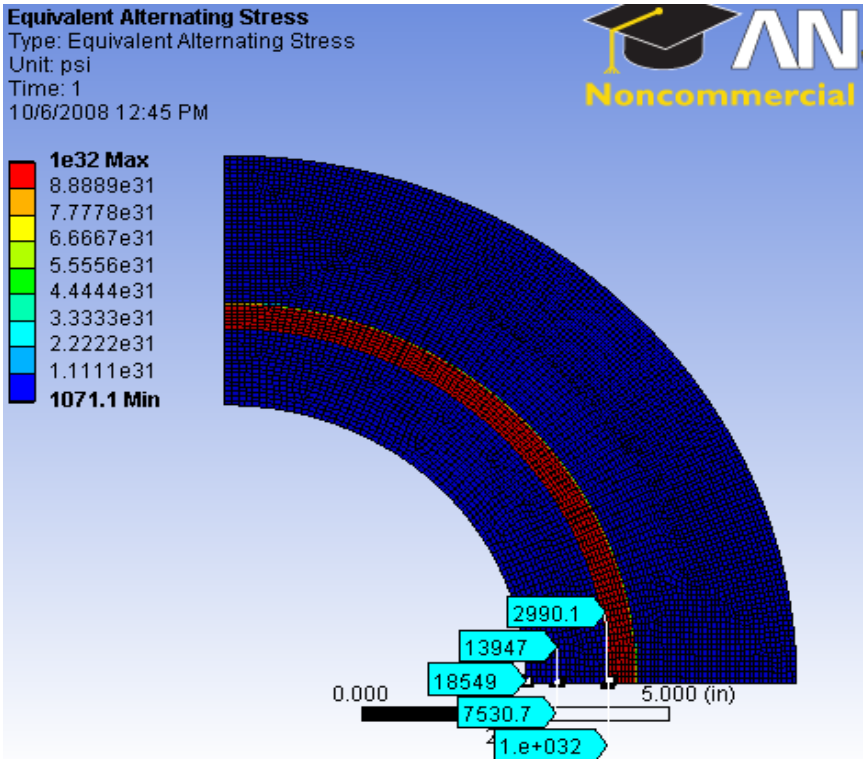

Fig 4.29: Alternating Stress for Zero Based Loading with Formation Property: $E_f = 1 \times 10^6$ psi, $\nu_f = 0.3$

FEA modeling of the fully reversed cyclic shear loading of cement sheath at the couplings (Figs. 4.30 and 4.31) also showed that the casing–cement boundary, which is the point of maximum shear, appears more vulnerable to fatigue failure.

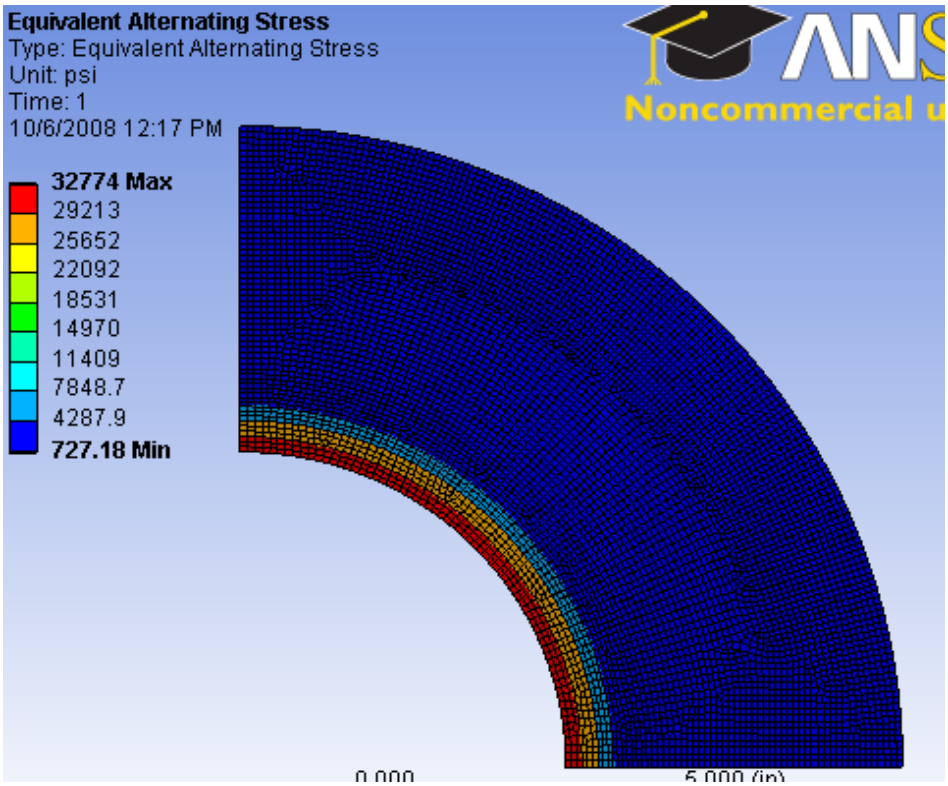

Fig 4.30: Alternating Stress for Fully Reversed Loading with Formation Property: $E_f = 3 \times 10^6$ psi, $\nu_f = 0.3$

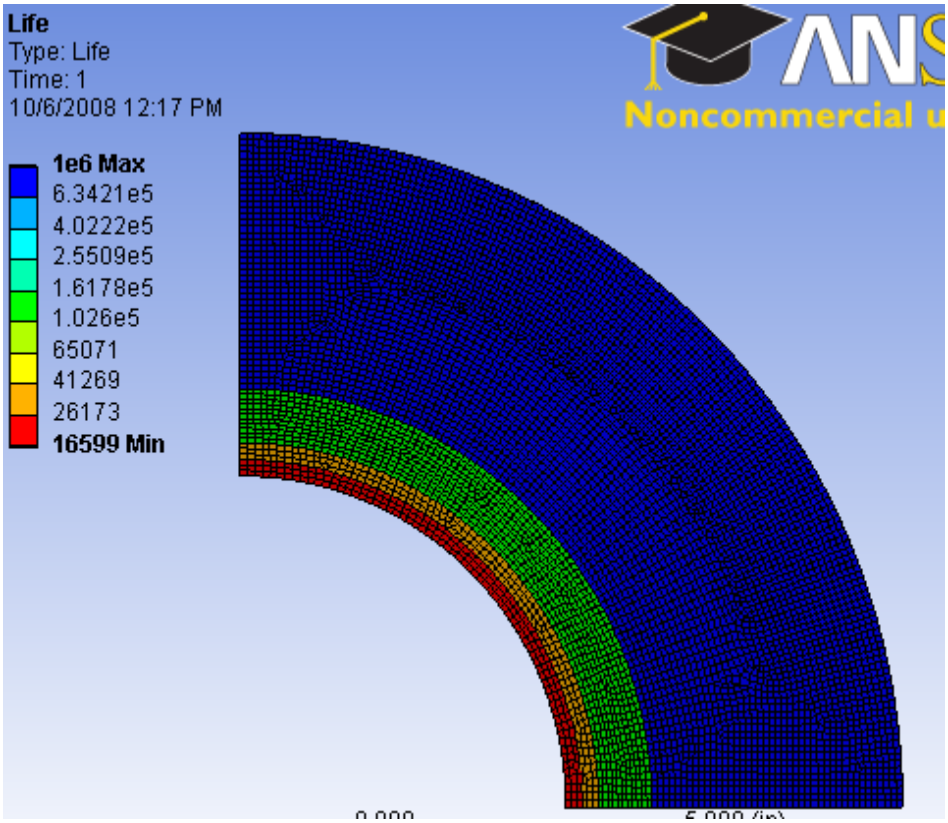

Fig 4.31: Life Cycle for Fully Reversed Loading with Formation Property: $E_f = 3 \times 10^6$ psi, $\nu_f = 0.3$

The fatigue sensitivity plots for life, damage and safety factor provide us with the number of life cycles to failure, the amount of damage done and the factor of safety for the casing–cement–formation system, but they do not clearly express the effects of fatigue loading on the cement sheath. In order to achieve this, the cement sheath was isolated and the contact pressures obtained from the analytical model were applied. A temperature change of 150°F was also considered. The response of cement systems 1 and 2 were modeled. The results are shown in Figs. 4.32 to 4.34. The fatigue sensitivity plots are shown in Figs. 4.35 to 4.37.

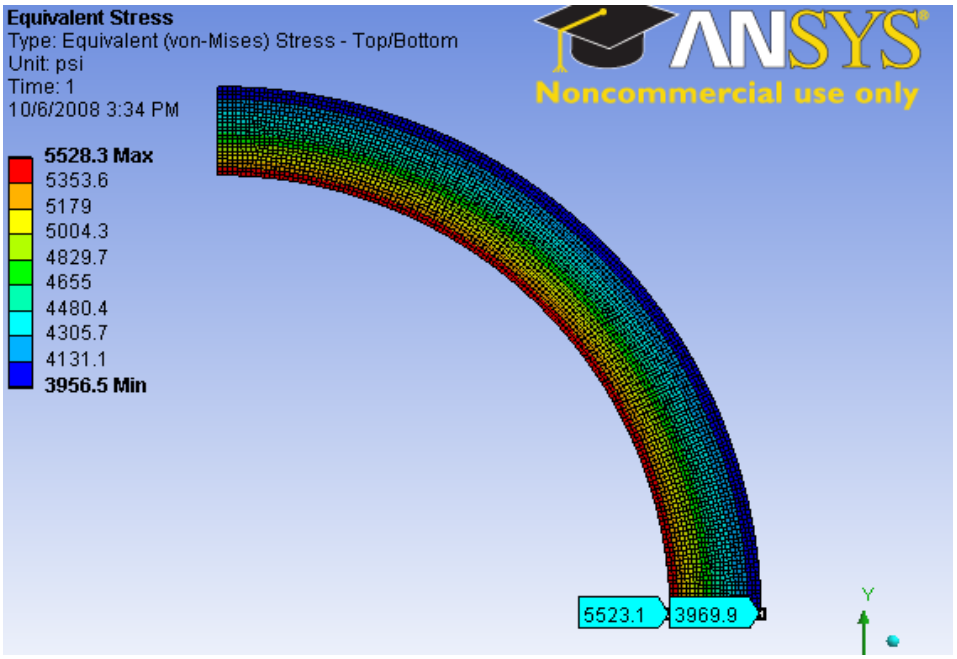

Fig 4.32: Equivalent Stress for Cement System 2 under Static Loading

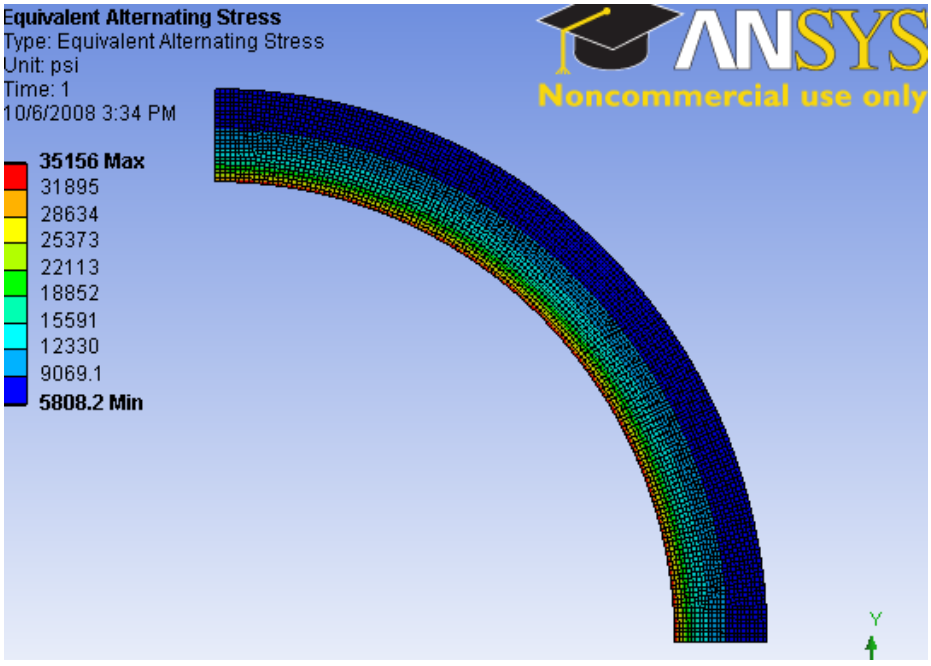

Fig 4.33: Alternating Stress for Cement System 2 under a Zero Based Cyclic Loading

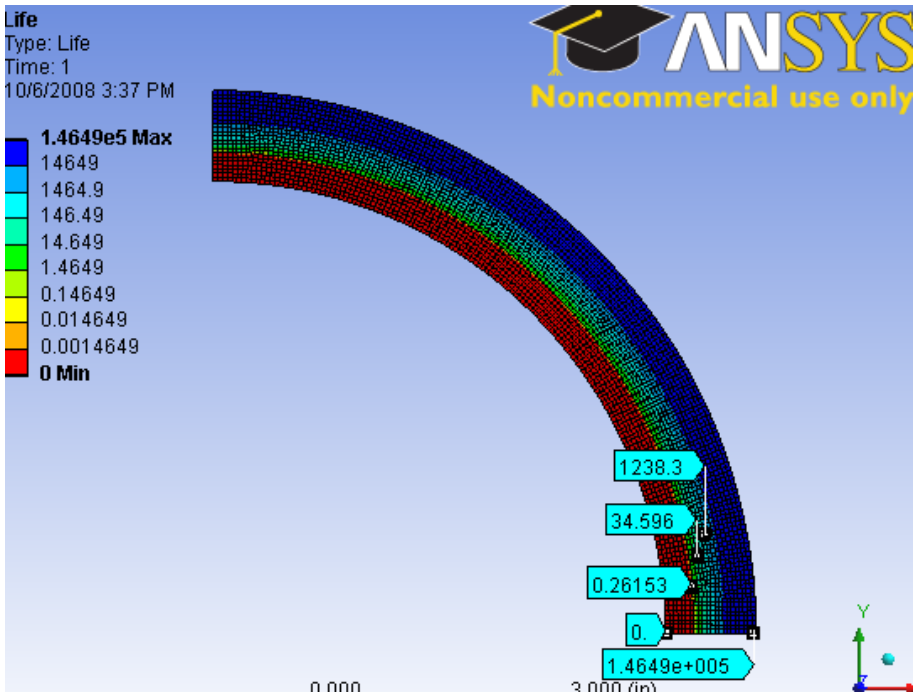

Fig 4.34: Life Cycle for Cement System 2 under a Zero Based Cyclic Loading

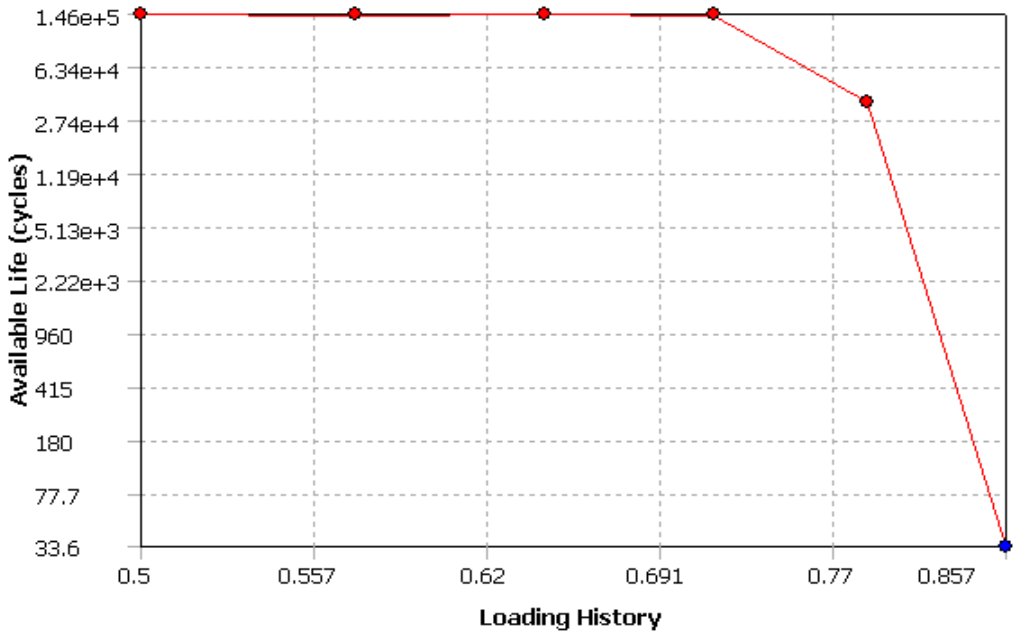

Fig 4.35: Fatigue Sensitivity to Life for a Zero Based Cyclic Loading with Cement 2

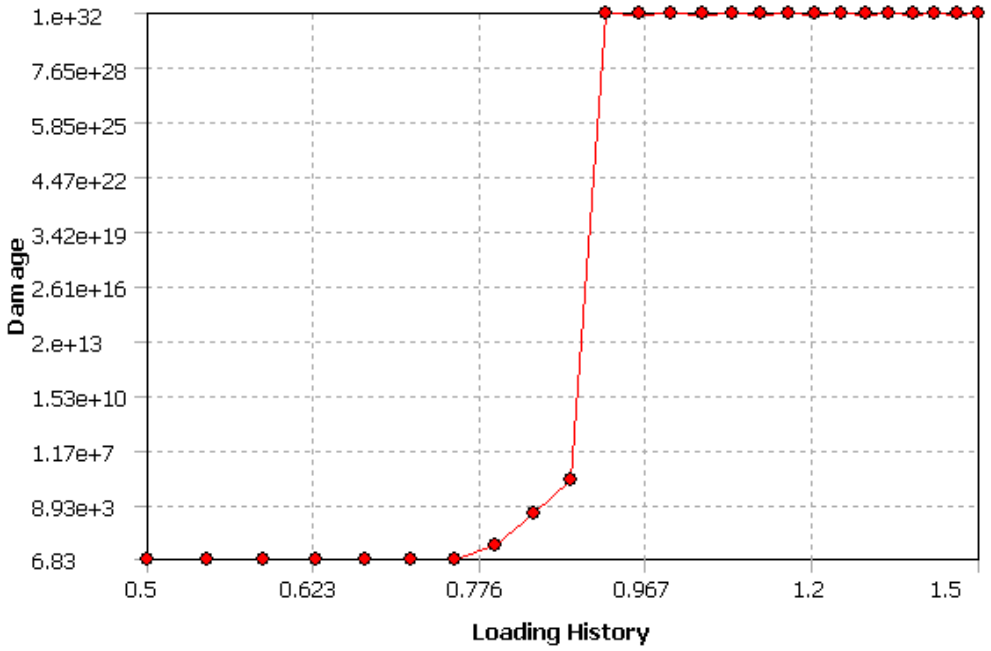

Fig 4.36: Fatigue Sensitivity to Damage Plot for a Zero Based Cyclic Loading with Cement 2

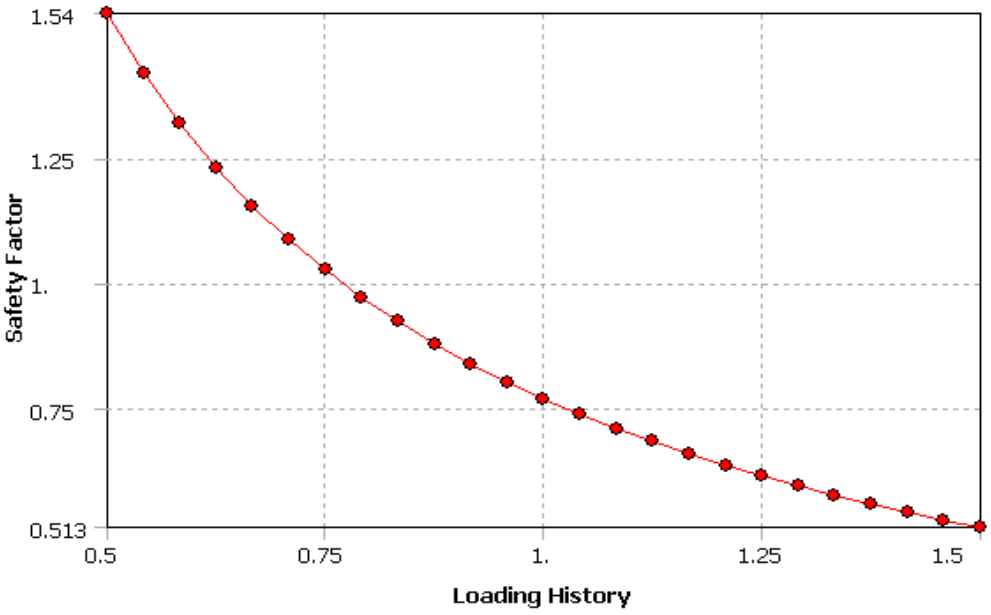

Fig 4.37: Fatigue Sensitivity to Safety Factor Plot for a Zero Based Cyclic Loading with Cement 2

From the fatigue sensitivity plots, it can be seen that the maximum load ratio that can be supported by cement system 2 before failure is about 0.75. The same analysis for the ductile cement (cement system 1) yields the results shown in Figs.4.38 to 4.40 below.

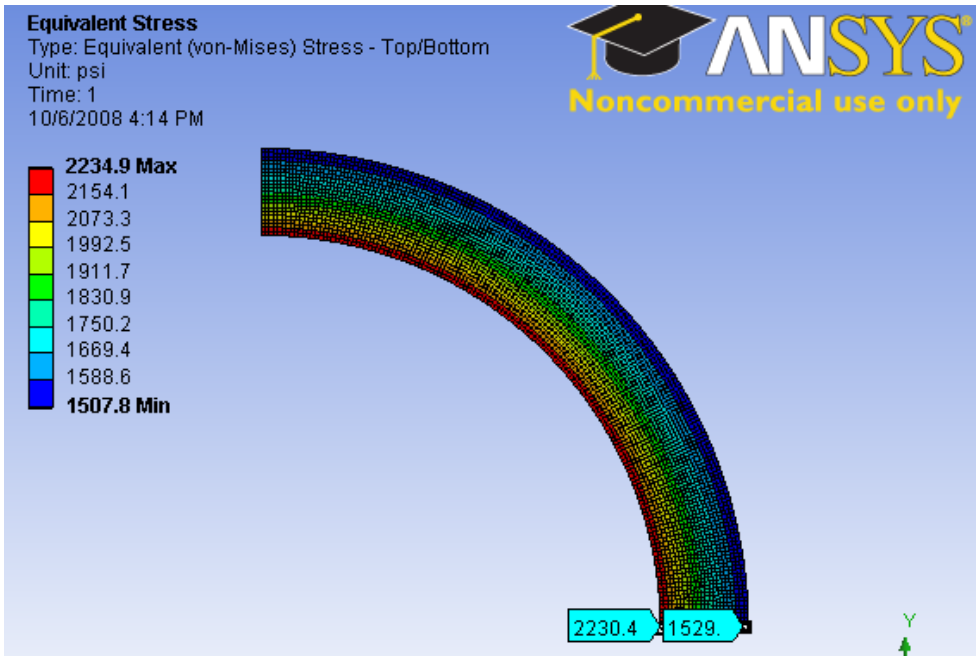

Fig 4.38: Equivalent Stress for Cement System 1 under Static Loading

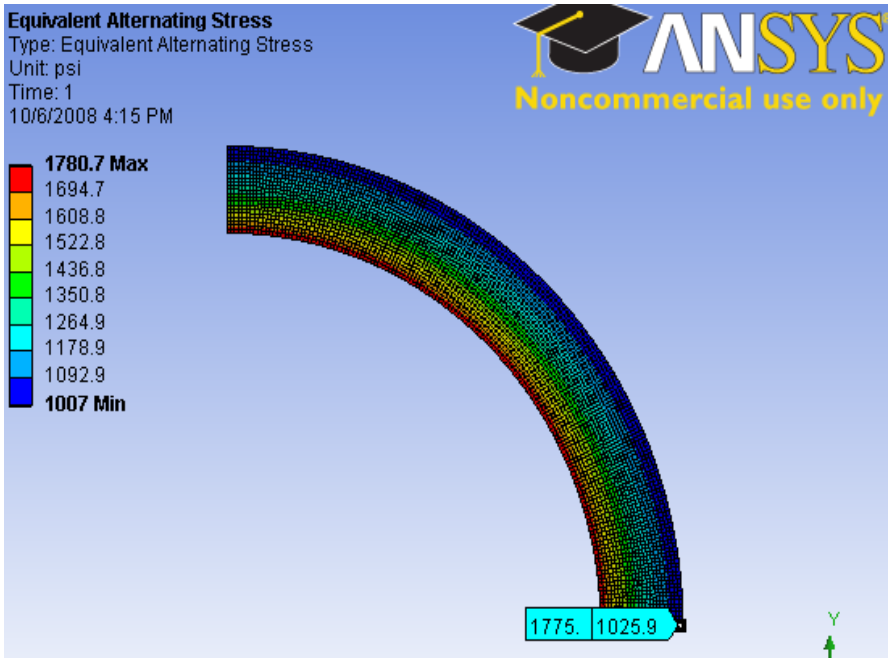

Fig 4.39: Alternating Stress for Cement System 1 under Zero Based Cyclic Loading

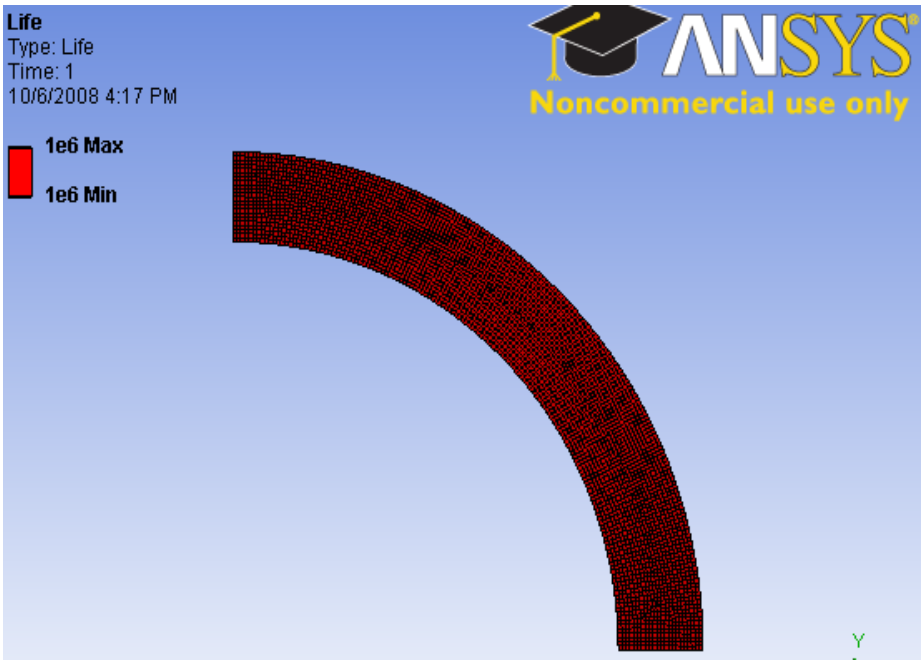

Fig 4.40: Life Cycle for Cement System 1 under Zero Based Cyclic Loading

For cement system 1, the magnitude of the alternating stress appears to be smaller than the equivalent stress under static loading (Figs. 4.38 and 4.39). This trend is quite different from what was obtained with cement system 2 where the minimum alternating stress under a zero based cyclic loading is greater than the maximum equivalent stress under static loading (Figs. 4.32 and 4.33). The fatigue sensitivity plots (Figs. 4.41 to 4.43) show that the maximum load ratio that can be supported by cement system 1 before failure is about 1.1.

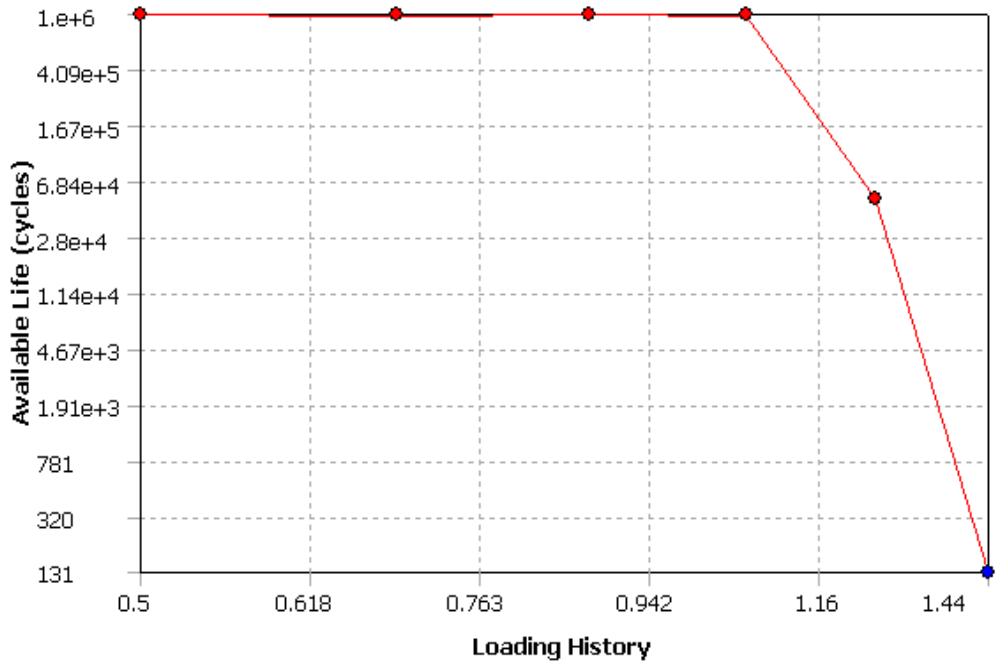

Fig 4.41: Fatigue Sensitivity to Life for Zero Based Cyclic Loading with Cement 1

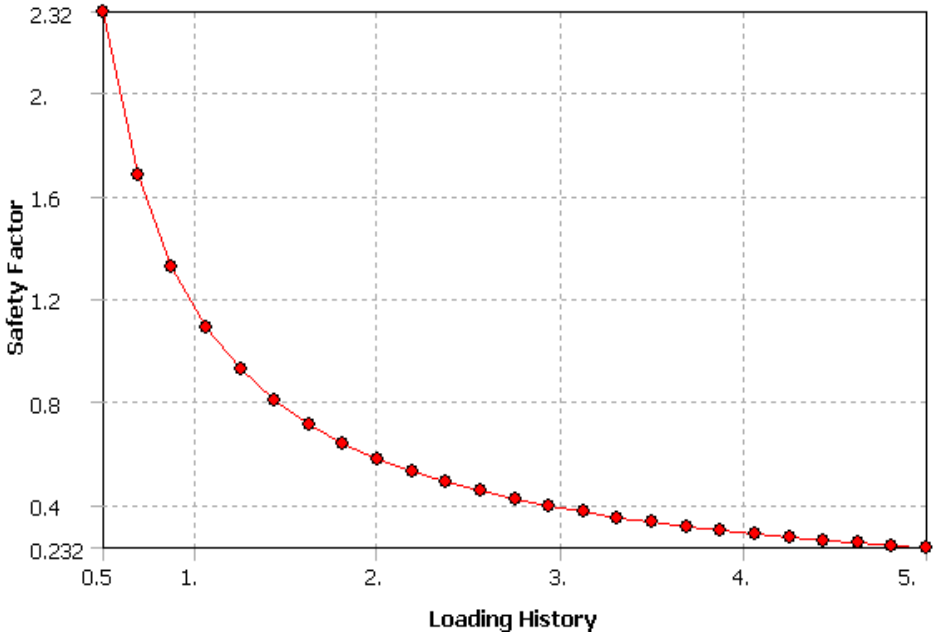

Fig 4.42: Fatigue Sensitivity to Safety Factor for Zero Based Cyclic Loading with Cement 1

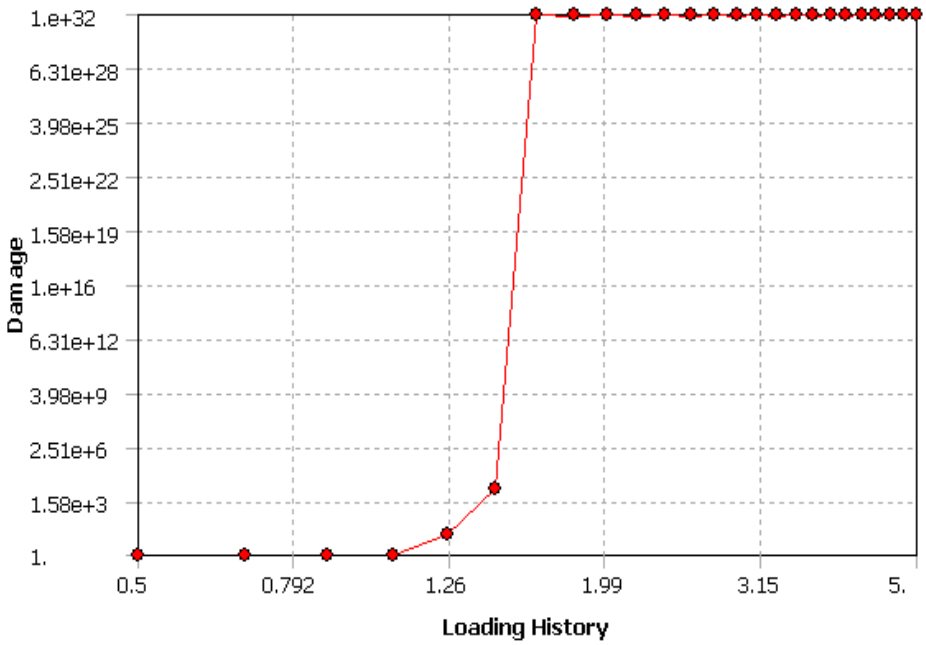

Fig 4.43: Fatigue Sensitivity to Damage for Zero Based Cyclic Loading with Cement 1

4.3 Experimental Studies

An experimental investigation was conducted on a prototype test cell to determine the performance of well cement under cyclic loading conditions.

A 2-½” ID steel pipe was cemented between two different sizes of PVC pipes acting as the confinements (formation). The PVC pipes were 4-½" and 3-½" inner diameter. The cement was a Class H premium cement and was mixed in two batches:

- 16 lb/gal slurry (water/cement ratio of 0.4)
- 14 lb/gal slurry (water/cement ratio of 0.7).

The two batches were mixed in an OFITE constant speed blender according to API specifications. The 16 lb/gal slurry was then poured between the steel pipe and both of the 4-½" and 3-½" ID pipes and allowed to cure under atmospheric pressure for 56 days. It was also poured into cube molds and allowed to cure under water and at atmospheric pressure for 56 days (Fig. 4.44). The 14 lb/gal slurry was cast only in the cube molds and cured under the same conditions as the 16 lb/gal slurry. The amount of shrinkage in the 14 lb/gal slurry was large compared to the 16 lb/gal slurry as shown in Fig. 4.45 with the 14 lb/gal mold having dimensions of 2×1.6 inches and the 16 lb/gal mold having dimensions of 2×2 inches.

Fig 4.44: Cubes Cured Under Water at Atmospheric Pressure

Fig 4.45: Shrinkage in Cured Cement

The cubes were tested for compressive strength after 56 days. The 14 lb/gal mold had a compressive strength of 3,162 psi while the 16 lb/gal mold had a strength of 7,887 psi. Cyclic tests were carried out on the cemented pipe-PVC setup. A maximum axial compressive force of 15,000 lbs was applied to the cement cyclically (from 0 lbs to 15,000 lbs and back to 0 lbs) using a compressive tester. This is shown in Fig 4.46.

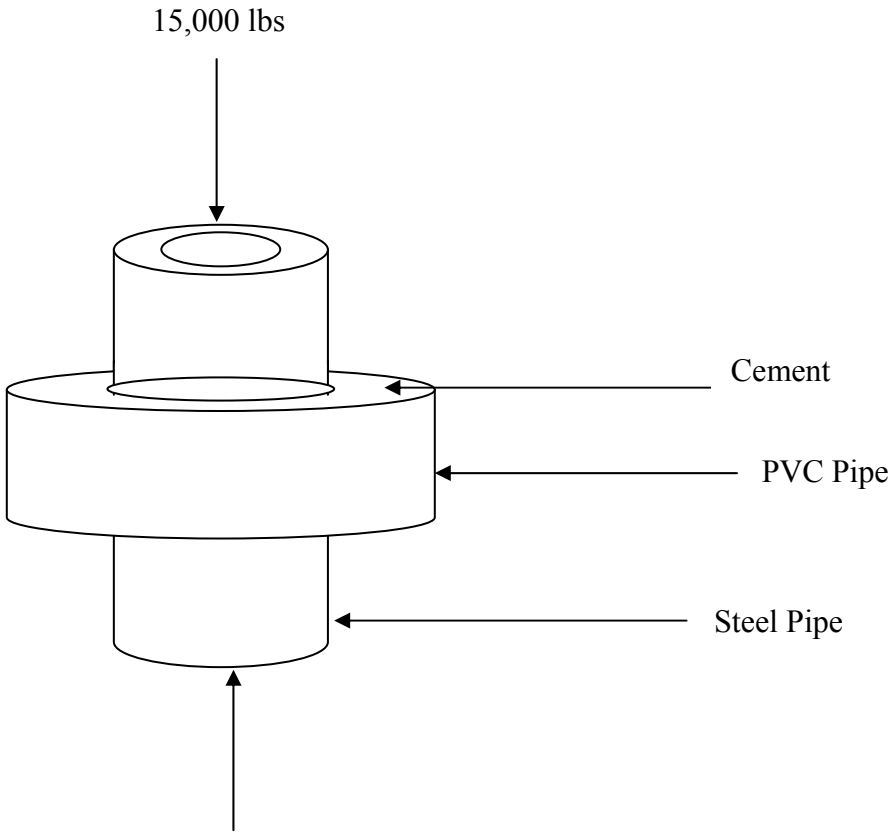

Fig 4.46: Cemented Pipe under Compression,

Cracks were observed on both slurry specimens at about 12 cycles and the cracks widened after 30 cycles. It should however be noted that tests were not conducted to see if these cracks went all the way to the surface as the integrity may not have been fully compromised at the presence of the cracks after 12 and 30 cycles. Another test was also conducted to determine the amount of force required to de-bond the cement from the casing. It was observed that this happened after a force of 2,500 lbs was applied to the 16 lb/gal slurry after 30 cycles of testing and at 4,000 lbs when no initial cycling force was applied.

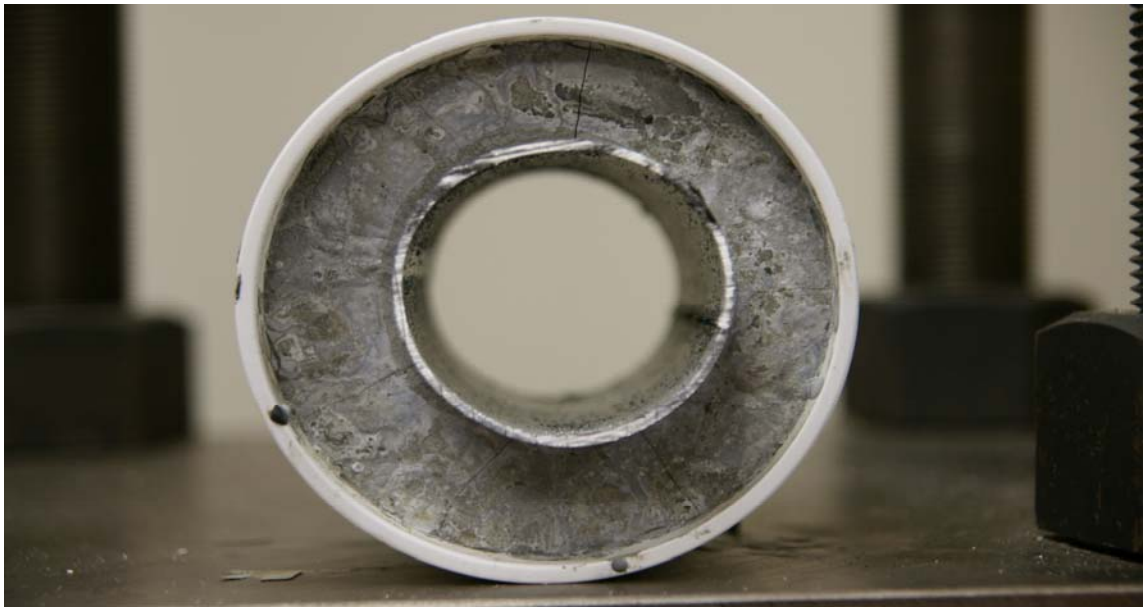

Fig 4.47: Cracks in 4-½" ID Pipe with 16 lb/gal Slurry after 12 Cycles

Fig 4.48: Cracks in 4-½" ID Pipe with 16 lb/gal Slurry after 30 Cycles

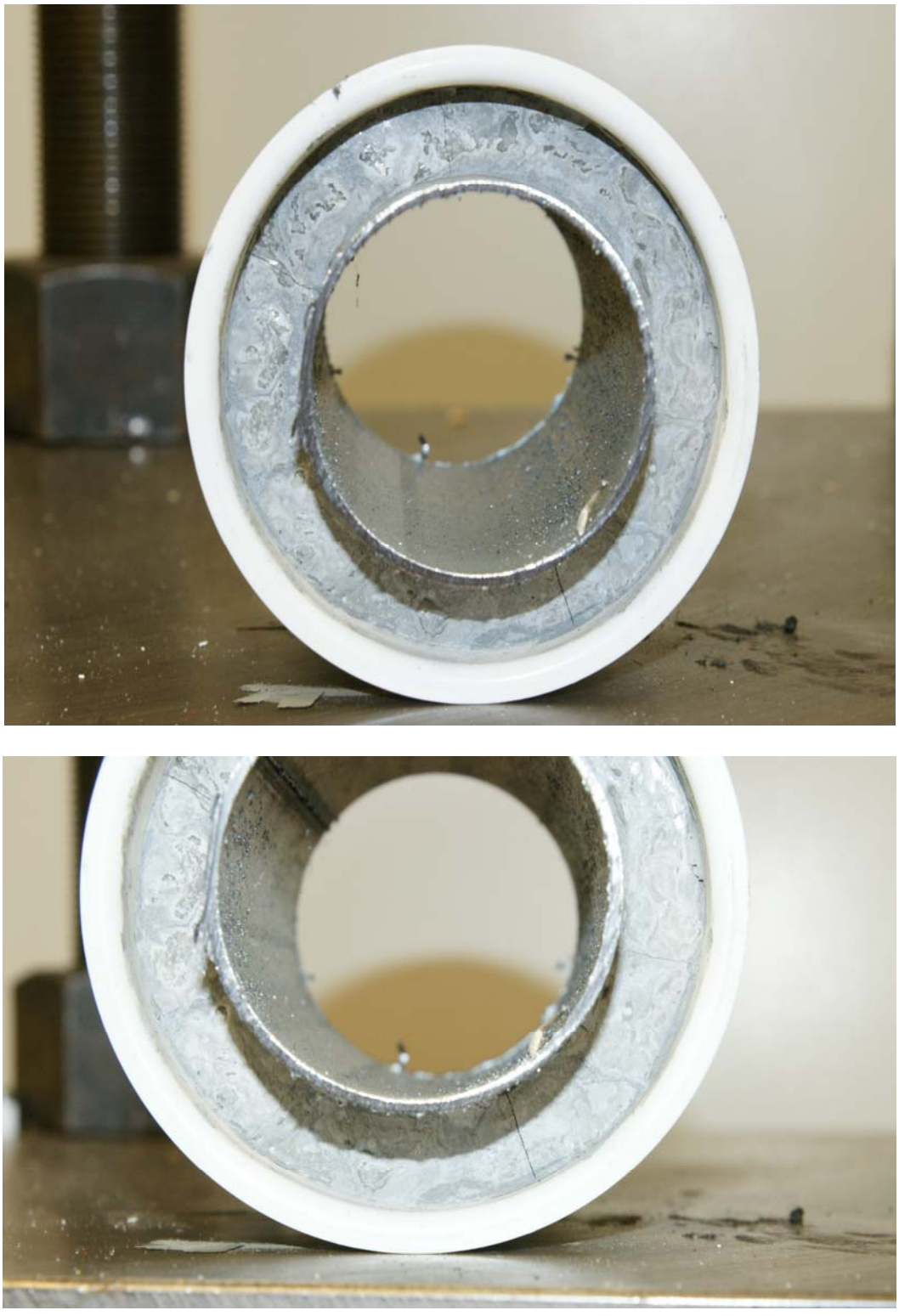

Fig 4.49: Cracks in 3-½" ID Pipe with 16 lb/gal Slurry after 12 Cycles

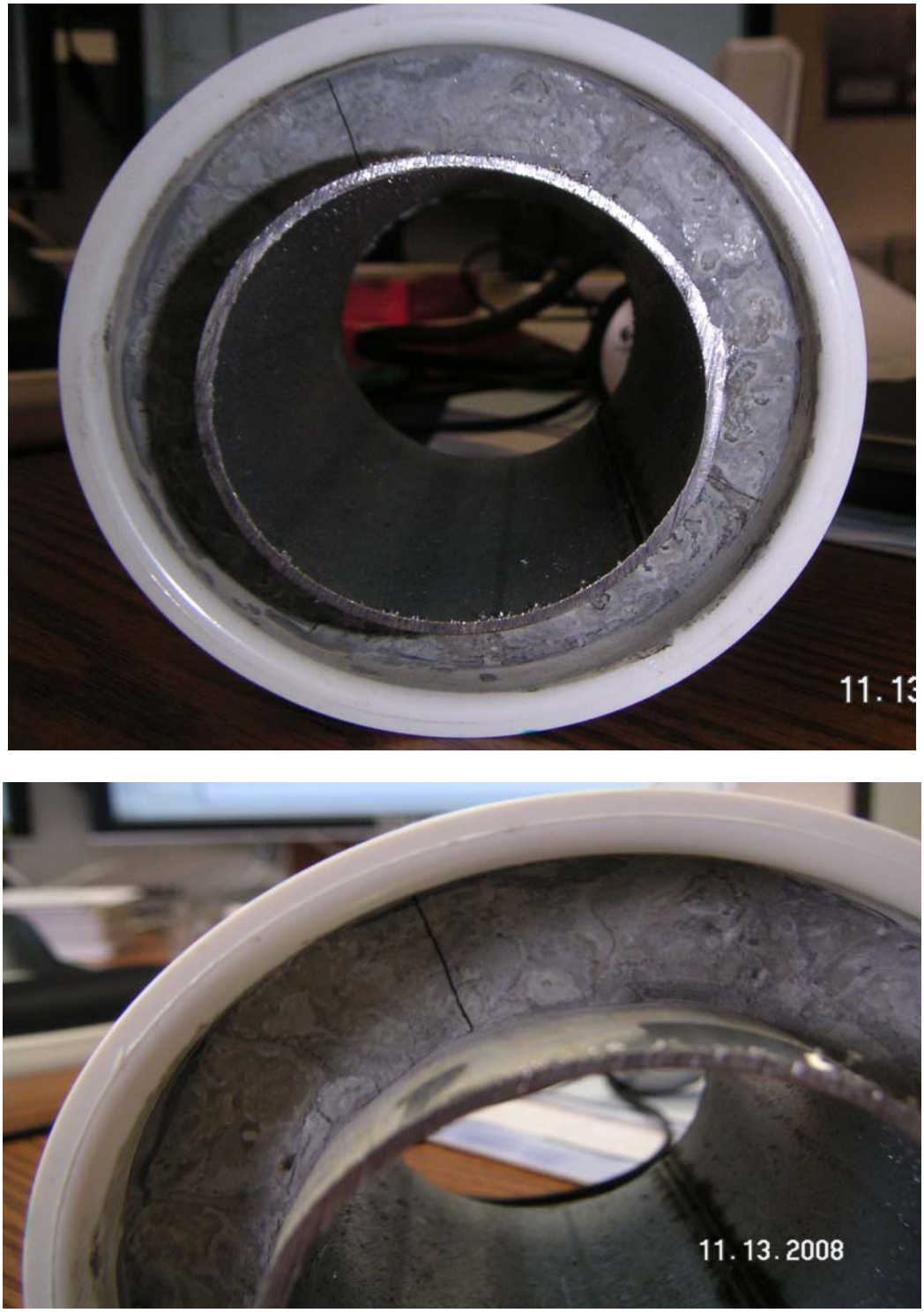

Fig 4.50: Cracks in 3-½" ID Pipe with 16 lb/gal Slurry after 30 Cycles

Fig 4.51: 4-½" ID Pipe with 16 lb/gal Slurry after De-bonding at 2,500 lb Force

5. CONCLUSIONS AND RECOMMENDATIONS

5.1 Conclusions

The drilling and completion of a well is a capital project that needs to be executed properly. As a consequence, a detailed design is required, putting into consideration all forces that may affect the integrity of a well throughout its life span.

An aid to such a detailed design is the analytical model which was developed in this project that utilizes the wellbore parameters to evaluate stresses in the cement sheath and has been developed into a software tool. It is a very flexible tool which enables cement designers to optimize their design for HTHP conditions while at the same time putting the design cost in perspective. Combined in synergy with finite element analysis, it can be used to evaluate the fatigue and static loading behavior of the cement, thereby helping to predict the life of the well. The analytical model can also be extended to include fatigue properties of cement in the next phase of this project.

Experimental studies provided us with an insight into some fatigue and static behavior of well cements. Fatigue failure in cement occurs when microscopic damage within the microstructure of the cement, caused by initial cyclic loading, turns into macroscopic cracks under gradually increasing loads. Cyclic loading impacts initial damage and if loading is continued at load ratios above the critical ratio for a particular cement mix, failure is imminent but may undergo many cycles when loaded below this ratio. Loading conditions may affect the fatigue property of cement only when the mechanical properties are such as to withstand static loading. Designs based solely on

static loading conditions may or may not be enough to ensure long term integrity depending on prevailing downhole conditions, thus the need to take the analysis further by also examining the effect of fatigue with additional experimental studies.

The mechanical properties of cement play a very important role in the static and fatigue performance of cement. Ductile cement systems – cements with low Young's modulus and a high Poisson's ratio – generally perform better under static and cyclic loading conditions as compared to brittle cement systems, i.e. cement systems with a high Young's modulus and low Poisson's ratio. Ductile cement systems generate significantly lower values of tangential and radial stresses, while brittle cements are more likely to generate higher tensile and radial stresses within their microstructure under a particular loading condition.

The magnitude of confining stress and the mechanical properties of the formation also play an important role in the static and fatigue behavior of both the cement and casing. A large far field stress (formation pressure) acts to increase the performance of the casing and counteracts high internal pressures, ensuring a minimal transfer to the cement sheath. Also, the more brittle the formation (in terms of Young's modulus and Poisson's ratio), the greater the stress transmitted to the casing and cement sheath.

5.2 Recommendations for Future Work

This study has focused on the effect of both static loading and fatigue behavior of well cement based on analytical and finite element models. A significant amount of experimental work is required in the following areas:

- Developing equations specific to well cement. Equations (3.3), (3.4) and (3.26) can be derived specifically for well cement from experimental data and linear regression analysis. New failure mechanisms, crack initiation and propagation and failure theories can also be developed from these data. This would help expand the analytical model to include fatigue life prediction.

- The findings reported in this work are centered mainly on the mechanical properties of the cement and on loading conditions. The effect of other factors like cement-water ratio etc should be investigated through experimental studies.

- The effect of additives on the static and fatigue properties of well cement.

- Performance of new cement systems with special properties like foam and expansive cements should also be studied and data generated for them.

REFERENCES

1. Hahn, D.: "Why Do HP and HT Completions Require Rigorous Engineering Design?", paper SPE 101509, SPE Distinguished Lecture Series.

2. Ravi, K., Bosma, M., and Hunter, L.: "Optimizing the Cement Sheath Design in HPHT Shearwater Field," paper IADC/SPE 79905, IADC/SPE Drilling Conference, Amsterdam, Netherlands, February 2003.

3. Kim, J. and Kim, Y.: "Experimental Study of the Fatigue Behavior of High Strength Concrete," *Cement and Concrete Research*, Vol. 26, No. 10, 1996. 1513-1523.

4. Antrim, J.D.: "The Mechanism of Fatigue in Cement Paste and Plain Concrete", *Highway Research Record*, 210 no 6, 1965.

5. Breitenbucher, R., Alawieh, H., and Ibuk, H.: "Influence of Cyclic Loading on the Degradation of Mechanical Concrete Properties," *Advances in Construction Materials*, (August 2007) 317–324.

6. Breitenbucher, R. and Ibuk, H.: "Experimentally Based Investigations on the Degradation-Process of Concrete under Cyclic Load," *Materials and Structures,* (June 2006) 39,717–724.

7. Nayeb, H., Hashemi I., Cohen, M. D., and Erturk, T.: "Evaluation of Fatigue Damage on the Mechanical Properties of Fiber Reinforced Cement Pastes," *Cement and Concrete Research*, (May 1985)15, 879-888.

8. Bourgoyne, A.T., Millheim, K.K., Chenevert, M.E., and Young, F.S.: *Applied Drilling Engineering*, SPE Textbook Series, Vol. 2, 1986.

9. Nelson, E.B.: "Well Cementing," *Development in Petroleum Science*, Vol. 28, 1990.

10. Halliburton Energy Services: "Halliburton Cementing Technology Manual", 2007.

11. US Department of Transport: "Portland Cement", www.fhwa.dot.gov/infrastructure/materialsgrp/cement.html , 2007.

12. Edgley, K., D., Sabins, F., L. and Watters, L., T.: "Supercement for Annular Seal and Long Term Integrity in Deep, Hot Wells " 'Deep Trek'," Phase II Annual Report, CSI Technologies, Houston. August 2005.

13. Pine, M., Hunter, L., Mutch, J., Adam, J., and Griffith, E.J.: "Selection of Foamed Cement for HPHT Gas Wells Proves Effective for Zonal Isolation-Case History," paper IADC/SPE 79909, IADC/SPE Drilling Conference, Amsterdam, Netherlands, February 2003.

14. Ravi, K and Xenakis, H.: "Cementing Process Optimized to Achieve Zonal Isolation". Halliburton, January 2007.

15. Stiles, D.: "Effects of Long-Term Exposure to Ultrahigh Temperatures on Mechanical Parameters of Cement," paper SPE 98896, IADC/SPE Drilling Conference, Miami, Florida, February 2006.

16. Godwin, K.J., and Crook R.J.: "Cement Sheath Stress Failure," SPE Drilling Engineering, pp. 291-296, December 1992.

17. Fleckenstein, W.W., Eustes, A.W., and Miller, M. G.: "Burst Induced Stresses in Cemented Well Bores," paper SPE 62596, SPE/AAPG Western Regional Meeting, Long Beach, California, June 2000.

18. Gray, K.E., Podnos, E., and Becker, E.: "Finite Element Studies of Near-Wellbore Region during Cementing Operations: Part 1," Paper SPE 106998, SPE Production and Operations Symposium, Oklahoma City, Oklahoma, April 2007.

19. Heathman, J., and Beck, F.E.: "Finite Element Analysis Couples Casing and Cement Design for HP/HT Wells in East Texas," paper SPE 98896, IADC/SPE Drilling Conference, Miami, Florida, February 2006.

20. Rodriguez, W. J., Fleckenstein W.W., and Eustes A.W.: "Simulation of Collapsed Load on Cemented Casing Using Finite Element Analysis," paper SPE 84566, SPE Annual Technical Conference, Denver, Colorado, October 2003.

21. Schubert, J.J., Shahri, M.A., and Amani, M.: "Detecting and Modeling Cement Failure in High Temperature/High Pressure (HP/HT) Wells Using Finite Element Methods," paper IPTC 10961, IPTC Conference, Doha, Qatar, November 2005.

22. Ravi, K., Bosma, M., and Gastebled, O.: "Improve the Economics of Oil and Gas Wells by Reducing the Risk of Cement Failure," paper SPE 74497, IADC/SPE Drilling Conference, Dallas, Texas, February 2002.

23. Krusche, K., Johnson, C.R., Braud, N.Y., and Ghazi, H.B.: "Application of Cement Engineered Solutions to Solve Long Term Cement Integrity Issues in Tunisia," paper SPE 100390, SPE Annual Technical Conference, San Antonio, Texas, September 2006.

24. Avram, C., Facaoaru, I., Mirsu, O., Filimon, I., and Tertea, I.: "Concrete Strength and Strains," *Developments in Civil Engineering*, Vol. 3, Elsevier Scientific Publishing Company, New York, 1981.

25. Newman, J., and Choo, B.S.: "Concrete Properties", *Advanced Concrete Technology*, Elsevier Butterworth-Heinemann, Boston, MA. 2003.

26. Cook, R.D. and Young, W.C.: *Advanced Mechanics of Materials*, 2nd ed. Prentice Hall, Upper Saddle River, NJ. 1999.

Supplemental Sources Consulted

1. Magalhaes, A.G. et al. : "Mechanical Behavior of Cementitious Matrix Composite", *Cement and Concrete Composites*, (1996)18 no 1, 9-22.

2. Bocca, P. and Crotti, M.: "Variations in the Mechanical Properties and Temperature of Concrete Subjected to Cyclic Loads, Including High Loads," *Materials and Structures*, (February 2003)36, 40-45.

3. Morris, A. D., and Garrett, G. G.: "A Comparative Study of the Static and Fatigue Behavior of Plain and Steel Fiber Reinforced Mortar in Compression and Direct Tension," *The International Journal of Cement Composites and Lightweight Concrete*, (May 1981) 3, no 2, 73-91.

4. Khandka R.K.: "Leakage behind Casing" M.S. Thesis, Norwegian University of Science and Technology, Trondheim, 2007.

5. Alliche, A., and Francois, D.: "Fatigue Behavior of Hardened Cement Paste," *Cement and Concrete Research*, (January 1986)16, 199-206.

6. LeRoy-Delage, S., Baumgarte, C., Thiercelin M., and Vidick B.: "New Cement Systems for Durable Zonal Isolation," paper SPE 59132, IADC/SPE Drilling Conference, New Orleans, Louisiana, February 2000.

7. O'Brien, B.T.: "Case against Cementing Casing - Casing Annuli," paper SPE 35106, IADC/SPE Drilling Conference, New Orleans, Louisiana, March 1996.

8. Hancq, D.A.: "Fatigue Analysis using ANSYS", ANSYS Inc. http://www.caeai.com/papers/Fatigue_ANSYS.pdf, 2007.

9. Thiercelin, M.J., Dargaud, B., Baret, J.F., Rodriguez, W. J.: "Cement Design Based on Cement Mechanical Response," SPE Annual Technical Conference, San Antonio, Texas, 337–348, 1997.